Universidade Federal do Rio Grande - FURG

Instituto de Oceanografia

Programa de Pós-Graduação em Oceanologia

VARIABILIDADE ESPAÇO-TEMPORAL DOS PARÂMETROS DO SISTEMA CARBONATO NO ESTREITO DE BRANSFIELD, NORTE DA PENÍNSULA ANTÁRTICA

MAURÍCIO SANTOS ANDRADE

Dissertação apresentada ao Programa de Pós-Graduação em Oceanologia, como parte dos requisitos para a obtenção do Título de Mestre.

Orientador: *Prof. Dr.* RODRIGO KERR DUARTE PEREIRA

Universidade Federal do Rio Grande (FURG), Brasil

Rio Grande, RS, Brasil

Julho 2022

VARIABILIDADE ESPAÇO-TEMPORAL DOS PARÂMETROS DO SISTEMA CARBONATO NO ESTREITO DE BRANSFIELD, NORTE DA PENÍNSULA ANTÁRTICA

Dissertação apresentada ao Programa de Pós-Graduação em Oceanologia, como parte dos requisitos para a obtenção do Título de Mestre

por

MAURÍCIO SANTOS ANDRADE

Rio Grande, RS, Brasil

Julho 2022

SANTOS-ANDRADE, MAURICIO

Variabilidade espaço-temporal dos parâmetros do sistema carbonato no estreito de Bransfield, norte da Península Antártica. / Mauricio Santos Andrade. – Rio Grande: FURG, Ano 2022.

Número de páginas p. 181.

Dissertação (Mestrado) – Universidade Federal do Rio Grande. Mestrado em Oceanologia. Área de Concentração: Biogeoquímica, Poluição e Ecossistemas Marinhos.

1. Processos biogeoquímicos. 2. Acidificação oceânica. 3. El Niño Oscilação Sul. 4. Modo Anular Sul. 5. Estreito de Bransfield. 6. Oceano Austral.

SERVIÇO PÚBLICO FEDERAL
MINISTÉRIO DA EDUCAÇÃO
UNIVERSIDADE FEDERAL DO RIO GRANDE - FURG
INSTITUTO DE OCEANOGRAFIA - IO
PROGRAMA DE PÓS-GRADUAÇÃO EM OCEANOLOGIA - PPGO
E-mail: ccpofqg@furg.br – home-page: www.ppgo.furg.br

ATA ESPECIAL DE DEFESA DE DISSERTAÇÃO DE MESTRADO 01/2022

Às oito horas do dia vinte e cinco de julho do ano de dois mil e vinte e dois, por Vídeo Conferência, reuniu-se a Comissão Examinadora da Dissertação de **MESTRADO** intitulada: **"Variabilidade espaço-temporal dos parâmetros dos sistema carbonato no estreiro de Bransfield, Norte da Península Antártica"**, do Acad. Maurício Santos Andrade. A Comissão Examinadora foi composta pelos seguintes membros: Prof. Dr. Rodrigo Kerr (Orientador – IO/FURG), Profa. Dra. Eunice da C. Machado (IO-FURG) e Profa. Dra. Leticia C. da Cunha (UERJ), Dando início à reunião, o Presidente da sessão, Prof. Dr. Rodrigo Kerr, agradeceu a presença de todos, e fez a apresentação da Comissão Examinadora. Logo após, esclareceu que o Candidato teria de 45 a 60 min para explanação do tema, e cada membro da Comissão Examinadora, um tempo máximo de 30 min para perguntas. A seguir, passou à palavra ao Candidato, que apresentou o tema e respondeu às perguntas formuladas. Após ampla explanação, a Comissão Examinadora reuniu-se em reservado para discussão do conceito a ser atribuído ao Candidato. Foi estabelecido que as sugestões de todos os membros da Comissão Examinadora, que seguem em pareceres em anexo, foram aceitas pelo Orientador/Candidato para incorporação na versão final da Dissertação. Finalmente, a Comissão Examinadora considerou o candidato **APROVADO** por unanimidade. Nada mais havendo a tratar, foi lavrada a presente ATA, que após lida e aprovada, será assinada pela Comissão Examinadora, pelo Candidato e pelo Coordenador do Programa de Pós-Graduação em Oceanologia (PPGO).

Prof. Dr. Rodrigo Kerr
Presidente

Profa. Dra. Eunice da C. Machado

Profa. Dra. Letícia C. da Cunha

Acad. Maurício Santos Andrade

Prof. Dr. Rodrigo Kerr
Coordenador do PPGO

Chave de Autenticidade: 9996.2DEA.5802.C2E2

1 / 1

Agradecimentos

Uma série de nomes podem ser citados aqui, os quais contribuíram direta ou indiretamente para o andamento dessa dissertação. Primeiro, agradeço às forças superiores que me guiaram, mesmo durante períodos de tempestades noturnas, para chegar agora onde vejo o arco-íris junto ao pôr do sol.

Em seguida, à minha família, em especial à minha mãe, Edite, por me apoiar de longe ou de perto e me incentivar, do seu jeito particular de ser, a seguir e chegar hoje onde estou. Também, agradeço ao meu pai, Joaquim (em memória), que, embora não tenha acompanhado essa etapa de minha vida, foi base sólida para todos os passos anteriores se consolidarem nessa jornada que nunca foi fácil e só nós sabemos o quanto.

Ao meu orientador, Rodrigo, por ter me recebido como seu orientando, pelas discussões, pelos momentos leves que foram fundamentais para manter forças durante esses dois últimos anos que tiveram uma pitada a mais de desafios.

Aos integrantes do CARBON Team, pela receptividade, pelas contribuições que cruzavam o ambiente acadêmico e atingiam pontos pessoais importantes que me proporcionaram uma grande abertura de mente quanto ao ser humano antes de tudo. Em especial, ao Anderson, que me acolheu enquanto estava sendo acolhido em Rio Grande, pelos momentos de risos e de apoio, e espero que tenhamos tempo para o calzone, que eu não esqueci.

Aos meus amigos de vida, de outras jornadas, que também me deram apoio, me tiraram risos, foram “ombros que me ouviram” e que fizeram parte indiretamente desse processo.

Ao LEOC e ao IO/FURG, pelo espaço cedido enquanto a atividade presencial ainda era possível. Aos professores do PPGO/FURG, pelo crescimento obtido ao longo as disciplinas e discussões ao longo desses dois anos. Ao CNPq pela bolsa e à CAPES pelo financiamento do projeto.

Índice

Lista de figuras

Capítulo I

Capítulo III

Capítulo IV

Capítulo V – Material Suplementar do Capítulo IV

Lista de tabelas

Capítulo III

Capítulo IV

Capítulo V – Material suplementar do Capítulo IV

Lista de Acrônimos e Abreviações

C

CDW – Água Profunda Circumpolar (*Circumpolar Deep Water*)

CO_2 – Dióxido de Carbono (*Carbon Dioxide*)

CO_3^{2-} - Íon Carbonato (*Carbonate Ion)*

CT – Carbono Inorgânico Total – (*Total Inorganic Carbon*)

CTD – *Condutivity, Temperature and Depth*

D

DSW – Água Densa de Plataforma (*Dense Shelf Water*)

E

ENSO – El Niño Oscilação Sul (*El Niño Southern Oscillation*)

G

GOAL – Grupo de Oceanografia de Altas Latitudes

H

HCO_3^- - Íon Bicarbonato (*Bicarbonate Ion*)

K

K – Constante de Dissociação (*Dissociation Constant*)

N

NAP – Norte da Península Antártica (*Northern Antarctic Peninsula*)

O

O_2 – Oxigênio Dissolvido (*Dissolved Oxygen*)

P

pCO_2 – Pressão Parcial do Dióxido de Carbono (*Partial Pressure of Carbon Dioxide*)

pH – Potencial Hidrogeniônico

R

RMSE – Erro Quadrático Médio (*Root Mean Square Error*)

S

S – Salinidade (*Salinity*)

SAM – Modo Anular Sul (*Southern Annular Mode*)

T

T – Temperatura (*Temperature*)

TA – Alcalinidade Total (*Total Alkalinity*)

W

WOD18 – *World Ocean Database 2018*

Θ

Θ – Tempreratura potencial (*Potential Temperature*)

Ω

Ω_{ar} – Estado de Saturação de Aragonita (*Saturation State for Aragonite*)

Ω_{ca} – Estado de Saturação de Calcita (*Saturation State for Calcite*)

Resumo

O estreito de Bransfield é um *hotspot* climático localizado ao norte da Península Antártica. Essa região é caracterizada como um ambiente de alta mistura de águas relativamente mais quentes do mar de Bellingshausen com águas densas de plataforma oriundas do mar de Weddell. Ainda, a camada profunda da bacia central do estreito (> 800 m) detém a capacidade de preservar assinaturas de alterações hidrográficas que estão ocorrendo na plataforma continental do noroeste do mar de Weddell. Dessa forma, essa dissertação visa avaliar as alterações de longo prazo da química do sistema carbonato no estreito de Bransfield. A configuração hidrográfica, caracterizada pela mistura entre a fração modificada da Água Profunda Circumpolar e da Água Densa de Plataforma (DSW), controla a variabilidade temporal do sistema carbonato. Ao longo das últimas três décadas (1996 – 2019), a bacia oeste apresentou tendências de redução de pH, na escala *seawater* – pH_{sws}, que variaram de –0,003 a –0,017 unidades de pH_{sws} ano^{-1}, enquanto a saturação de carbonato de cálcio (Ω) apresentou tendência de –0,010 a –0,070 unidades de Ω ano^{-1} ao longo de toda a coluna de água. Essas tendências são mais intensas do que quaisquer outras estimativas reportadas para zonas costeiras e oceano aberto ao redor da Antártica. A bacia central foi caracterizada pelas altas contribuições de DSW, visto que a ventilação dos níveis profundos da bacia responde às altas concentrações de dióxido de carbono (CO_2) dissolvido na água do mar antes desta deixar o contato com a atmosfera, ainda no mar de Weddell. Somado a esse processo, a camada profunda da bacia central apresentou ser afetada por decomposição de matéria orgânica, controlando a variabilidade do sistema carbonato. Com baixo grau de variabilidade interanual para todos os parâmetros

da química do carbonato, a bacia leste provavelmente está associada com processos de mistura interna mais acentuados e/ou diferentes composições de águas-fontes. A alta contribuição de DSW para a bacia central do estreito de Bransfield pode conduzir a um mais rápido incremento de CO_2 (ocasionado pelo aumento da concentração na atmosfera devido as ações antrópicas) e, assim, um mais rápido alcance do limite de saturação desse gás quando comparado à bacia oeste, que é influenciada principalmente por processos naturais. Portanto, o estreito de Bransfield atua como uma região sentinela de alterações biogeoquímicas ocorrendo no entorno do norte de Península Antártica, podendo assumir um papel importante na assimilação de mudanças temporais dos parâmetros do sistema carbonato ocorrendo no oceano Austral.

Palavras-chave: Processos biogeoquímicos; acidificação oceânica; El Niño Oscilação Sul; Modo Anular Sul; Estreito de Bransfield; Oceano Austral.

Abstract

The Bransfield Strait is a climate change hotspot at the tip of the northern Antarctic Peninsula. The region is marked by a mixture of relatively warm waters from the Bellingshausen Sea with cold shelf waters from the Weddell Sea. Additionally, its deep central basin (>800 m) preserves the seawater properties from the north-western Weddell Sea continental shelf. This study assesses the carbonate chemistry long-term changes in the Bransfield Strait and identified that the hydrographic setting (i.e., a mixture between modified-Circumpolar Deep Water with Dense Shelf Water – DSW) drives the temporal variability of the carbonate properties. Over the last three decades (1996-2019), the western basin presented a pH_{sws} decrease varying from -0.003 and -0.017 pH_{sws} units yr^{-1}, while the Ω decreased from -0.010 to -0.070 yr^{-1} throughout the water column. The central basin was characterized by a high contribution of DSW, responding to high concentrations of carbon dioxide (CO_2) dissolution and the decomposition of organic matter produced and transported into its deep layer. With smoother levels of variability for the whole carbonate system parameters, the eastern basin was likely regulated by internal mixing. The high contribution of DSW may swiftly lead to CO_2 saturation threshold as identified in the central basin relative to the western side of the Strait. Therefore, the Bransfield Strait does act as a sentinel for chemical changes experienced around the Antarctic Peninsula, which may play an important role in assimilating any temporal changes in the carbon system in the Southern Ocean.

Keywords: Biogeochemical processes; ocean acidification; El Niño Southern Oscillation; Southern Annular Mode; Bransfield Strait; Southern Ocean.

Capítulo I: Introdução

I.1. O ciclo do carbono global e o sistema carbonato marinho

O ciclo do carbono constitui um dos principais ciclos biogeoquímicos no planeta Terra (Figura I.1). A participação do carbono na composição bioquímica de ~50% das estruturas orgânicas existentes, a comparável magnitude entre a ciclagem desse elemento e os fluxos de energia em superfície e o seu papel no clima, principalmente pela atuação dos gases dióxido de carbono (CO_2) e metano, proporcionam tamanha importância a esse ciclo biogeoquímico (Houghton, 2003). Assim, distintas formas de carbono tendem a percorrer por diferentes reservatórios, desde endógenos, tais como depósitos sedimentares e manto, até exógenos, tais como atmosfera, continente e oceano, permitindo que fluxos sejam estabelecidos (Green e Byrne, 2004) em distintas escalas temporais que

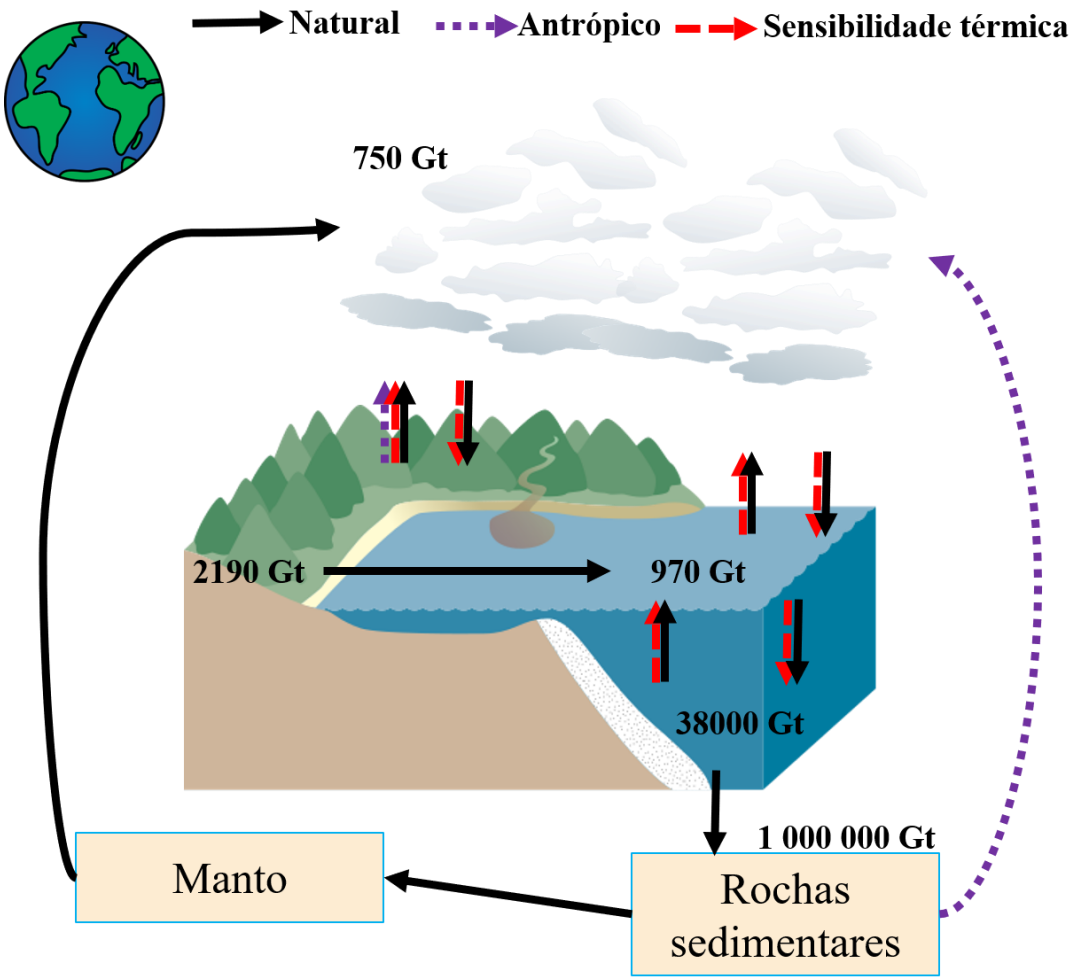

Figura I.1. Esquema representativo dos principais reservatórios de carbono em ambiente exógeno e endógeno e os fluxos (setas pretas) entre eles. Os valores dos estoques (Gt) em cada reservatório foram extraídos de Abbas *et al.* (2017). As setas roxas representam fluxos resultantes da atividade antrópica, enquanto as setas vermelhas representam os fluxos que são sensíveis às alterações térmicas experimentadas diante das mudanças do clima. As escalas dos fluxos no ambiente exógeno são maiores do que as escalas endógenas, mas as ações antrópicas reduzem essa escala temporal.

variam de segundos a milhares de anos (Houghton, 2003; Zeebe, 2012). Em escala global, os depósitos sedimentares constituem um dos principais reservatórios de carbono, com estoques que giram em torno de 10^6 Gt (Abbas *et al.*, 2017). Uma vez que esses depósitos têm sido explorados como fonte de combustíveis fósseis, a escala temporal de reciclagem do carbono nas rochas sedimentares reduz drasticamente de milhares de anos para anos. Em

superfície, o maior reservatório de carbono é o oceano, que totaliza ~3,9 x 10^4 Gt. Esse valor é o resultado da soma dos conteúdos de carbono em toda a coluna de água e do conteúdo de carbono que compõe a fauna marinha (Abbas *et al.*, 2017; Houghton, 2013).

Boa parte do conteúdo de carbono oceânico ocorre na forma de carbono inorgânico total (do inglês, *total inorganic carbon,* CT), representando um total de 3,7 x 10^4 Gt (Zeebe, 2012). Por sua vez, o CT é a soma de quatro formas de compostos de carbono: o CO_2 em sua fração dissolvida na água do mar, o ácido carbônico e os íons bicarbonato (HCO_3^-) e carbonato (CO_3^{2-}), sendo o bicarbonato a maior dessas frações (~91% do CT, Figura I.2, Zeebe e Wolf-Gladrow, 2001). Esses componentes estão interrelacionados através de um sistema químico que é responsável pela regulação do potencial hidrogeniônico (pH) da água do mar, o sistema carbonato (Millero, 2007; Stips *et al.*, 2016).

Na interface oceano-atmosfera, gradientes de CO_2 são estabelecidos, permitindo que fluxos ocorram entre ambos os reservatórios. Os fluxos são associados às variações da pressão parcial do CO_2 (pCO_2). Assim, se o gradiente ocorrer do oceano para a atmosfera, o fluxo ocorre no sentido contrário, o que caracteriza o oceano como um sumidouro de CO_2. O CO_2 deixando a atmosfera se encontra na fase gasosa e passa à fração dissolvida na água do mar. Rapidamente, CO_2 dissolvido sofre hidrólise e forma o ácido carbônico. Uma vez que CO_2 e o ácido carbônico são altamente reativos na água do mar, medidas isoladas de ambos os compostos são difíceis. Para suprir essa dificuldade analítica, ambos os compostos são geralmente indicados na literatura como CO_2^*. Em seguida, o áci-

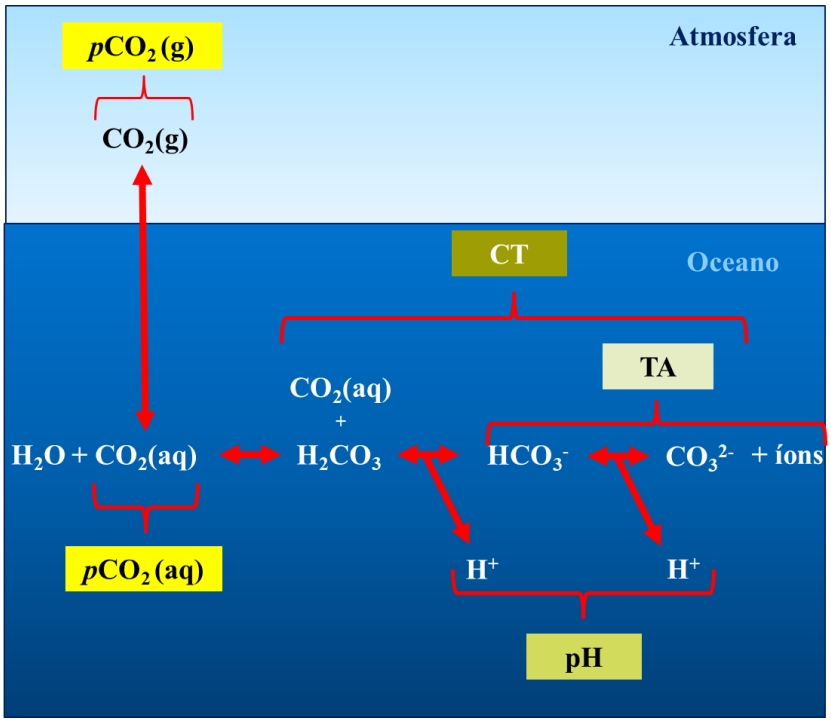

Figura I.2. Esquema representativo das reações químicas e dos principais parâmetros associados ao sistema carbonato marinho. Esquema adaptado de Stips *et al.* (2016).

do carbônico dissocia sucessivamente em dois compostos iônicos, HCO_3^- e CO_3^{2-}. Essas dissociações ocorrem devido ao desequilíbrio das espécies químicas na água do mar e produzem prótons livres de hidrogênio na água do mar (H^+) que estão associados ao controle do pH oceânico. Além do CT, pCO_2 e pH, o sistema carbonato é composto por um quarto parâmetro, chamado alcalinidade total (do inglês, *total alkalinity*, TA). TA é composto pelos íons que estão dissolvidos na água do mar, promovendo um balanço de carga. Esse balanço de carga apresenta influência no pH, atuando como um sistema tampão da água do mar. Nesse sentido, TA pode ser definida como o "excesso de bases/prótons aceptores de elétrons em relação aos ácidos/doadores de prótons em uma solução" e tem ~75% de sua contribuição advinda do HCO_3^- (Emerson e Hedges, 2008). As relações químicas aqui descritas, bem como as equações relacionadas ao equilíbrio químico desse sistema, estão descritas em diversos

documentos (e.g. Millero, 2007, 2016; Zeebe, 2012; Zeebe e Wolf-Gladrow, 2001).

I.2. Os problemas do dióxido de carbono

A história recente ao longo do tempo geológico que marca o registro do homem no planeta registra alterações do sistema Terra até então não experimentadas nos últimos 800 mil anos. Atividades como o uso de combustíveis fósseis e os diferentes usos da terra têm redimensionado as trocas de CO_2 entre os distintos reservatórios (Friedlingstein *et al.*, 2021), o que tem resultado em dois principais efeitos. Uma vez que o carbono na forma de CO_2 é novamente disponibilizado na superfície terrestre, a atmosfera é o primeiro reservatório por onde ele circula (IPCC, 2018). As concentrações de CO_2 na atmosfera têm, portanto, aumentado desde a Revolução Industrial, atingindo concentrações em torno de 421 ppm no mês de junho de 2022, segundo o *Scripps Institution of Oceanography* da Universidade da Califórnia (https://www.keelingcurve.ucsd.edu/). Essa concentração atual representa um incremento de aproximadamente 66% de CO_2 na atmosfera quando comparado ao ano de 1700. Como consequência, a capacidade de retenção de calor na atmosfera é intensificada, promovendo o aumento de temperatura em escala global e, então, o primeiro problema do CO_2 (IPCC, 2018).

O segundo problema do CO_2 atua como uma consequência do primeiro acima citado. O aumento da sua concentração na atmosfera altera o gradiente de pCO_2 na interface oceano-atmosfera, promovendo uma maior captação oceânica de carbono de origem antrópica, o carbono antropogênico (Gruber *et al.*, 2019).

Esse incremento altera o sistema carbonato, o qual guia a um desequilíbrio que favorece uma maior formação do íon HCO_3^- e uma liberação de prótons de hidrogênio, reduzindo o pH e a concentração do íon CO_3^{2-} (Cao, Caldeira e Jain, 2007; Orr *et al.*, 2005). Como consequência, o processo de acidificação oceânica é caracterizado (Doney *et al.*, 2009; Feely, Doney e Cooley, 2009), sendo que o impacto destas alterações ainda tem sido associado aos diversos cenários climáticos desenvolvidos através dos prognósticos de concentração representativa do Painel Intergovernamental da Mudança do Clima (Raven *et al.*, 2005; Turley e Findlay, 2016).

I.3. A sensibilidade oceânica aos problemas do dióxido de carbono

Diferentes regiões oceânicas respondem de formas distintas quanto ao incremento antrópico de CO_2 na atmosfera. Essa relação pode ser expressa por um parâmetro derivado do sistema carbonato, o fator Revelle (Zeebe e Wolf-Gladrow, 2001). Esse parâmetro é determinado através da relação entre a pCO_2 e o CT (Jiang *et al.*, 2019; Millero, 2007; Sabine *et al.*, 2004), representando a mudança proporcional do CO_2 dissolvido na água do mar em relação ao CT (Renforth e Henderson, 2017) e, assim, a sensibilidade de uma região oceânica à adição de CO_2 oriundo da atividade antrópica. Maiores valores de fator Revelle indicam que uma região oceânica está mais próxima de atingir a saturação de CO_2 (Ito, Woloszyn e Mazloff, 2010; Sabine *et al.*, 2004). Com um gradiente meridional bem marcado, as altas latitudes detêm os mais altos valores do fator Revelle (Figura I.3, Jiang *et al.*, 2019), as caracterizando como as áreas mais sensíveis quanto à absorção de carbono antropogênico e sua consequente

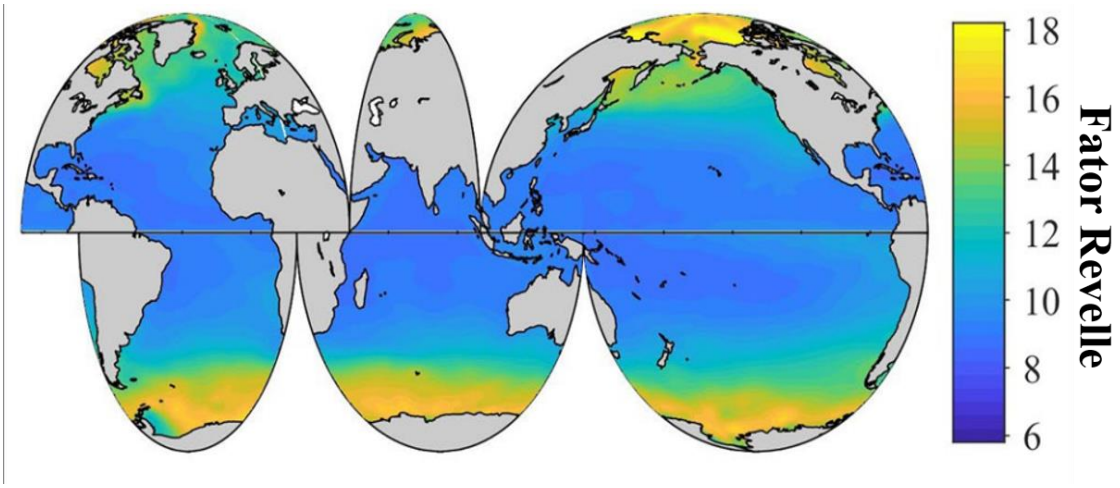

Figura I.3. Distribuição espacial do fator Revelle ao longo da superfície oceânica em todo o globo. Figura retirada e adaptada de Jiang et al (2019).

dispersão pela circulação oceânica. No entanto, as altas latitudes oceânicas são cruciais na remoção de CO_2 atmosférico: enquanto o oceano global é responsável pela absorção de 25 a 30% do excesso de carbono antropogênico no sistema Terra (Watson *et al.*, 2020), o oceano Austral é responsável sozinho por ~40% da captação oceânica total (Gruber, Landschützer e Lovenduski, 2019).

Porém, o oceano Austral tem experimentado uma série de impactos associados às mudanças do clima. Uma das principais respostas climáticas é caracterizada pelas mais frequentes fases positivas de importantes modos de variabilidade climática que desempenham forte influência no entorno da Antártica, como o Modo Anular Sul (do inglês *Southern Annular Mode,* SAM) (Ruiz Barlett *et al.*, 2018; Thompson e Solomon, 2002). Como consequência, o cinturão de ventos de oeste no entorno do continente antártico intensifica e promove alterações nos padrões de circulação oceânica (Jones *et al.*, 2017), incluindo os fluxos das correntes costeiras, no bombeamento de Ekman (Wang *et al.*, 2022; Yanjun *et al.*, 2021) e um maior transporte de calor para as zonas costeiras (Henley *et al.*,

2020) que resulta na perda de volumes significativos de glaciares (Cook *et al.*, 2005, 2016; Rignot *et al.*, 2019) e alterações na extensão, espessura e sazonalidade do gelo marinho (Ruiz Barlett *et al.*, 2018; Shepherd *et al.*, 2018; Shepherd, Wingham e Rignot, 2004). Associado a esses efeitos oriundos do SAM, outro modo de variabilidade climática também influencia nesses impactos, o El Niño Oscilação Sul (do inglês, *El Niño Southern Oscillation*, ENSO). O impacto da mudança do clima tem afetado, neste caso, a intensidade desse modo nas últimas décadas, o qual tem potencializado as suas distintas fases (Loeb *et al.*, 2009; Torres Parra, Caicedo Laurido e Iriarte Sánchez, 2020). Somado a esses pontos, o aumento da temperatura superficial oceânica ao longo dos últimos anos no entorno da Antártica (Cook *et al.*, 2005; Kapsenberg *et al.*, 2015; Meredith e King, 2005) além de alterações na estratificação oceânica (Ducklow *et al.*, 2013; Kapsenberg *et al.*, 2015; Wang *et al.*, 2022) e nas propriedades de salinidade e densidade ao longo das últimas décadas (Dotto *et al.*, 2016; Ruiz Barlett *et al.*, 2018) são alguns dos impactos já identificados.

Por outro lado, a acidificação oceânica promove uma série de implicações ecossistêmicas, principalmente àquelas associadas à química do carbonato de cálcio. Dentre os diversos minerais de carbonato, a aragonita e a calcita são os mais comuns no processo de síntese de estruturas carbonatadas em organismos marinhos (Emerson e Hedges, 2008). As condições atuais de tendência de redução do pH oceânico estão conduzindo para configurações geoquímicas que favorecem a dissolução de estruturas carbonatadas, promovendo condições de subsaturação desses minerais (Fabry, 2008; Tynan *et al.*, 2016). Estados de subsaturação (favorecendo a dissolução com valores menores do que 1), saturação (em equilíbrio químico com valores iguais a 1) e de supersaturação

(favorecendo a precipitação com valores maiores do que 1) são usualmente definidos por Ω (Ω_{ar} para a aragonita e Ω_{ca} para calcita). Dessa forma, uma vez que o oceano Austral apresenta uma baixa capacidade tamponante natural (i.e., TA e pH naturalmente baixos), é esperado que essa região seja a segunda a experimentar condições de subsaturação ($\Omega < 1$) em toda a coluna de água, depois do oceano Ártico. Essa condição é passível de ocorrer principalmente em relação à aragonita devido a sua maior instabilidade se comparado a calcita (Lauvset *et al.*, 2020; Sabine *et al.*, 2004; Tynan *et al.*, 2016). Isso se deve, segundo Orr *et al.* (2005), às tendências que mostram que a concentração do íon CO_3^{2-} no oceano em 2100 será aproximadamente 60% menor do que as atuais. Recentes estudos indicam que condições de subsaturação em algumas regiões da Antártica sejam atingidas já na década de 2030, como o mar de Ross e o oeste da Península Antártica (Lencina-Avila *et al.*, 2018; McNeil e Matear, 2008). A baixa concentração desse íon, então, pode alterar o funcionamento de ecossistemas antárticos através de danos aos organismos que desempenham funções ecológicas cruciais. Nesses, podem ser citados cocolitoforídeos em oceano aberto e briozoários, equinordermos e moluscos em ambiente costeiro com funções ecológicas como produção primária, formação de hábitats, fluxos de energia e ciclagem biogeoquímica (Acqua *et al.*, 2019; Figuerola *et al.*, 2020, 2021; Henley *et al.*, 2020).

Como ponto alarmante, algumas regiões ao redor do continente antártico são mais sensíveis do que outras quanto aos impactos das mudanças do clima. Conhecida como um *hotspot* climático, o entorno da Península Antártica é um exemplo de uma região com alta sensibilidade climática (Kerr, Mata, *et al.*, 2018). Nesta região já foram identificados incrementos da pCO_2 nas camadas

profundas no mar de Weddell, leste da península (Heuven, van *et al.*, 2014), aumento da capacidade de absorção de dióxido de carbono nos verões austrais desde 2012 no estreito de Gerlache, oeste da península (Monteiro *et al.*, 2020), área onde foi quantificada as concentrações de carbono antropogênico no verão de 2015 oriundas de processos advectivos de águas densas de plataforma do mar de Weddell (Kerr, Goyet, *et al.*, 2018) que apresenta uma tendência de aumento nos últimos 60 anos (Lencina-Avila *et al.*, 2018). Em relação as alterações de pH e Ω, praticamente todo o entorno da península demonstra padrões de redução desse parâmetro ao longo das últimas décadas (Hauck *et al.*, 2010; Lencina-Avila *et al.*, 2018). É interessante notar que reduções pH e Ω têm ocorrido mesmo em regiões associadas ao oeste da Península Antártica, principalmente abaixo da superfície (Jones *et al.*, 2017; Legge *et al.*, 2017). No caso do mar de Weddell, reduções de pH também foram identificadas e variaram entre 0,002 a 0,005 unidades de pH entre 1992 a 2008 devido às intrusões de carbono antropogênico (Hauck *et al.*, 2010). De um modo geral, áreas costeiras com alta propensão de captação de CO_2, como ocorre no entorno da Península Antártica (Jones *et al.*, 2017; Monteiro *et al.*, 2020), são associadas com impactos consideráveis na química do carbonato.

Contudo, uma região no extremo norte da península detém escassa quantidade de estudos sobre distribuições e alterações biogeoquímicas no sistema carbonato, o estreito de Bransfield. Até então, os estudos da temática na região se limitam a avaliações de apenas alguns meses de dados referente a uma única campanha amostral em uma pequena porção do estreito, como ocorreu com os dados gerados durante os cruzeiros FRUELA (Anadón e Estrada, 2002), ou um conjunto pequeno de anos de dados, embora com ampla cobertura espacial,

como os cruzeiros do Grupo de Oceanografia de Altas Latitudes (Ito *et al.*, 2018; Torres-Lasso, 2019). Recentemente, Orselli *et al.* (2022) avaliaram o estado da arte do ciclo do carbono inorgânico ao longo do norte da Península Antártica (do inglês, *northern Antarctic Peninsula*, NAP), incluindo avaliações sazonais, da compreensão da dinâmica do carbono antropogênico e alterações hidrográficas associadas, por exemplo, à interação entre modos de variabilidade climática e seus impactos na variação no sistema carbonato entre 2008 e 2020.

O estreito de Bransfield se torna um ambiente importante na caracterização de processos biogeoquímicos e suas mudanças diante das alterações do clima devido a duas características particulares. A primeira está associada à sua atuação como região de conexão entre o leste e o oeste da Península Antártica, promovendo interações entre os mares de Weddell e Bellingshausen, respectivamente. Enquanto o primeiro é caracterizado como uma região de formação de águas densas de plataforma, as quais apresentam altas salinidade e oxigênio dissolvido, mas temperaturas próximas ao ponto de congelamento da água do mar (Avelina *et al.*, 2020; Azaneu, Kerr e Mata, 2014; Damini *et al.*, 2022; Dotto *et al.*, 2016), o segundo é caracteristicamente associado à assinatura de águas relativamente mais quentes oriundas de intrusões de massas de água antigas (Huneke, Huhn e Schröeder, 2016; Sangrà *et al.*, 2011, 2017). A segunda característica peculiar do estreito é a sua capacidade de preservar alterações hidrográficas nas bacias profundas, as quais estão ocorrendo no entorno da península e são advectadas para o interior do estreito (Caspel, van *et al.*, 2018; Dotto *et al.*, 2016). Advindo principalmente das plataformas continentais no noroeste do mar de Weddell, as águas de plataforma preenchem as zonas profundas das bacias do estreito de Bransfield sem

apresentar grande mistura com as águas da região (Orselli *et al.*, 2022 e referências incluídas). Uma vez que ocorre a preservação das características hidrográficas, é possível que o estreito possa atuar como uma região sentinela das alterações biogeoquímicas, como das alterações na química do sistema carbonato ao longo da península.

Capítulo II: Objetivos

Diante da problemática acima levantada, essa dissertação tem como objetivo principal:

- Avaliar a variabilidade espaço-temporal dos parâmetros do sistema carbonato na região do estreito de Bransfield, no norte da Península Antártica.

Assim, esse objetivo se distingue nos seguintes objetivos específicos, que foram desenvolvidos ao longo dessa pesquisa:

- Avaliar as mudanças dos estados de acidificação e de saturação dos minerais de carbonato de cálcio ao longo do estreito de Bransfield;
- Caracterizar os principais processos responsáveis pela variabilidade dos parâmetros do sistema carbonato nas diferentes bacias do estreito.

Capítulo III:
Material e Métodos

III.1. Obtenção dos dados

Dados hidrográficos do verão austral (janeiro, fevereiro e março) para a região do estreito de Bransfield foram acessados em diferentes bancos de dados oceanográficos disponíveis e de livre acesso. Apenas dados de garrafa e CDT foram utilizados. Os dados de temperatura [°C], salinidade prática (S) e oxigênio dissolvido (O_2) [µmol kg^{-1}] foram acessados dos bancos de dados do *World Ocean Database 2018* (WOD18) (https://www.nodc.noaa.gov/OC5/WOD/wod18-notes.html) (Boyer *et al.*, 2018), e do Grupo de Oceanografia de Altas Latitudes (GOAL) (Dotto *et al.*, 2021; Mata, Tavano e Garcia, 2018). O conjunto de dados totalizou uma série temporal de trinta anos (i.e., de 1990 a 2019), não necessariamente consecutivos, e sua

distribuição espacial está ilustrada na Figura III.1. Junto aos dados hidrográficos, dados de TA e CT também foram acessados. Estes estavam disponíveis nos anos de 1996, 2006, 2010 e entre 2015 e 2019. Para os dados de 1996, TA foi determinada através de titulação potenciométrica automática com o uso de ácido clorídrico, enquanto o CT foi estimado através de dados de pH a 15°C e TA a partir do uso de equações termodinâmicas próprias do sistema carbonato (Alvarez, Aida e Ros, 2002). Para os dados do GOAL, TA e CT foram medidos simultaneamente por titulação potenciométrica em cela fechada com o uso de um titulador automático (Kerr, Orselli, *et al.*, 2018). Os dados referentes aos cruzeiros do GOAL (projeto *NAUTILUS*) foram corrigidos e submetidos a um controle de qualidade padrão, determinando dados de boa qualidade (*flag*) e de *offsets* (Boyer *et al.*, 2018; Dotto *et al.*, 2016). Ambas as análises foram realiza-

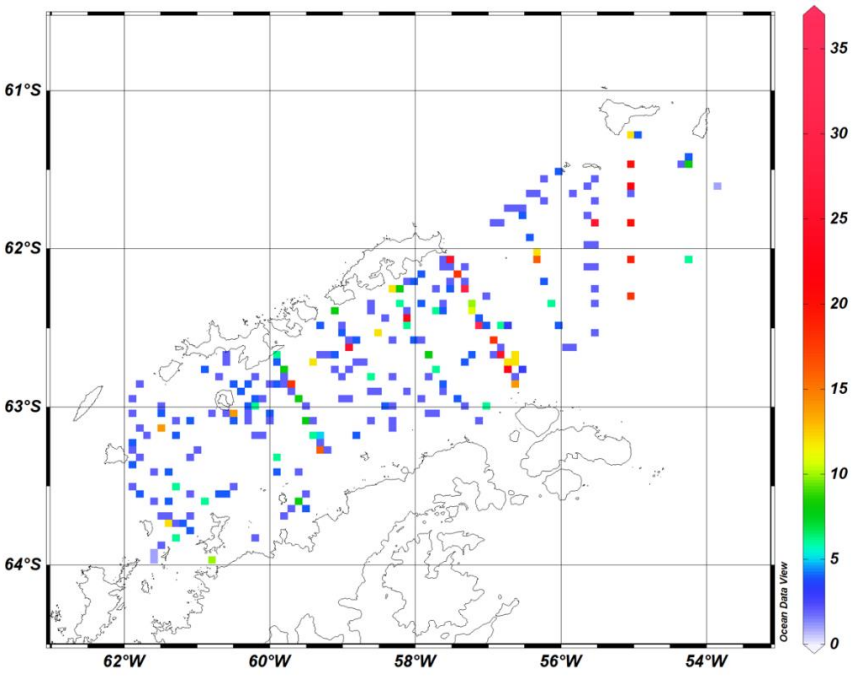

Figura III.1. Distribuição espacial e quantidade de estações oceanográficas utilizadas no desenvolvimento desse estudo.

das principalmente no *software* livre *Ocean Data View*®, onde somente dados com *flag* 0 ou 1 (i.e., dados bons ou de boa qualidade, respectivamente) foram

mantidos enquanto dados considerados espúrios foram excluídos antes de qualquer outra análise. A acurácia dos dados hidrográficos é de 0,001 – 0,005 °C e de 0,003 – 0,02 para os oriundos do *WOD18* (Boyer *et al.*, 2018) e de aproximadamente ~0,001 °C e ~0,003 para os oriundos do GOAL (Dotto *et al.*, 2021) para temperatura e salinidade, respectivamente. Já a precisão média para os dados de TA foi de 3,2 ± 1,3 μmol kg^{-1}, enquanto para CT, foi de 4,0 ± 0,8 μmol kg^{-1}. Os dados anuais de precisão de TA e CT dos bancos de dados acessados são apresentados na Tabela III.1.

Tabela III.1. Precisão dos dados de TA e CT por ano disponíveis nos bancos de dados WOD18 e GOAL. Dados de precisões não disponibilizados nos respetivos bancos de dados referentes a cada ano estão assinalados por ND.

Ano **Parâmetro**	**1996**	**2006**	**2010**	**2015**	**2016**	**2017**	**2018**	**2019**
TA μmol kg^{-1}	1,4 Alvarez et al., 2002	ND	ND	3,0 Kerr et al., 2018	3,4	2,8	5,5	2,9
					LEOC/GOAL			
CT μmol kg^{-1}	4,0 Alvarez et al., 2002	ND	ND	5,0 Kerr et al., 2018	4,4	2,9	3,4	4,5
					LEOC/GOAL			

III.2. Controle de qualidade dos dados do WOD18 e GOAL

Brevemente, os dados foram classificados de acordo com diferentes valores de *flags*, os quais os caracterizam como bons (*flag* = 0 e *flag* = 1), de qualidade baixa ou questionável (*flag* = 4) ou ruins (*flag* = 8, Boyer *et al.*, 2018). Por outro lado, a determinação de *offset* visou identificar amostras cujos valores medidos não condiziam com valores esperados. Para isso, dados espúrios foram caracterizados como dados que apresentaram valores maiores ou menores que

duas vezes o desvio padrão relativo à média do perfil vertical de cada estação. Assim, todos os perfis foram avaliados individualmente e os dados com *flag* maior ou igual a 4 e classificados como *offset* foram excluídos.

III.3. Estimativa de variáveis derivadas

A temperatura potencial (θ) [°C] e densidade neutra (γ^n) [kg m^{-3}] foram calculadas a partir de rotinas pré-estabelecidas no *software Ocean Data View*®. Para isso, foi utilizada a convenção baseada na "*Thermodynamic Equation of SeaWater 2010*" (Intergovernmental Oceanographic Commission, Scientific Committee on Oceanic Research e International Association for the Physical Sciences of the Oceans, 2010). A pressão de referência requerida para os cálculos de variáveis derivadas, como ocorreu para a γ^n, foi estabelecida como a pressão na superfície do oceano (i.e., 0 dbar).

III.4. Setorização da área de estudo

Para melhor caracterizar a região, o estreito de Bransfield foi dividido em três bacias: oeste, central e leste. Os limites associados à essa divisão foram determinados a partir de estruturas de *sills* que delimitam contornos batimétricos inferiores a 1000 m de profundidade (Clowes, 1934). As distinções em diferentes bacias auxiliaram na melhor descrição dos processos ocorrendo ao longo do estreito, já que o mesmo apresenta alta variabilidade de mistura de distintas massas de água (Sangrà *et al.*, 2011, 2017). Além disso, verticalmente, a coluna de água foi separada em três camadas com base nos valores de γ^n. Essas

camadas foram definidas como superfície ($\gamma^n \leq 28.00$ kg m^{-3}), intermediária (28.00 kg $m^{-3} < \gamma^n < 28.27$ kg m^{-3}) e profunda ($\gamma^n \geq 28.27$ kg m^{-3}).

III.5. Reconstrução dos parâmetros do sistema carbonato

O conjunto de dados do *WOD18* (1996, 2006 e 2010) e do GOAL (2015 a 2019) que apresentaram medidas de campo para TA e CT, juntamente com suas respectivas medidas de S, θ e O_2, foi utilizado na determinação de equações de reconstrução aplicáveis ao estreito de Bransfield. Essas equações lineares multivariadas seguiram o modelo:

$$TA\ (\theta\ [°C], S);\ CT\ (\theta\ [°C], S, O_2\ [\mu mol\ kg^{-1}]) \qquad \text{Eq. 1}$$

Para isso, esse conjunto de dados foi distinguido em dois grupos, o primeiro associado a desenvolver equações de reconstrução, enquanto o segundo foi utilizado para validar os dados modelados. O conjunto de reconstrução considerou diferentes composições de anos e entre os parâmetros de entrada, buscando identificar a melhor combinação de entrada de dados que gerassem a melhor equação de reconstrução. No total, três configurações de equações foram testadas:

1. *Set01*: equações mais restritas, aplicáveis a cada camada (i.e., superfície, intermediária e profunda) de cada bacia (i.e., oeste, central e leste) do estreito de Bransfield. No total, esse conjunto produziu oito equações para TA e outras oito para CT. Somente a camada profunda da bacia oeste não foi testada devido ao seu baixo número de dados que, portanto, não garantiram robustez das estimativas aqui realizadas;

2. *Set02*: equações mais gerais, aplicáveis a cada camada (i.e., superfície, intermediária e profunda) de todo o estreito. No total, esse conjunto produziu três equações para TA e outras três para CT. Esse *set* utilizou combinações de certos anos de dados como entrada para o desenvolvimento das equações;
3. *Set03*: equações também mais gerais, aplicáveis a cada camada (i.e., superfície, intermediária e profunda) de todo o estreito com um total de três equações tanto para TA quanto para CT. A diferença referente ao *set02* decorreu dos dados de entrada, os quais foram utilizados em combinações randômicas.

O melhor *set* de equações para cada conjunto acima descrito foi primariamente avaliado através dos melhores ajustes entre os dados para validação e os modelados. As equações com melhores validações foram então avaliadas através das melhores correlações, os menores erros quadráticos médios, (do inglês, *Root Mean Square Error*, RMSE), maiores significâncias estatísticas e melhores F de significação (i.e., um indicativo de quão bem representados por equações lineares esses dados reconstruídos são). A partir da intercomparação dos *sets* desenvolvidos com os dados oriundos das bases de dados do *WOD18* e GOAL, o *set* com melhor caracterização dos dados observados *in situ* foi o *set*03 (Figura III.2). O conjunto de equações de reconstrução aqui identificado como *set*03 está descrito na Tabela III.2. Verificando a robustez do *set*03, foi realizada uma intercomparação com outros conjuntos de equações de reconstrução de TA e CT baseados nas relações expressas na Eq. 1 para regiões oceânicas mais amplas, como os oceanos Austral (Lee *et al.*, 2006; Millero, Lee e Roche, 1998; Takahashi *et al.*, 2014) e Ártico (Arrigo *et al.*, 2010),

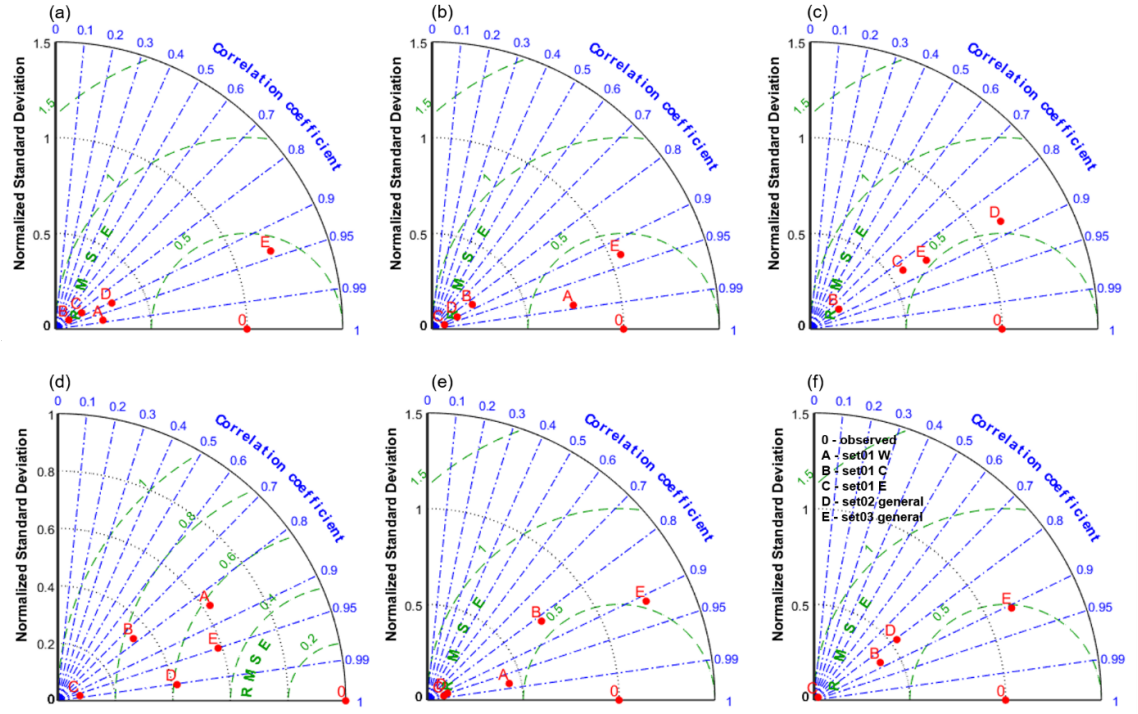

Figura III.2. Diagrama de Taylor apresentando a intercomparação dos diferentes *sets* de equações geradas nesse estudo para (a, b e c) alcalinidade total – TA e (d, e e f) carbono inorgânico total – CT. As avaliações consideraram *sets* de equações aplicáveis à camada (a e d) superficial, (b e e) intermediária e (c e f) profunda. Os dados observados são assinalados por 0; o *set*01 está assinalados por A, B e C, representando os *sets* aplicáveis às bacias oeste, central e leste, respectivamente; o *set*02 está assinalado pela letra D; e o *set*03, pela letra E.

além de equações mais locais no entorno da Península Antártica (Hauri *et al.*, 2015; Lencina-Avila *et al.*, 2018; Monteiro *et al.*, 2020; Monteiro, Kerr e Machado, 2020). Monteiro, Kerr e Machado (2020) é aqui identificado como Monteiro *et al.* (2020a) enquanto Monteiro *et al.* (2020), Monteiro *et al.* (2020b). Assumindo que a coluna de água é bem mistura, as equações aplicáveis à camada superficial de todos os estudos foram aplicadas ao longo da coluna de água do estreito de Bransfield. Verticalmente, Lencina-Avila *et al.* (2018) apresentam dois *sets* de equações ao longo da coluna de água: o primeiro para a camada de mistura e o segundo para a camada abaixo da camada de mistura. Assumindo que as cama-

Tabela III.2. Conjunto de equações que compõem o *set*03 desenvolvido neste estudo e identificado como mais robusto para reconstruir os dados de TA e CT no estreito de Bransfield. As equações são apresentadas por camada definida por densidade neutra (γ^n). Dados estatísticos relacionados à cada equação são apresentados, como o coeficiente de correlação (*r)*, o erro quadrático médio (do inglês, *root mean square error*, RMSE), número de amostras usadas para desenvolver cada equação (*n*), o valor *p* (*p*) e o valor F de significância (uma expressão de quanto esses dados são bem representados através de equações lineares; altos valores de F indicam alta representatividade dos dados através de equações multivariadas lineares). Os acrônimos utilizados são γ^n – densidade neutra, TA – alcalinidade total, CT – carbono inorgânico total, θ – temperatura potencial, S – salinidade prática e O_2 – oxigênio dissolvido.

Camada	TA	CT
Superfície $\gamma^n \leq$ 28,0 kg m^{-3}	TA = –31,9*θ –54,5*S +4236 *r* = 0,93 RMSE = 6,35 µmol kg^{-1} *n* = 72; *p* < 0,01 F = 247,7	CT = –29,3*θ –26,1*S –0,57*O_2 +3311,5 *r* = 0,95 RMSE = 8,92 µmol kg^{-1} *n* = 49; *p* < 0,01 F = 139,2
Intermediária 28,0 kg m^{-3} < γ^n < 28,27 kg m^{-3}	TA = –57,1* θ +143,6*S –2652,3 *r* = 0,93 RMSE = 6,35 µmol kg^{-1} *n* = 41; *p* < 0,01 F = 115,0	CT = –0,73*θ +61,2*S +1,86*O_2 –352,1 *r* = 0,91 RMSE = 8,99 µmol kg^{-1} *n* = 37; *p* < 0,01 F = 53,8
Profunda $\gamma^n \geq$ 28,27 kg m^{-3}	TA = 59,7*θ –126,2*S +6805,3 *r* = 0,86 RMSE = 6,22 µmol kg^{-1} *n* = 49; *p* < 0,01 F = 63,1	CT = 135,9*θ +797,8*S +3,2*O_2 –26019,9 *r* = 0,91 RMSE = 9,63 µmol kg^{-1} *n* = 30; *p* <0,01 F = 39,86

das intermediária e superficial do estreito de Bransfield são bem misturadas, o *set* de equações aplicáveis à camada de mistura de Lencina-Avila *et al.* (2018) foi utilizado para camadas superiores do estreito de Bransfield. O mesmo estudo distingue sua área de estudo em sul e norte. Aqui, as equações ao sul da área de estudo de Lencina-Avila *et al.* (2018) são definidas como *set*01; a área ao norte, *set*02. Nesse caso, as intercomparações de equações de outros estudos com o melhor *set* desenvolvido nesse estudo são apresentados para TA (Figura III.3) e CT (Figura III.4). O conjunto de equações para cada estudo utilizados nessa intercomparação está descrito na Tabela III.3.

Em ambas as intercomparações, embora todas as equações utilizadas apresentam uma boa correlação e baixo desvio padrão, o RMSE do *set*03 deste estudo é mais equiparável ao erro observado, fazendo deste *set* de equações o

Tabela III.3. Equações de reconstrução para TA e CT utilizadas na intercomparação de diferentes autores aplicáveis a distintas regiões oceânicas. As equações mencionadas sequem as relações expressas pela Eq. 1. Cada equação segue acompanhada dos valores de seus respectivos RMSE (µmol kg^{-1}), a área para a qual a equação foi desenvolvida e sua referência bibliográfica.

Equação		**RMSE**	**Área oceânica**	**Referência**
TA	**CT**			
$2305 + 52{,}48 \times (S - 35) + 2{,}85 \times (S - 35)^2 - 0{,}49 \times (\theta - 20) + 0{,}086 \times (\theta - 20)^2$		8,4	Oceano Austral	(Lee *et al.*, 2006)
$2291 - 2{,}52 \times (\theta - 20) + 0{,}056 \times (\theta - 20)^2$		5,0	Oceano Austral	(Millero, Lee e Roche, 1998)*
$74{,}13 \times S - 192{,}2$		9,1	Oceano Austral	(Takahashi *et al.*, 2014)
$57{,}01 \times S + 373{,}86$		15,2	Oeste da Península Antártica	(Hauri *et al.*, 2015)
$-22 \times S^2 + 1564 \times S - 25027$** $66 \times S + 72$***	$-31 \times \theta - 1 \times O_2 + 15 \times S + 1923$** $-28 \times \theta - 1 \times O_2 + 55 \times S + 587$***	1,0; 2,0** 2,0; 3,0***	Oeste da Península Antártica	(Lencina-Avila *et al.*, 2018) *set*01****
$49 \times S + 661$** $76 \times S^2 - 5162 \times S + 90042$***	$-20 \times \theta - 1 \times O_2 - 36 \times S + 3751$** $-1 \times \theta - 0{,}2 \times O_2 + 48 * S + 634$***	4,0; 1,0** 8,0; 1,0***	Oeste da Península Antártica	(Lencina-Avila *et al.*, 2018) *set*02****
$36{,}72 \times S + 1052$		4,4	Oeste da Península Antártica	(Monteiro, Kerr e Machado, 2020)****
$685{,}34 + 3{,}85 \times \theta + 47{,}91 \times S$		16,8	Oeste da Península Antártica	(Monteiro *et al.*, 2020)****
$200{,}13 + 4{,}42 \times \theta + 63{,}06 \times S$		26,9	Oceano Ártico	(Arrigo *et al.*, 2010)*

* Aplicável ao setor Atlântico.

**Aplicável à camada de mistura.

***Aplicável à camada abaixo da camada de mistura.

****Equações desenvolvidas para o estreito de Gerlache.

mais apropriado para reconstruir os demais parâmetros do sistema carbonato no estreito de Bransfield. Assim, O *set*03 com melhor resultado foi aplicado na reconstrução de TA e CT através do uso dos dados hidrográficos entre 1990 e 2019 nas amostras nas quais ambos os parâmetros não foram medidos *in situ*. Com os dados da série reconstruídos, TA, CT e seus respectivos parâmetros hidrográficos foram, então, utilizados como dados de entrada para o *software* CO2Sys v2.1 (Lewis e Wallace, 1998) para a determinação dos parâmetros pCO_2, pH, estados de saturação da aragonita e da calcita e do fator Revelle. Pa-

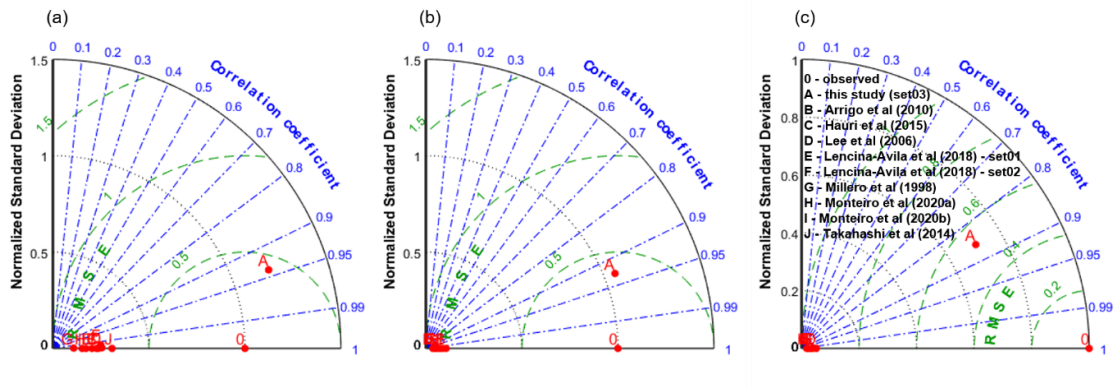

Figura III.3. Diagrama de Taylor apresentando a intercomparação de diferentes equações desenvolvidas por outros autores e do *set*03 deste estudo, identificada como a melhor aqui desenvolvidas, para alcalinidade total – TA na camada (a) superficial, (b) intermediária e (c) profunda.

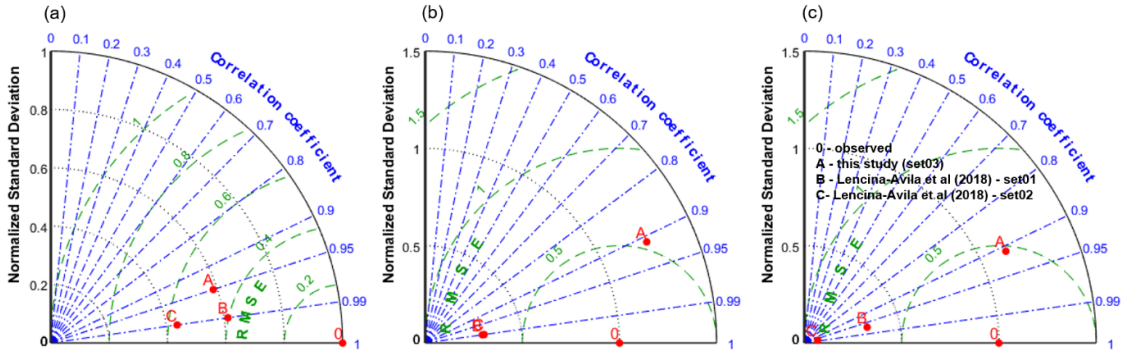

Figura III.4. Diagrama de Taylor apresentando a intercomparação de diferentes equações desenvolvidas por outros autores e do *set*03 deste estudo, identificada como a melhor aqui desenvolvidas, para carbono inorgânico total – CT na camada (a) superficial, (b) intermediária e (c) profunda.

ra isso, as constantes de dissociação do ácido carbônico (K1, na dissociação para o íon bicarbonato, e K2, na dissociação para o íon carbonato) de Goyet e Poisson (1989), além das constantes do sulfato (Dickson, 1990) e do borato total (Uppström, 1974), foram utilizadas. Em particular, as constantes do ácido carbônico aqui empregadas apresentam boas respostas para ambientes polares, como já verificado anteriormente na literatura (Kerr, Goyet, *et al.*, 2018; Laika *et al.*, 2009; Lencina-Avila *et al.*, 2018; Wanninkhof *et al.*, 1999).

III.6. Controle de qualidade das reconstruções via o CO2Sys

Duas abordagens foram aplicadas para verificar a robustez da reconstrução, além da validação acima citada. A primeira foi o teste de sensibilidade (Figura III.5). Esse teste visou identificar qual o impacto do uso de diferentes constantes de dissociação do ácido carbônico nos resultados reconstruídos através do CO2Sys. Para isso, foi realizado uma subtração entre os dados obtidos das reconstruções a partir das demais constantes em relação às constantes de Goyet e Poisson (1989). A nível de comparação, conjuntos de constantes do ácido carbônico com aplicações em ambientes oceânicos foram empregadas. São elas: Dickson e Millero (1987); Hansson (1973); Lueker, Dickson e Keeling (2000); Mehrbach *et al.* (1973); Millero *et al.* (2002, 2006); e Roy *et al.* (1993). A segunda abordagem foi baseada no uso de uma rotina de propagação de incertezas a partir do *software* do CO2Sys (Orr *et al.*, 2018). As incertezas são apresentadas na Tabela III.4. Uma vez que Orr *et al.* (2018) não propaga erro para pH, os dados de erro propagado para os prótons livres de hidrogênio também são apresentados como um *proxy*.

Figura III.5. Resultado do teste de sensibilidade comparando os resultados da reconstrução dos parâmetros do sistema carbonato pelas constantes de dissociação do ácido carbônico de Goyet & Poisson (1989) e outras constantes de aplicações a ambientes oceânicos. Os dados de pH_{sws} (unidades de pH), pCO_2 (µatm), Ω_{ar} (unidades de estado de saturação) e Ω_{ca} (unidades de estado de saturação) ao longo das bacias (a, b, c) oeste, (d, e, f) central e (g, h, i) leste nas camadas de (a, d, g) superfície, (b, e, h) intermediária e (c, f, i) profunda.

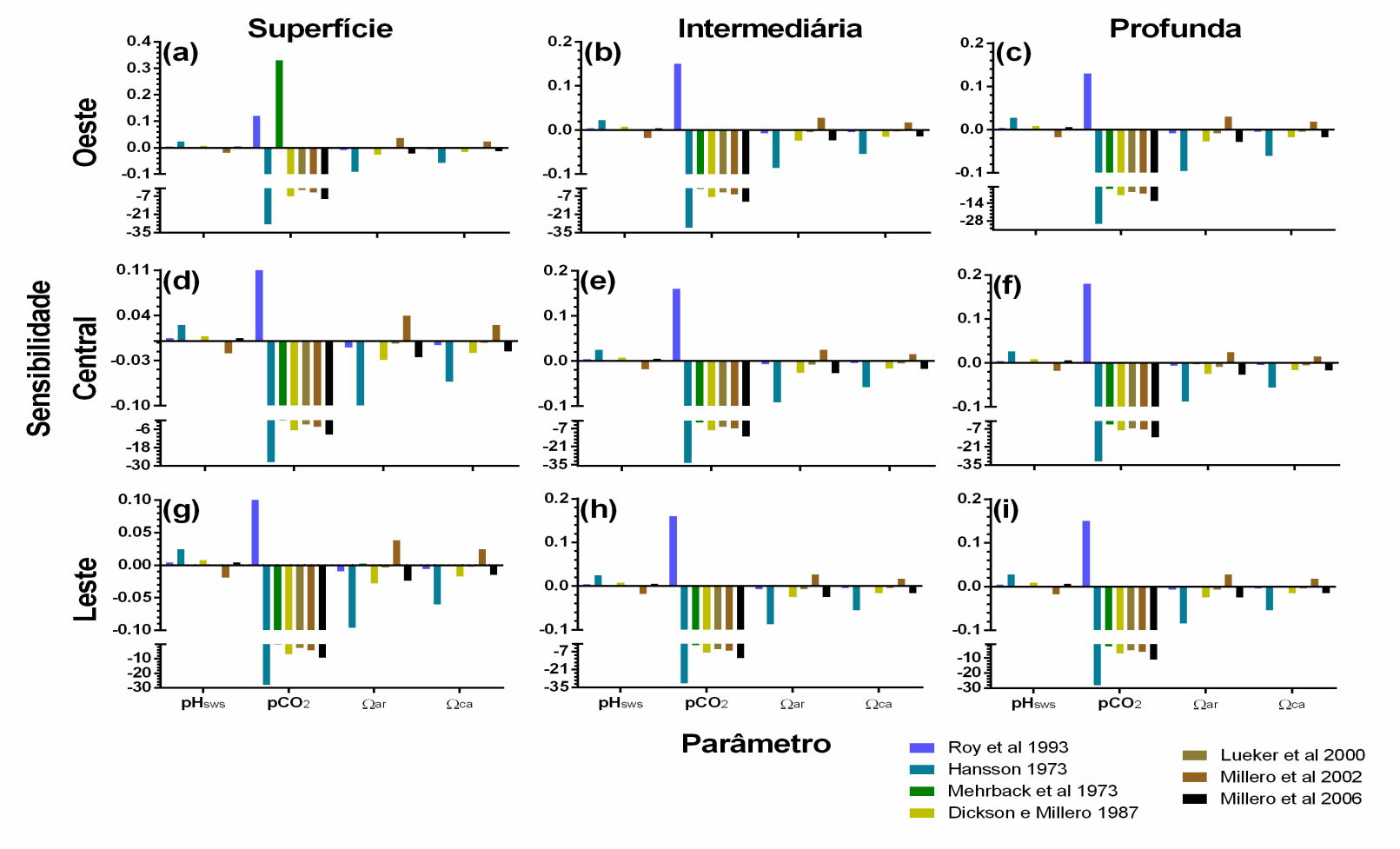

Tabela III.4. Erros propagados dos dados de saída do *software* CO2Sys de acordo com as descrições e rotinas estabelecidas em Orr et al 2018 para as bacias (a) oeste, (b) central e (c) leste. Essa rotina não propaga erro para pH, logo, a concentração dos prótons livres de hidrogênio é apresentada abaixo.

(a) Bacia oeste

Parâmetro	Superfície	Intermediária	Profunda
pCO_2 (µatm)	91,3 ± 22,0	14,1 ± 4,6	100,4 ± 26,5
$[H^+]$ (nmol kg^{-1})	1,56 ± 0,40	0,24 ± 0,08	1,71 ± 0,44
Ω_{ca}	0,136 ± 0,014	0,016 ± 0,002	0,143 ± 0,012
Ω_{ar}	0,085 ± 0,008	0,010 ± 0,001	0,090 ± 0,008

(b) Bacia central

Parâmetro	Superfície	Intermediária	Profunda
pCO_2 (µatm)	79.7 ± 12.1	14.7 ± 3.9	115.0 ± 39.3
$[H^+]$ (nmol kg^{-1})	1.36 ± 0.20	0.25 ± 0.07	1.97 ± 0.67
Ω_{ca}	0.140 ± 0.005	0.056 ± 0.002	0.124 ± 0.020
Ω_{ar}	0.090 ± 0.005	0.001 ± 0.001	0.079 ± 0.013

(c) Bacia leste

Parâmetro	Superfície	Intermediária	Profunda
pCO_2 (µatm)	83.5 ± 12.2	13.2 ± 2.8	91.9 ± 25.6
$[H^+]$ (nmol kg^{-1})	1.42 ± 0.20	0.23 ± 0.05	1.57 ± 0.43
Ω_{ca}	0.141 ± 0.008	0.015 ± 0.002	0.124 ± 0.015
Ω_{ar}	0.088 ± 0.005	0.010 ± 0.001	0.079 ± 0.010

III.7. Variabilidade temporal dos parâmetros do sistema carbonato no estreito de Bransfield

Duas distinções temporais foram tomadas para a avaliação da variabilidade dos parâmetros do sistema carbonato no estreito de Bransfield. A primeira foi baseada na escala interanual e a segunda, decenal. A variabilidade interanual foi avaliada através das anomalias dos parâmetros do sistema carbonato determinadas pela diferença entre a média anual e a média ao longo da década de 2010 para cada parâmetro

avaliado. A década de 2010 foi utilizada como referência pois é a década que apresenta uma maior cobertura temporal ao longo da série temporal, apenas com ausência de dados no ano de 2012. A partir das anomalias, as tendências (± limites de confiança) de longo prazo foram estimadas. Essas tendências foram significativas quando a tendência foi maior do que o limite de confiança, o que implica em um nível de confiança de 95% ($p < 0,05$).

A variabilidade decenal foi avaliada através dos perfis verticais dos parâmetros do sistema carbonato ao longo das três décadas aqui avaliadas (i.e., 1990s, 2000s e 2010s). Assim, a média a cada 50 m de profundidade ao longo de cada bacia por década foi calculada, permitindo a avaliação dos padrões de distribuição ao longo do tempo e entre as bacias. Cada nível de profundidade foi, então, comparado estatisticamente através de um teste de Mann-Whitney. O nível de significância de 95% de intervalo de confiança (i.e., $p < 0,05$) foi aqui considerado.

Uma vez que os modos de variabilidade climática do ENSO e SAM, suas distintas fases e interações acopladas alteram a hidrografia da região, uma análise de composição foi realizada para caracterizar os seus efeitos na distribuição dos parâmetros do sistema carbonato no estreito de Bransfield. Dados dos índices de ambos os modos de variabilidade climática foram considerados para o verão austral de acordo com os dados disponibilizados em https://origin.cpc.ncep.noaa.gov/products/analysis_monitoring/ensostuff/ONI_v5.php para o ENSO e http://www.nerc-bas.ac.uk/icd/gjma/sam.html para o SAM. No caso do ENSO, os dados acessados foram do Índice Niño Oceânico. Para determinar cada composição, limiares dos índices foram utilizados: índices abaixo de -0,5 foram caracterizados como fases negativas; índices acima de 0,5 foram caracterizados

como fases positivas; valores de índices entre -0,5 e 0,5 foram caracterizados como eventos neutros. O número de anos para cada fase de cada modo de variabilidade climática ao longo do estreito de Bransfield é apresentada na Figura III.6. Composições singulares (i.e., considerando cada fase específica de cada modo de forma isolada, sendo elas o ENSO e o SAM em fases neutra, positiva e negativa) e compostas (i.e., considerando combinações de fases de ambos os modos, sendo elas

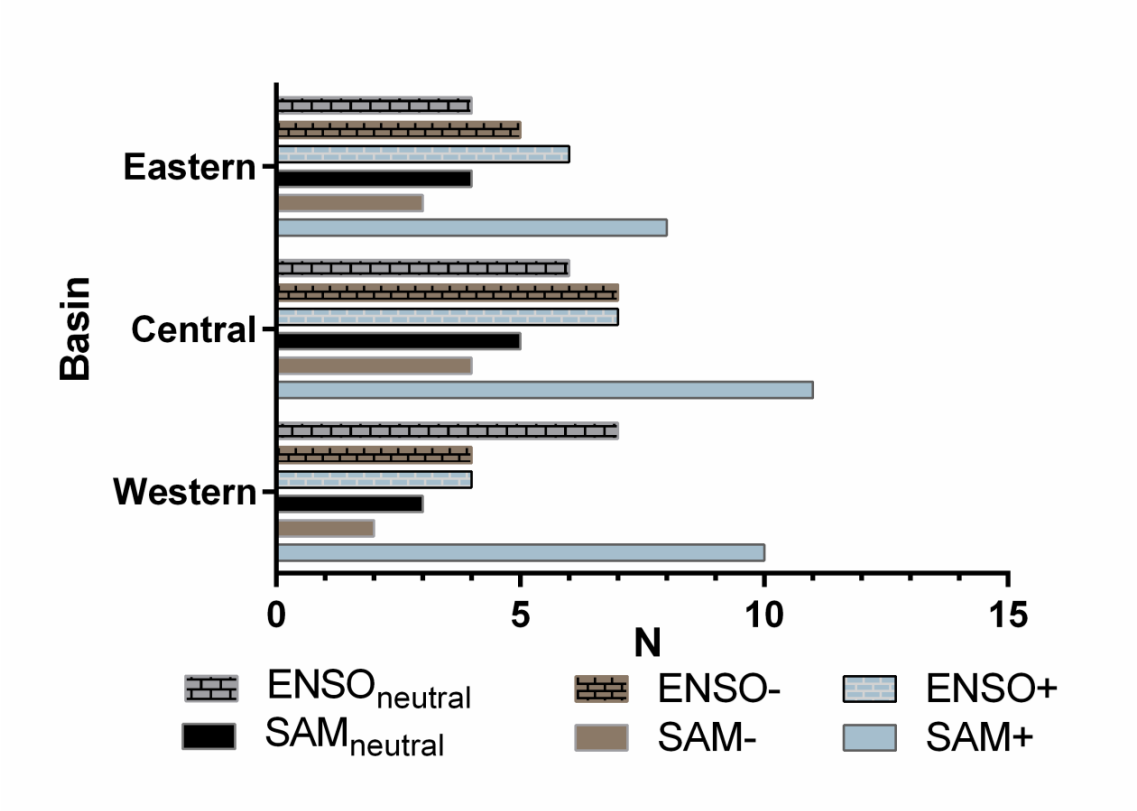

Figura III.6. Número de anos utilizados para a caracterização de cada fase dos modos de variabilidade climática do ENSO e SAM. A quantidade de anos das composições é baseada na mesma distribuição temporal de dados dos parâmetros do sistema carbonato reconstruídos.

ENSO e SAM em fase neutra, ENSO e SAM em fase positiva, e das fases opostas entre ambos) foram identificadas e suas médias foram calculadas a cada 50 m de profundidade ao longo dos perfis verticais referentes a cada composição. As suas

diferenças foram verificadas estatisticamente através do teste de Mann-Whitney para cada intervalo de profundidade e com um nível de significância de 95% ($p < 0,05$).

Capítulo IV:
Artigo Científico

Este capítulo apresenta o artigo científico que está em revisão na revista científica *Global Biogeochemical Cycles* seguindo a própria formatação criada pela *American Geophysical Union*.

Drivers of Marine CO_2-Carbonate Chemistry in the Northern Antarctic Peninsula

Maurício Santos-Andrade[1,2], Rodrigo Kerr[1,2], Iole B. M. Orselli[1,2], Thiago Monteiro[1,2], Mauricio M. Mata[1,2], and Catherine Goyet[3,4]

[1]Laboratório de Estudos dos Oceanos e Clima, Instituto de Oceanografia, Universidade Federal do Rio Grande – FURG, Rio Grande, RS, 96203-900, Brazil.

[2]Programa de Pós-Graduação em Oceanologia, Instituto de Oceanografia, Universidade Federal do Rio Grande – FURG, Rio Grande, RS, 96203-900, Brazil.

[3]IMAGES_ESPACE-DEV, Université de Perpignan Via Domitia, 52 ave. Paul Alduy, 66860 Cedex Perpignan, France.

[4]ESPACE-DEV UMR UG UA UM IRD, Maison de la télédétection, 500 rue Jean-François Breton, 34093 Montpellier Cedex 5, France.

Corresponding authors: Mauricio Santos-Andrade (mauriciosa@furg.br) and Rodrigo Kerr (rodrigokerr@furg.br)

Key Points:

- Carbonate chemistry in the Bransfield Strait responds to modes of climate variability.
- Source water masses intruding the region modulate carbonate system variability and influence CO_2 saturation.

- The western basin of the Bransfield Strait reveals steeper pH decrease than surrounding areas.

IV.1. Abstract

The Bransfield Strait is a climate change hotspot at the tip of the northern Antarctic Peninsula. The region is marked by a mixture of relatively warm waters from the Bellingshausen Sea with cold shelf waters from the Weddell Sea. Additionally, its deep central basin (>800 m) preserves seawater properties from the north-western Weddell Sea continental shelf. This study assessed long-term changes in carbonate chemistry in the Bransfield Strait and found that the hydrographic setting (i.e., a mixture between modified-Circumpolar Deep Water with Dense Shelf Water – DSW) drives temporal variability of carbonate parameters. Over the last three decades (1996 – 2019), the western basin presented pH_{sws} decreases varying from -0.003 to -0.017 pH_{sws} units yr^{-1}, while Ω decreased from -0.010 to -0.070 yr^{-1} throughout the water column. The central basin was characterized by a high contribution of DSW, responding to high concentrations of carbon dioxide (CO_2) dissolution and the decomposition of organic matter produced and transported into its deep layer. With smoother levels of variability for all carbonate system parameters, the eastern basin was likely regulated by internal mixing. The high contribution of DSW may swiftly lead to CO_2 saturation threshold as identified in the central basin relative to the western side of the Strait. Therefore, the Bransfield Strait does act as a sentinel for chemical changes experienced around the Antarctic Peninsula, which may play an important role in assimilating any temporal changes in the carbon system in the Southern Ocean.

IV.2. Plain Language Summary

Although the entire world is experiencing the impacts of climate change, some regions may experience them faster, such as the northern Antarctic Peninsula. At the northern tip of this area is the Bransfield Strait, which can act as a sentinel for identifying what is happening around the area during current climate change. Areas from the strait connected to the open ocean showed a rapid increase in acidification over time than areas mainly influenced by coastal zones. This occurs because most-connected areas to the open ocean experience the effects of old and deep-water masses governed by natural processes such as the decomposition of organic particles from the ocean around Antarctica. Conversely, coastal zones are much more influenced by the atmospheric carbon dioxide from human activities. The impact of these higher acidification trends in some parts of the northern Antarctic Peninsula may draw our attention to the effects of climate change on ocean acidification and its biological and chemical impacts on the ocean. Moreover, there are many areas, such as the Bransfield Strait, with scarce studies about these effects, delaying the identification of severe impacts even after changes have already been experienced, as was found in our assessment.

IV.3. Introduction

The Southern Ocean is expected to be the next oceanic region, after the Arctic Ocean, to experience a subsaturated aragonite condition throughout the water column in the next few decades (Henley *et al.*, 2020; Orr *et al.*, 2005). Moreover, many other climate-driven impacts have been registered around the Antarctic continent, including: (i) increase in atmospheric and ocean surface temperatures (Cook *et al.*, 2005; Meredith

e King, 2005; Siegert *et al.*, 2019); (ii) intensification of westerly winds related to modes of climate variability and their impacts surrounding Antarctica (Turner *et al.*, 2007); and (iii) glacial retraction and changes in the concentration, duration, and extension of sea ice (Cook *et al.*, 2016; Rignot *et al.*, 2019). Concomitantly, hydrographic and biogeochemical changes in ocean water masses are taking place around Antarctica, such as freshening trends (Azaneu *et al.*, 2013; Dotto *et al.*, 2016; Haumann *et al.*, 2016; Hellmer *et al.*, 2011), increased frequency of Circumpolar Deep Water (CDW) intrusions into coastal environments (Henley *et al.*, 2019; Moffat e Meredith, 2018), and pH reduction over different time scales (McNeil e Matear, 2008; Midorikawa *et al.*, 2012; Roden *et al.*, 2013; Sabine *et al.*, 2008). These changes are already impacting and reflecting on changes in the behavior of Southern Ocean ecosystems, which impact ocean health for the development of the sensitive Antarctic biota (Figuerola *et al.*, 2020, 2021; Henley *et al.*, 2020).

In this sense, Southern Ocean coastal zones, such as the northern Antarctic Peninsula (NAP; Kerr, Mata, et al., 2018), are more sensitive to climate change effects. The surrounding waters of NAP have experienced (i) an increase in partial pressure of carbon dioxide (CO_2, pCO_2) in the deep waters, as observed in the Weddell Sea (Heuven, van *et al.*, 2014); (ii) glacier retraction and sea ice thickness changes over the last decades, such as for the Larsen ice shelves (Cook *et al.*, 2005, 2016; Dinniman, Klinck e Hofmann, 2012; Dinniman, Klinck e Smith, 2011); and (iii) impacts of modes of climate variability altering hydrographic patterns in the region, such as the frequency and intensity of water masses coming from open ocean regions (Ruiz Barlett *et al.*, 2018). Other biogeochemical impacts have been highlighted around NAP such as the anthropogenic carbon observed in recently ventilated waters (Kerr, Goyet, *et*

al., 2018) and its effect on decreasing pH along NAP (Lencina-Avila *et al.*, 2018), in addition to increasing CO_2 uptake during the summer since 2012 in coastal zones (Monteiro *et al.*, 2020). Even with many efforts to comprehend the carbonate system along NAP over recent decades (Orselli et al., 2022 and references there in), the Bransfield Strait remains a subregion with relatively few studies when compared to the southern regions of the western Antarctic Peninsula (Kerr, Goyet, *et al.*, 2018; Kerr, Orselli, *et al.*, 2018; Legge *et al.*, 2017; Lencina-Avila *et al.*, 2018; Monteiro *et al.*, 2020; Monteiro, Kerr e Machado, 2020; Rivaro *et al.*, 2014; Sandrini *et al.*, 2007). Current knowledge regarding the carbonate system in the Bransfield Strait is limited to regional (e.g., the FRUELA cruise in 1996 in the western basin of the Bransfield Strait) and temporal (either only one year of summer data or short-time series) assessments (e.g., Anadón & Estrada, 2002; Ito et al., 2018). Besides acting as a transitional environment between polar and sub-polar domains, the NAP region interconnects the warm and old intermediate waters derived from the Bellingshausen Sea with the cold and young waters sourced in the Weddell Sea continental shelf (Caspel, van, Hellmer e Mata, 2018; Ruiz Barlett *et al.*, 2018). In addition, the Bransfield Strait is considered a sentinel to understanding hydrographic and biogeochemical processes occurring in the surroundings, since its deep layers preserve the seawater properties of the Weddell Sea shelf water masses (Azaneu *et al.*, 2013; Gordon *et al.*, 2000; Hofmann *et al.*, 1996).

Thus, considering the key role of the Bransfield Strait in NAP, we evaluated the spatial and temporal variability of carbonate system parameters (i.e., total alkalinity – TA, total inorganic carbon – CT, pCO_2, pH, and the saturation state with respect to aragonite and calcite carbonate minerals – Ω_{ar} and Ω_{ca}, respectively) in a period spanning 30

years during 1990 – 2019. To address this, we used hydrographic and biogeochemical data available in historical (1996, 2006, and 2010) and recent (2015 – 2019) databases to estimate equations able to reconstruct carbonate system parameters in the three basins of the Bransfield Strait over the last three decades. Thus, our results will lead to a better understanding of the main drivers of interannual variability, as well as decadal changes, of carbonate chemistry in the area.

IV.4. Oceanographic Features of the Bransfield Strait

The Bransfield Strait (Figure IV.1a) is a coastal area of NAP consisting of three deep basins formed recently on the geological time scale. Dated from the Quaternary (Keller *et al.*, 1992), a rifting system that split the South Shetland Islands from the Antarctic Peninsula led to a heritage of some volcanoes and fault systems in this post-arc system (Fisk, 1990) so that the release of hydrothermal fluids and magma in deep, such as around the Humpback volcano (Almendros *et al.*, 2020), and shallow waters, such as Deception Island (Álvarez-Valero *et al.*, 2020), have been recently identified. The bathymetry of the Bransfield Strait increases from southwest towards northeast, from ~1200 m in the western basin, reaching ~2000 m in the central basin and then a maximum of ~2500 m in the eastern basin, which are bound by sills with depths shallower than 800 m and deep canyons (Clowes, 1934; Lopez *et al.*, 1999; Masqué *et al.*, 2002). While the western basin has an open connection to the Bellingshausen Sea, the others are semi-closed systems with much more influence from the continental shelf of the Weddell Sea.

The main water mass contribution influencing the intermediate levels of the Bransfield Strait is advected from the Bellingshausen Sea and the Drake Passage, with relatively

warm temperature, hereinafter called the modified-CDW. It is derived from a mixture of surface waters with intrusions over the shelf of CDW that is transported by the Antarctic Circumpolar Current (Huneke, Huhn e Schröeder, 2016; Moffat e Meredith, 2018; Sangrà *et al.*, 2011). In addition, the deep basins of the Bransfield Strait are fulfilled with dense shelf waters advected from the western and southern continental shelf of the Weddell Sea and characterized by high density and extremely low temperature (i.e., close to seawater freezing point), hereinafter called Dense Shelf Water (DSW; Figure IV.1b; Clowes, 1934; Frölicher et al., 2015; García et al., 2002; Hellmer et al., 2017; Sangrà et al., 2011, 2017).

The Peninsula Front (at surface) and the Bransfield Front (at subsurface; Sangrà et al., 2011, 2017) are formed in the boundary between the modified-CDW and DSW. The latter front is associated with intense baroclinic jets to the northeast, called the Bransfield Current (Sangrà *et al.*, 2011, 2017), with a crucial role in the transport of metal, nutrients, and organisms (Zhou *et al.*, 2006). Furthermore, another source for the complex hydrography has been related to the glacier and sea ice melting processes around Antarctica (Castro *et al.*, 2002). For a broad review of the hydrography of the Bransfield Strait, the reader is referred to see Azaneu et al. (2013), van Caspel et al. (2018), Clowes (1934), Damini et al. (2022), Dotto et al. (2016), García et al. (2002), Huneke et al. (2016), Sangrà et al. (2011, 2017), Ruiz Barlett et al. (2018) and Wilson et al. (1999).

The coastal zones along NAP are areas of high biological productivity holding high stocks and concentrations of phytoplankton (Karl, Tilbrook e Tien, 1990; Mendes *et al.*, 2012), with diatoms being the most abundant phytoplanktonic group found in the north-western Weddell Sea (Mendes *et al.*, 2012). This, therefore, implies high organic

matter sedimentation around the entire peninsula (Fischer, 1991; Masqué *et al.*, 2002). Also, intense primary production in the north-western Weddell Sea continental shelf (Detoni *et al.*, 2015; Mendes *et al.*, 2012) likely promotes high dissolved organic carbon concentrations in the deep basins of the Bransfield Strait (Avelina *et al.*, 2020). Furthermore, regions related to islands and coastal zones in the strait are also associated with high organic carbon concentrations, such as Deception Island and Admiralty Bay (Costa *et al.*, 2022; Doval *et al.*, 2002). Considering the inorganic carbon cycle, the strait experiences large interannual variability, swinging between periods of net CO_2 source to the atmosphere (2009) and net CO_2 sink towards the ocean (2008 and 2010; Ito et al., 2018). A long-term assessment of CO_2 fluxes nearby the Bransfield Strait has shown that coastal zones have acted as strong CO_2 sink zones since 2012 (Monteiro *et al.*, 2020), which is also observed southwards (Brown *et al.*, 2019). The region has also experienced storage of ~20–50 µmol kg^{-1} of anthropogenic carbon around NAP (Anderson *et al.*, 1991; Lencina-Avila *et al.*, 2018; Pardo *et al.*, 2014), which likely comes from recent ventilated DSW (Kerr, Goyet, *et al.*, 2018).

It is also worth mentioning that the variability of modified-CDW and DSW intrusions into the Bransfield Strait mainly respond to coupled interactions between two modes of climate variability, i.e., the El Niño Southern Oscillation (hereinafter ENSO) and the Southern Annular Mode (hereinafter SAM, Loeb et al., 2009; Ruiz Barlett et al., 2018). In general, ENSO imposes strong control over the Weddell Gyre, which intensifies (weakens) in the negative phase, hereinafter ENSO- (positive phase, hereinafter ENSO+), allowing a low (strong) connection between the eastern and western Antarctic Peninsula through a less (high) contribution of DSW into the Bransfield Strait. On the other hand, the SAM promotes an intensification (weakening) of the westerlies

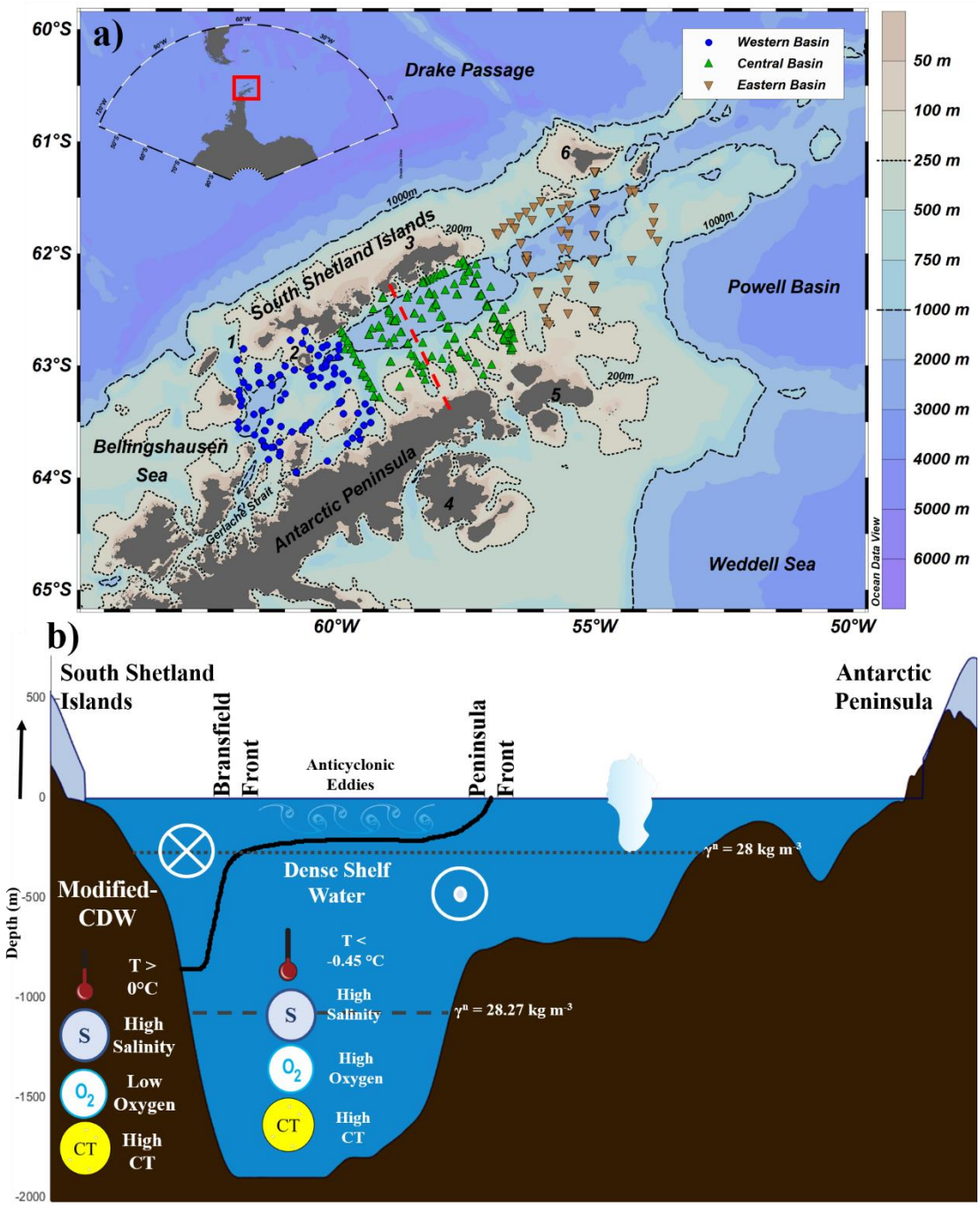

Figure IV.1. The Bransfield Strait and its main characteristics. (a) Distribution of the oceanographic stations used in this study. Stations in the western, central, and eastern basins of the Bransfield Strait are marked by blue dots, green triangles, and brown inverted triangles, respectively. The black dashed line shows the 1000 m isobath, while the black dotted line shows the 200 m isobath. The red dashed line indicates the section described in (b). The numbers indicate: 1. Boyd Strait, 2. Deception Island, 3. King George Island, 4. James Ross Island, 5. Joinville Island, and 6. Clarence Island. (b) Scheme of the main hydrographic properties (seawater temperature – T, salinity – NaCl, dissolved oxygen – O_2, total inorganic carbon – CT, and modified-Circumpolar Deep Water - modified-CDW) and ocean dynamics along the red dashed line depicted in (a). The in and out arrows represent the direction of the main current flow in the region, which is northward around the South Shetland Islands and southward near the Antarctic Peninsula. The dotted and dashed lines indicate mean depth related to neutral density (γ^n) = 28 kg m^{-3} and γ^n = 28.27 kg m^{-3}, respectively. The black line represents the boundary between modified-CDW and Dense Shelf Water.

around the continent in a positive (negative) phase, hereinafter SAM+ (negative phase, hereinafter SAM-), implying stronger (weaker) modified-CDW intrusions into the strait. Furthermore, some recent studies have also shown the impacts of ENSO or SAM on physical, biological, and biogeochemical parameters in the strait (Avelina *et al.*, 2020; Costa *et al.*, 2020; Damini *et al.*, 2022; Dotto *et al.*, 2016).

IV.5. Methods

IV.5.1 Data collection

Hydrographic data (i.e., temperature in °C, salinity, and dissolved oxygen as O_2 in µmol kg^{-1}) with broad coverage for austral summer (i.e., January, February, and March) in the Bransfield Strait were accessed from two databases: (i) World Ocean Database 2018 (WOD18, https://www.nodc.noaa.gov/OC5/WOD/wod18-notes.html, Boyer et al., 2018) during 1990 – 2011 and (ii) Brazilian High Latitude Oceanography Group (GOAL, Dotto et al., 2021; Mata et al., 2018) during 2003 – 2019. Thus, the time series totalizes 30 years of data spanning during 1990 – 2019. The spatial distribution and the number of occupations of each station are presented in Figure V.1. The precision for temperature and salinity measurements was 0.001–0.005°C and 0.003–0.02 for WOD18 (Boyer *et al.*, 2018) and ~0.001°C and ~0.003 for GOAL (Dotto *et al.*, 2021), respectively. These data sets were used to reconstruct carbonate system parameters (see Section IV.5.2).

Derived parameters, such as neutral density (γ^n, kg m^{-3}) and potential temperature (θ, °C), were estimated according to the Thermodynamic Equation of Seawater 2010 (Intergovernmental Oceanographic Commission, Scientific Committee on Oceanic

Research e International Association for the Physical Sciences of the Oceans, 2010). The γ^n values were applied to split the vertical layer structure in each basin (marked by their boundaries with sills shallower than 800 m, Clowes, 1934; Gàrcia et al., 1997), defining the surface ($\gamma^n \leq 28.00$ kg m^{-3}), intermediate (28.00 kg $m^{-3} < \gamma^n < 28.27$ kg m^{-3}), and deep ($\gamma^n \geq 28.27$ kg m^{-3}) layers. The surface layer is occupied by Antarctic Surface Water highly modified locally by sea ice melting and continental meltwater, the intermediate water is mainly composed of a mixture of modified-CDW and DSW, while the deep layer is occupied by DSW that flows down the hills and canyons in the region (Caspel, van, Hellmer e Mata, 2018; Huneke, Huhn e Schröeder, 2016; Ruiz Barlett *et al.*, 2018).

The TA and CT in situ measurements of WOD18 were available for the years 1996, 2006, and 2010, while GOAL data spanned during 2015 – 2019. Data from WOD18 for 1996 were measured during the FRUELA cruise, when TA was determined through automatic potentiometric titration with hydrochloric acid while CT was estimated from pH at 15°C and TA through thermodynamic equations of the carbonate system (Alvarez, Aida e Ros, 2002). Data of TA and CT available from the GOAL database were measured simultaneously by potentiometric titration in a closed cell with an automated titrator (Kerr, Orselli, *et al.*, 2018). The averaged precision for these data (Table V.1) was 3.2 ± 1.3 µmol kg^{-1} and 4.0 ± 0.8 µmol kg^{-1} for TA and CT, respectively. Only data marked with good quality by the post-processing procedure in the databases (flag = 0 or 1) were used in this study (Boyer *et al.*, 2018). Furthermore, offsets were evaluated and spurious data greater than two standard deviations from the mean value of each vertical profile were excluded. These data sets were used to build the

equations used to reconstruct the carbonate system parameters (see Section IV.5.2) when not directly measured.

IV.5.2. Reconstruction of marine carbonate chemistry

The data for in situ TA and CT were used to estimate the best-fitted multivariate linear equations to reconstruct both parameters along the time series used in this study. For this, the following relationship (Eq. 1) was applied:

$$TA\ (\theta, S);\ CT\ (\theta, S, O_2), \qquad \text{Eq. 1}$$

where TA is total alkalinity and CT is total inorganic carbon, both in µmol kg^{-1}; θ is potential temperature in °C, S is practical salinity, and O_2 is dissolved oxygen in µmol kg^{-1}. The equations aim for the reconstruction of TA and CT in those stations where they were not available. Briefly, in situ data and the respective hydrographic parameters were tested in two different groups (i.e., reconstruction and assessment) for many sets to find the best equation suitable to be applied in the Bransfield Strait. The equations were evaluated through the best correlation, smaller root-mean-square error (RMSE), significance (95% confidence interval; $p < 0.05$), and significant F (high values indicate good representation through a linear regression). Comparisons of different sets for each layer (Figure V.2) and among equations for broad (Lee *et al.*, 2006; Millero, Lee e Roche, 1998; Takahashi *et al.*, 2014), including the Arctic Ocean (Arrigo *et al.*, 2010), and regional (Hauri *et al.*, 2015; Lencina-Avila *et al.*, 2018; Monteiro *et al.*, 2020; Monteiro, Kerr e Machado, 2020) oceanic areas for TA (Figure V.3) and CT (Figure V.4) were tested. The best-fitted equations for the Bransfield Strait are presented in Table IV.1. Only equations with the same input data used here were considered in this intercomparison. Validation showed correlations of 0.99 ($p < 0.01$; *n*

= 22), 0.99 ($p < 0.01$; $n = 19$), and 0.81 ($p < 0.01$; $n = 12$) for TA of surface, intermediate, and deep layers, respectively, whereas validation for CT resulted in correlations of 0.99 ($p < 0.01$, $n = 26$), 0.96 ($p < 0.01$, $n = 17$) and 0.98 ($p < 0.01$, $n = 9$), respectively. Reconstructed TA and CT data were used as input for CO2Sys v2.1 (Lewis e Wallace, 1998) to estimate the other carbonate system parameters (i.e., pH in seawater scale, pH_{sws}; pCO_2 in µatm; Revelle Factor; Ω_{ar} and Ω_{ca}). Since measured TA was an input and considers all minor TA components, we used pH in seawater scale, which is 0.01 unit higher than pH in total scale (pH_T, Millero, 2007). This estimate was performed by the use of dissociation constants of carbonic acid by Goyet and Poisson (1989), which is recognized for its good responses in high latitude environments (Kerr, Goyet, *et al.*, 2018; Laika *et al.*, 2009; Lencina-Avila *et al.*, 2018; Wanninkhof *et al.*, 1999). To comprehend the impact of different constant sets on the output data from CO2Sys, we performed a sensitivity test, the results of which are described in the Supplementary Material (Tables V.2, V.3, and V.4). Dickson (1990) and Uppström (1974) were used for sulphate and total borate constants, respectively. Uncertainties related to this reconstruction were calculated following the error propagation of Orr et al. (2018), and they are shown in Table V.5.

IV.5.3. Time series and decadal/mode of climate variability composited vertical profiles of carbonate system parameters

Interannual variability was assessed by parameter trends (± confidence bounds) based on time series anomalies for each density layer of the respective basin in the Bransfield Strait. Anomalies were estimated based on the decadal average of each carbonate

Table IV.1. Reconstruction equations for carbonate system parameters with the best fit for this study. Statistical data related to each reconstruction are presented along with their respective equation, such as correlation (*r*), root mean square error (RMSE), number of samples used for each reconstruction (*n*), *p*-value (*p*), and the signification value (F, which expresses how many of these data are well represented via linear regressions, with high values meaning best fit via linear regressions). Note that these specific relationships present a RMSE about half that of those for broad oceanic areas. Acronyms are: TA – total alkalinity; CT – total inorganic carbon; θ – potential temperature; S – salinity; O_2 – dissolved oxygen; γ^n – neutral density.

Layer	TA	CT
Surface $\gamma^n \leq 28.0$ kg m^{-3}	TA = -31.9*θ -54.5*S + 4236 *r* = 0.93 RMSE = 6.35 µmol kg^{-1} *n* = 72; *p* < 0.01 F = 247.7	CT = -29.3*θ -26.1*S -0.57*O_2 + 3311.5 *r* = 0.95 RMSE = 8.92 µmol kg^{-1} *n* = 49; *p* < 0.01 F = 139.2
Intermediate 28.0 kg m^{-3} < γ^n < 28.27 kg m^{-3}	TA = -57.1* θ + 143.6*S -2652.3 *r* = 0.93 RMSE = 6.35 µmol kg^{-1} *n* = 41; *p* < 0.01 F = 115.0	CT = -0.73*θ + 61.2*S + 1.86*O_2 -352.1 *r* = 0.91 RMSE = 8.99 µmol kg^{-1} *n* = 37; *p* < 0.01 F = 53.8
Deep $\gamma^n \geq 28.27$ kg m^{-3}	TA = 59.7*θ -126.2*S + 6805.3 *r* = 0.86 RMSE = 6.22 µmol kg^{-1} *n* = 49; *p* < 0.01 F = 63.1	CT = 135.9*θ +797.8*S + 3.2*O_2 -26019.9 *r* = 0.91 RMSE = 9.63 µmol kg^{-1} *n* = 30; *p* <0.01 F = 39.86

system parameter with higher temporal coverage (i.e., the 2010s) and then, annual anomalies were calculated by subtraction of each annual from the 2010s average. Annual trends were statistically significant when the confidence bound was less than the trend value (i.e., 95% confidence level; $p < 0.05$).

Decadal variability was assessed through decadal averaged (± standard error) vertical profiles for the carbonate system parameters at bins of 50 m over the three decades (i.e., 1990s during 1990 – 1999, 2000s during 2000 – 2009, and 2010s during 2010 – 2019, Table V.6). Each calculated mean level of depth in the vertical profile was assessed, point by point, through the Mann-Whitney test to identify significant differences among these three decades, considering a significance level of 95% ($p < 0.05$). Vertical variability was also assessed through a composite analysis, which verified the role played by coupled interactions of ENSO and SAM (see Figure V.5) and their effects on carbonate chemistry within the strait. Significant differences for

composite analysis were tested through the Mann-Whitney test for each depth interval of 50 m in each basin. Each vertical profile shown here represents a composited profile.

IV.6. Results

IV.6.1. Western basin of the Bransfield Strait

The surface layer of the western basin was characterized by annual average ± standard deviation ranging from 2315 ± 24 to 2381 ± 16 µmol kg^{-1} for TA and 2195 ± 15 to 2291 ± 31 µmol kg^{-1} for CT (Figure V.6a and b). Higher pH_{sws}, Ω_{ar}, and Ω_{ca} were observed in the surface layer than in the intermediate and deep layers, with annual average values reaching 8.14 ± 0.02, 1.78 ± 0.10, and 2.84 ± 0.15, respectively (Figure V.6d, e, and f). Total average pCO_2 was higher in the intermediate layer with 484.1 ± 105.5 µatm, likely associated with the presence of modified-CDW. Furthermore, total averages for pH_{sws}, Ω_{ar}, and Ω_{ca} in the intermediate layer were 7.91 ± 0.10 (minimum of 7.8), 1.03 ± 0.21 (minimum of 0.7), and 1.63 ± 0.33 (minimum of 1.1), respectively (Figure V.6). For TA, the annual average vertical distribution was lower in the intermediate layer, 2276 ± 10 µmol kg^{-1}, relative to the surface layer, and reached 2392 ± 1 µmol kg^{-1} in the deep layer (Figure V.6). CT increased, on annual average, with increasing depth, reaching 2355 ± 1 µmol kg^{-1} in the deep layer (Figure V.6).

In general, interannual variability showed sharp trends in the deepest layers, except for TA (Table IV.2, Figure V.7a). The deep layer had a sharp positive trend for CT per year, ten-fold higher than in intermediate layer (Table IV.2, Figure V.7b). Although data were restricted to solely the 2010s in the deep layer within the western basin, because of its high variability the CT trend was well marked. Moreover, the annual trend for

pCO_2 in the deep layer also showed a sharp positive trend of 17.3 ± 6.9 µatm yr^{-1}, being eight-fold higher than the surface (Table IV.2). Interannual trends showed a clear reduction per year for pH_{sws} and Ω, which are more intense with depth and characterize the deep layer with trends three- and five-fold higher than intermediate and surface layers, respectively (Table IV.2).

Decadal-average vertical profiles of TA and CT showed no long-term variability in the surface layer (Figure IV.2a and b, $p > 0.05$, Table V.8). However, TA and CT decreased between the 1990s and 2000s ($p < 0.01$, Table V.8) for the intermediate layer around 450–1000 m (Figure IV.2a and b). During the 2010s, TA and CT recovered to values of the 1990s ($p < 0.01$, Table V.8). A progressive increase of pCO_2 below 200 m is observed from the 1990s to the 2010s, consequently related to a reduction of both pH_{sws} and Ω (Figure IV.2c-f). It is noted that the vertical distribution of the carbonate system parameters was mainly affected by the SAM (Figure IV.3 and V.8). During both SAM+ and SAM- phases, TA and CT below ~450 m increased when compared to the vertical distribution observed in years marked by neutral SAM. However, the highest increase occurs during periods of SAM- (Figure IV.3a and b). Furthermore, although changes were noted in TA and CT concentrations, pCO_2, pH_{sws}, and Ω did not experience well-marked changes throughout the water column, except for increased pCO_2 and decreased pH_{sws} and Ω between 300 and 500 m during combined periods of SAM+ and ENSO- (Figure V.8).

IV.6.2. Central basin of the Bransfield Strait

The surface layer of the central basin had total average concentrations for TA and CT

of 2368 ± 10 and 2243 ± 20 µmol kg^{-1}, respectively (Figure V.9a and b), which are close to those of the surface waters of the western basin (Figure V.6a and b). The total average value of pCO_2 in the surface layer was 394.8 ± 40.8 µatm, whereas pH_{sws}, Ω_{ar}, and Ω_{ca} values reached 8.13 ± 0.03, 1.71 ± 0.03, and 2.72 ± 0.29, respectively (Figure V.9). The average values in the intermediate layer were marked by a minimum of annual average for pH_{sws} of 7.76 ± 0.05 and a maximum for pCO_2 of 750.2 ± 90.7 µatm relative to the other layers in the basin (Figure V.9). Low TA and CT variabilities were observed throughout depths, with total average varying roughly 10 and 13 µmol kg^{-1} between surface and deep layers, respectively, while average values of Ω_{ar} and Ω_{ca} decreased with depth, with Ω_{ar} reaching subsaturated condition in most of vertical profiles and Ω_{ca} in a few in the deep layer (Figure V.9).

Increasing TA and CT trends were observed only in the intermediate layer (Table IV.2, Figure V.10), with CT in particular being the variable with higher interannual variability (Figure V.10b). Although with no significant trends, pH_{sws} and Ω increased in the entire water column for the evaluated period (Table IV.2, Figure V.10). Unfortunately, the carbonate chemistry reconstruction is limited to those years with available hydrographic data, thus limiting a better spatiotemporal coverage in the 1990s in this basin. This is reinforced by the lack or bad quality of available O_2 data. The last 30 years have been marked by reduced TA below 500 – 600 m and increased CT below 1000 m in the 2010s over the 2000s (Figure IV.4a and b). The parameter pCO_2 increased, whereas pH_{sws} and Ω decreased over the last two decades in the entire vertical profile (Figure IV.4c, d, e, and f). Particularly for Ω_{ar}, depths below 200 m were under subsaturated conditions (i.e., $\Omega_{ar} < 1$) in the 2010s (Figure IV.4e). Furthermore,

low TA was associated with the deep layer during joint periods of SAM- and ENSO+ (Figure IV.3a and b, respectively). Both pH_{sws} and Ω were lowest in the deep layer du-

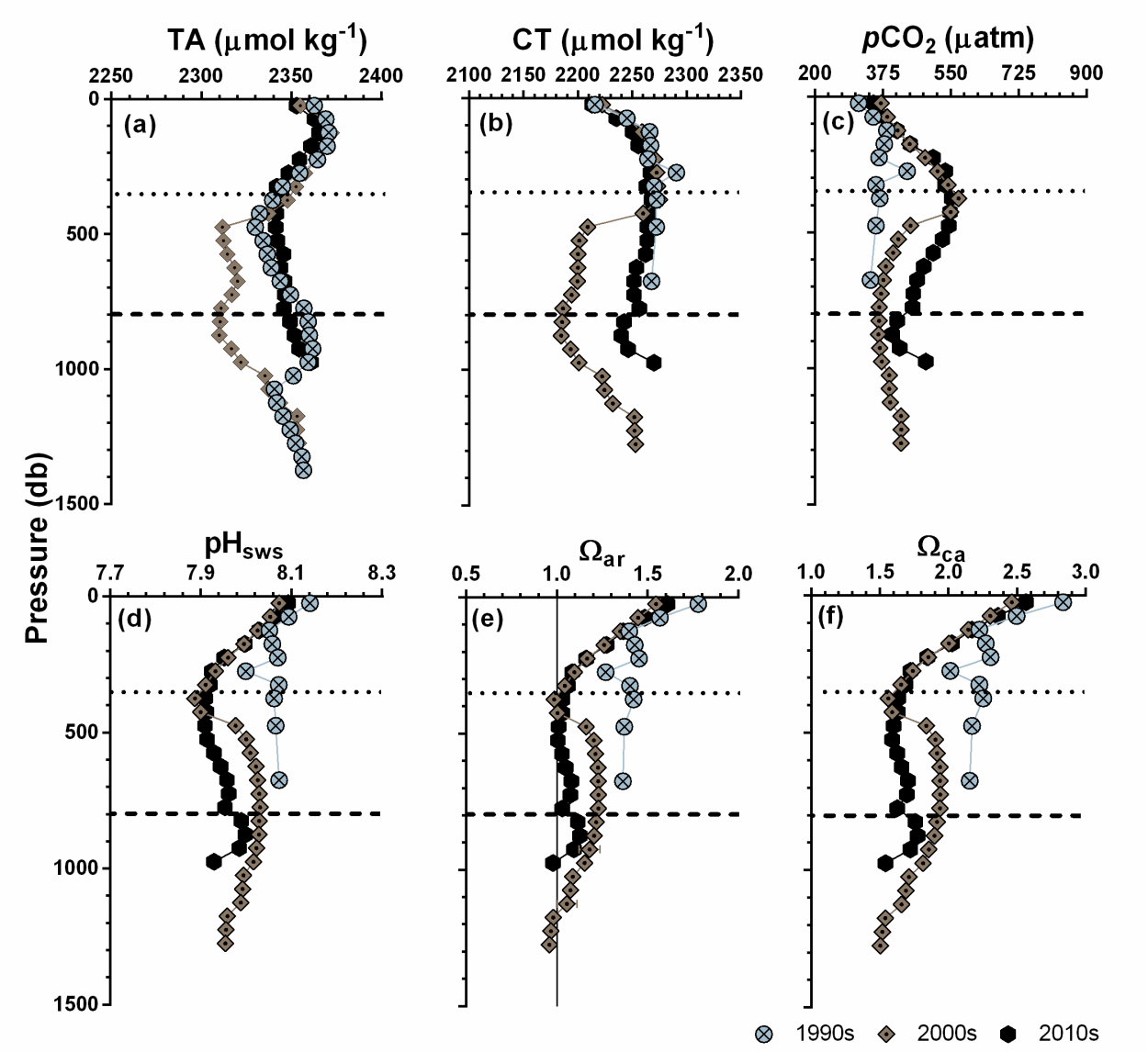

Figure IV.2. Vertical profiles of decadal averages of carbonate system parameters in the western basin of the Bransfield Strait during 1990–2019 for total alkalinity (TA) and during 1996–2019 for the other parameters. Data plotted are (a) total alkalinity – TA, (b) total inorganic carbon – CT, (c) partial pressure of carbon dioxide – pCO_2, (d) pH_{sws} (seawater scale), (e) aragonite saturation state – Ω_{ar}, and (f) calcite saturation state – Ω_{ca}. The standard errors are < 1.9 µmol kg^{-1} for TA, < 2.4 µmol kg^{-1} for CT, < 5.2 µatm for pCO_2, < 0.004 pH_{sws} units, and < 0.04 for both Ω_{ar} and Ω_{ca}. The averaged values are calculated for 50-m bins until the deepest sample in each decade. The black horizontal dotted and dashed lines in the panels represent the average value of the neutral density levels of 28.00 kg m^{-3} and 28.27 kg m^{-3}, respectively. The vertical line in panel (e) indicates Ω_{ar} = 1, with values below 1 referring to subsaturation of calcium carbonate. Only the 2010s presented γ^n, with the value 28.27 kg m^{-3}, to characterize the deep layer in this basin for CT and the other CO_2-carbonate system parameters, except for TA.

Table IV.2. Trends (± confidence bound) for carbonate system parameters based on a time series of 30 years of reconstructed data between 1990 and 2019 in the Bransfield Strait. If the confidence bound is higher than the trend, then, the trend is not statistically significant (i.e., $p > 0.05$; 95% confidence interval). Significant values are highlighted in bold.

Layer	Basin	Period of TA data (other parameters)	TA (μmol kg^{-1} yr^{-1})	CT (μmol kg^{-1} yr^{-1})	pCO_2 (μatm yr^{-1})	pH_{sws} (pH_{sws} units yr^{-1})	Ω_{ar} (yr^{-1})	Ω_{ca} (yr^{-1})
Surface	Western	1990–2019 (1996–2019)	-0.108 ± 0.231	-0.127 ± 0.461	**2.893 ± 2.570**	**-0.003 ± 0.002**	**-0.010 ± 0.006**	**-0.015 ± 0.010**
	Central	1990–2019 (2000–2019)	-0.169 ± 0.274	**-0.989 ± 0.856**	-0.334 ± 0.656	0.0004 ± 0.0007	0.002 ±0.002	0.003 ±0.004
	Eastern	1999–2019 (1999–2019)	**-0.176 ± 0.041**	**-0.152 ± 0.074**	**0.266 ± 0.102**	**-0.0002 ± 0.0001**	-0.0002 ± 0.0003	-0.0004 ± 0.0006
Intermediate	Western	1990–2019 (1996–2019)	**0.460 ± 0.370**	0.680 ± 1.527	**5.946 ± 0.786**	**-0.008 ± 0.002**	**-0.018 ± 0.009**	**-0.026 ± 0.007**
	Central	1990–2019 (2000–2019)	**0.490 ± 0.196**	0.421 ± 1.050	**-3.286 ± 2.245**	0.0002 ± 0.0003	0.003 ± 0.007	0.005 ± 0.012
	Eastern	1999–2019 (1999–2019)	**-0.044 ± 0.021**	**-0.078 ± 0.047**	**-0.249 ± 0.164**	0.0001 ± 0.0003	**0.0006 ± 0.0003**	**0.0009 ± 0.0006**
Deep	Western	1990–2019 (2013–2019)	**0.262 ± 0.167**	**6.807 ± 3.770**	**17.270 ± 6.851**	**-0.017 ± 0.010**	**-0.044 ± 0.027**	**-0.070 ± 0.043**
	Central	1990–2019 (2000–2019)	**-0.415 ± 0.149**	-0.244 ± 2.067	2.569 ± 4.965	0.0007 ± 0.0062	0.003 ± 0.013	0.004 ± 0.020
	Eastern	1999–2019 (1999–2019)	**0.017 ± 0.006**	**-0.115 ± 0.038**	**-0.312 ± 0.121**	**0.0003 ± 0.0001**	**0.0007 ± 0.0002**	**0.0011 ± 0.0004**

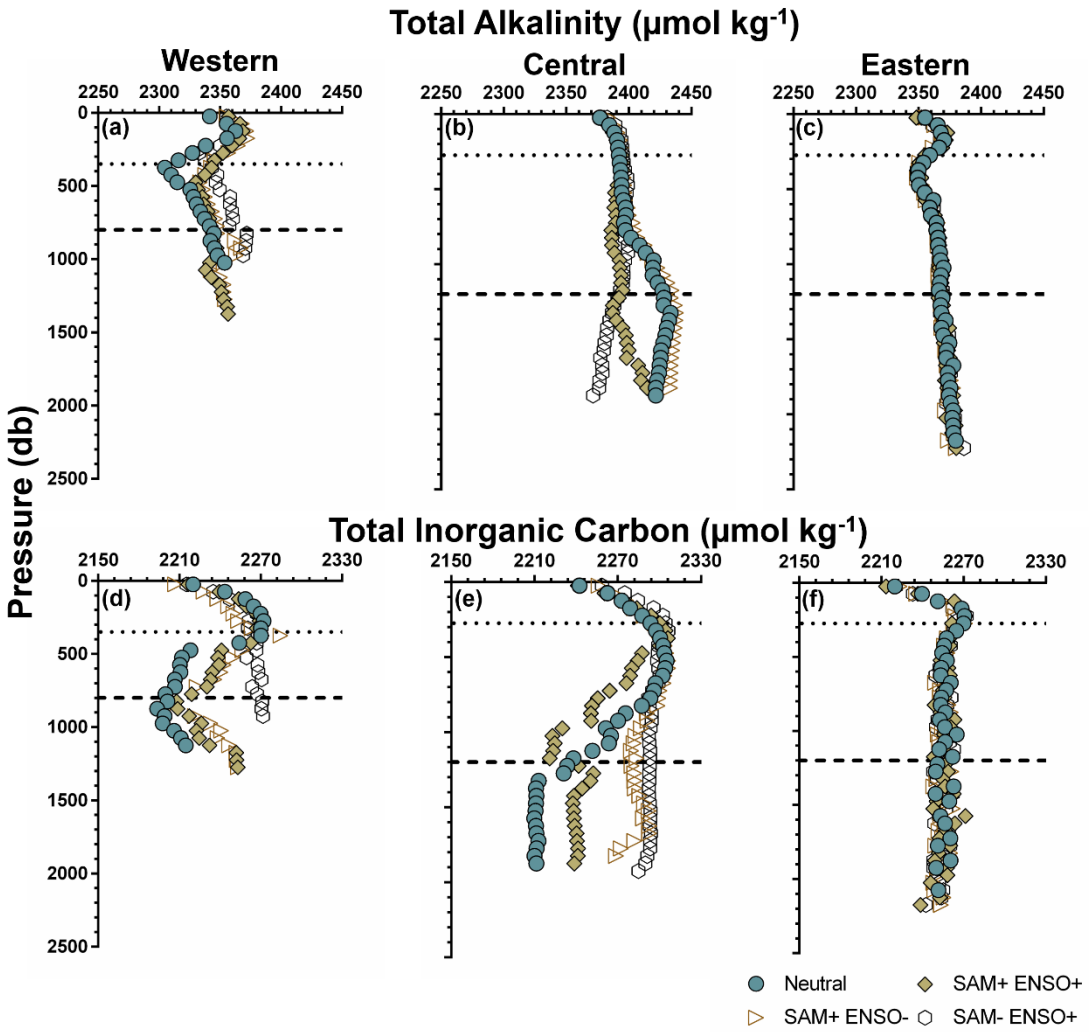

Figure IV.3. Composited vertical profiles of (a, b, and c) total alkalinity – TA (µmol kg^{-1}) and (d, e, and f) total inorganic carbon – CT (µmol kg^{-1}) considering the phases of the modes of climate variability El Niño-Southern Oscillation (ENSO) and Southern Annular Mode (SAM). Averaged TA and CT profiles at the (a, d) western, (b, e) central, and (c, f) eastern basins of the Bransfield Strait. The years used for each composition are presented in Table V.7. The neutral vertical profile for the central basin was estimated by the averaged vertical profile for the neutral situation of SAM and ENSO presenting a standard deviation lower than 1.0 µmol kg^{-1}.

ring joined events of SAM- and ENSO+ or SAM+ and ENSO- (Figure V.8f, g, and h).

IV.6.3. Eastern basin of the Bransfield Strait

The eastern basin is filled with water masses with relative homogeneity in the vertical distribution of carbonate chemistry, implying low interannual and decadal variability (Fi-

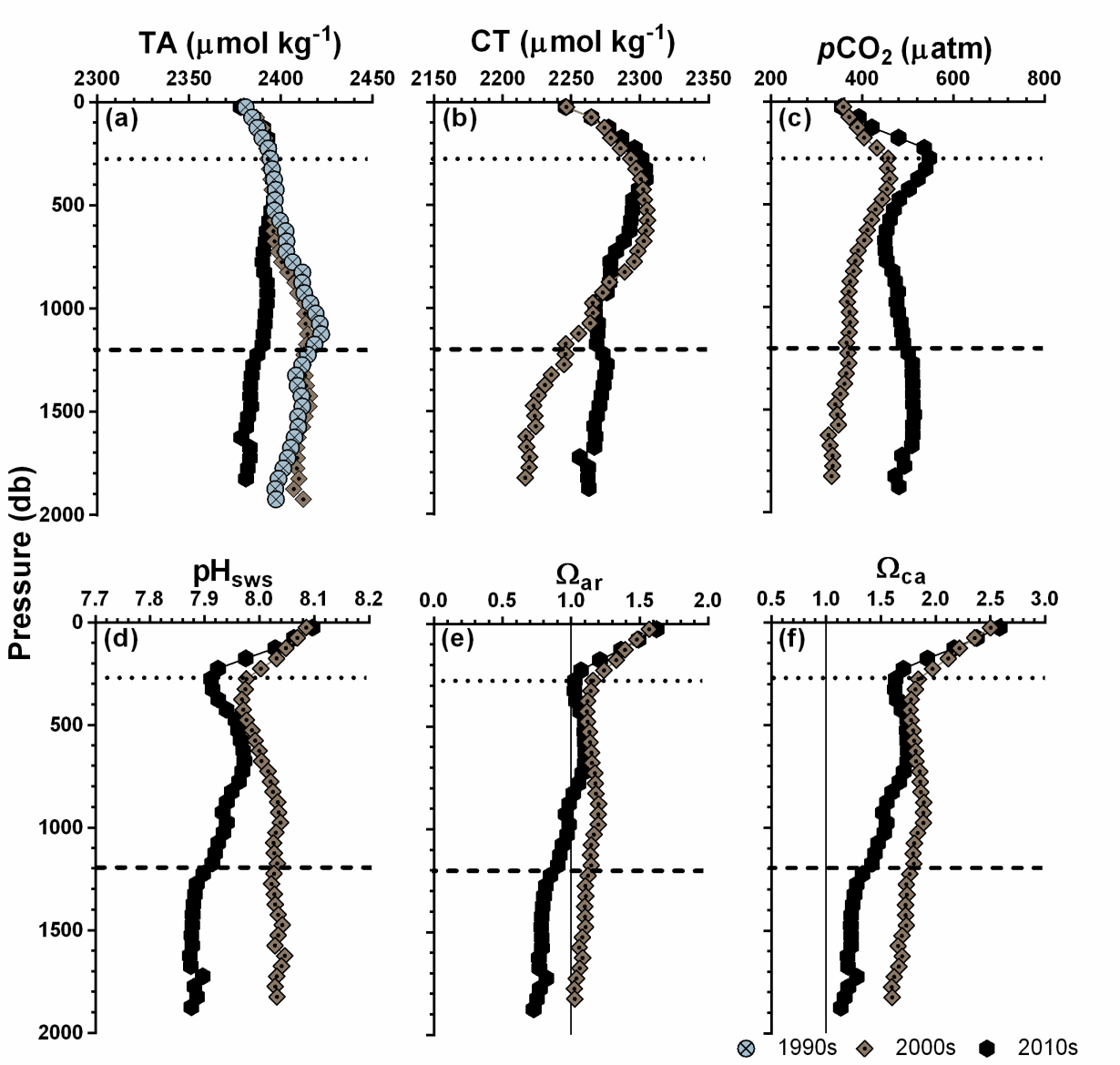

Figure IV.4. Vertical profiles of decadal averages for carbonate system parameters in the central basin of the Bransfield Strait during 1990–2019 for total alkalinity (TA) and during 2000–2019 for the other parameters. Data plotted are (a) total alkalinity – TA, (b) total inorganic carbon – CT, (c) partial pressure of carbon dioxide – pCO_2, (d) pH_{sws} (seawater scale), (e) aragonite saturation state – Ω_{ar}, and (f) calcite saturation state – Ω_{ca}. The standard errors are < 1.2 µmol kg^{-1} for TA, < 1.5 µmol kg^{-1} for CT, < 5.3 µatm for pCO_2, < 0.005 for pH_{sws}, and < 0.02 for both Ω_{ar} and Ω_{ca}. The solid vertical line in panels (e) and (f) indicates Ω_{ar} = 1 and Ω_{ca} = 1, respectively, with values below 1 referring to subsaturation of calcium carbonate.

gure V.11, V.12, and V.13). Interannual trends were small compared to the other basins of the strait (Table IV.2, Figure V.11). Although with low temporal variability, most carbonate system parameters had a negative trend, except for surface pCO_2 at

0.27 ± 0.10 µatm yr^{-1}, and pH_{sws} and Ω in the deep layer with a positive trend of 0.0003 ± 0.0001 pH_{sws} units yr^{-1}, and 0.0014 ± 0.0021 yr^{-1} (for aragonite) and 0.0021 ± 0.0014 yr^{-1} (for calcite), respectively (Table IV.2, Figure V.11).

IV.7. Discussion

IV.7.1. What drives carbonate system variability in the Bransfield Strait?

The temporal and spatial variability of carbonate chemistry in the Bransfield Strait evolves based on changes related to intrusions of water masses in the region. Thus, hydrographic and chemical changes in water column structure primarily respond to the coupled interactions between ENSO and SAM (Avelina *et al.*, 2020; Caspel, van, Hellmer e Mata, 2018; Loeb *et al.*, 2009; Renner *et al.*, 2012; Ruiz Barlett *et al.*, 2018), which regulate the main source water mass that intrudes into the region (Damini *et al.*, 2022). This occurs because high or low influx into the strait of modified-CDW from the western side of the Antarctic Peninsula (i.e., a relatively old, warm, salty, less oxygenated, and TA- and CT-rich water mass) and/or DSW from the eastern side (i.e., a recently ventilated, cold, salty, high oxygenated, and TA- and CT-rich water mass) are regulated by the prevailing mode of climate variability (Bellerby, Turner e Robertson, 1995; Karl, Tilbrook e Tien, 1990; Sangrà *et al.*, 2011). However, the magnitude of the mixing processes along the water column depends on the ocean dynamics and bathymetry of each basin of the Bransfield Strait. While the western and eastern basins of the strait are more exposed to receiving a higher amount of modified-CDW at intermediate levels, the same is not true for the central basin, because the Bransfield Gyre tends to constrain this water mass towards the South Shetland Islands

(Huneke, Huhn e Schröeder, 2016; Sangrà *et al.*, 2011). In addition, the purest form of DSW (i.e., less mixture with ambient waters) is mainly constrained by the central basin at deep levels after sinking into the region (Damini *et al.*, 2022; Dotto *et al.*, 2016).

Interannual and decadal variabilities in the western basin of the Bransfield Strait (Figure V.10) respond to the dynamics of the Antarctic Circumpolar Current and the modes of climate variability prevailing over time. For example, during the early 2000s, both SAM+ and ENSO- were characterized by increasing intrusions of modified-CDW (Figure V.14 and V.15, Loeb et al., 2009; Renner et al., 2012), mainly up to 500 m in depth (Figure V.14), in the western Antarctic Peninsula continental shelf (Moffat, Owens e Beardsley, 2009; Wang *et al.*, 2022). Because the origin of modified-CDW implies high TA and CT concentrations, it should be associated with an increase in the concentrations of both carbonate system parameters, but this is not the case. The heat transported alongside by the intense modified-CDW intrusions during periods of SAM+, which reach the coastal areas of Antarctica, influences glacial retraction with consequent meltwater input into the ocean (Shepherd et al., 2004; Abernathey et al., 2016; Meredith et al., 2008, 2014; Shepherd et al., 2018). The freshwater input and the consequent dilution may contribute with a characteristic signature (i.e., low TA and CT relative to surrounding seawater) to the surface layer from the western basin in the Bransfield Strait, which eventually is advected from the western Antarctic Peninsula (Moffat e Meredith, 2018; Shepherd *et al.*, 2018) and then, into the water column because of the vertical mixing (Gille, 2008). It is a possible countereffect of the high TA and CT content associated with the modified-CDW, but with no or minimized impact on pCO_2, pH_{sws}, and Ω (Figure IV.2). Indeed, the meltwater contribution may reduce TA and CT between 500 – 1000 m in depth (Figure IV.2a and b) as previously detected

on the western Antarctic Peninsula (Legge *et al.*, 2017; Lencina-Avila *et al.*, 2018). Since SAM+ events have been associated with most positive trends over the last decades (Marshall *et al.*, 2006), negative trends for TA and CT due to dilution but the intensification of pCO_2, pH_{sws}, and Ω trends (Table IV.2) may be marked over time if melting contributions become more intense. The central and eastern basins showed a less intense influence of modified-CDW intrusions, but it may be significant to perform a TA:CT ratio like for the upper layers from the western basin. Thus, the presence and variability of modified-CDW intrusions into the upper layers in the Bransfield Strait contribute to the key process driving carbonate chemistry variability through dilution and concentration of salts (Figure IV.5a and b).

However, DSW is the main water mass filling the water column below 500 m in the Bransfield Strait (Figure V.10; Damini et al., 2022) and then, it is responsible for controlling the rapid changes of carbonate system parameters in deep layers. In the western basin, the deep layer showed a positive trend for DSW contribution over the last decade (Figure V.14a; Ruiz Barlett et al., 2018). Its high carbon signature, added to the mixing with modified-CDW, may be associated with the sharp positive trend of CT (Table IV.2). Positive trends of carbonate system parameters associated with modified-CDW intrusions were also observed in the southern Gerlache Strait and DSW in the northern Gerlache Strait (Lencina-Avila *et al.*, 2018) and in the deep layers of the Weddell Sea (Heuven, van *et al.*, 2014). For the central and eastern basins, DSW contributed up to ~60% of the source water masses mixture filling the deep layers (Damini et al., 2022; Figure V.14b and c). This water sinks from the shallow shelf zones directly to the seafloor as dense and cold plumes flowing down the sills, a ventilation process with relatively low mixing with surrounding waters (Caspel, van, Hellmer e

Mata, 2018; Dotto *et al.*, 2016), thus, advecting DSW properties from the north-western Weddell Sea continental shelf into the Bransfield Strait. In fact, the Bransfield Front also acts to constrain the contributions of modified-CDW close to the South Shetland Islands. Thereby, the presence of DSW may increase interannual trends or decadal variability of CT and pCO_2 and decrease pH_{sws} and Ω in the deep layer in both western (Table IV.2) and central (Figure IV.4) basins, respectively. Indeed, DSW transports an anthropogenic carbon signature westward (Kerr et al 2018a), which was estimated via the TrOCA method (Touratier, Azouzi e Goyet, 2007; Touratier e Goyet, 2004a; b) at concentrations of about 50 µmol kg^{-1} in the central basin of the Bransfield Strait in the late 2010s (Torres-Lasso, 2019). Additionally, high primary productivity is highlighted from the north-western Weddell Sea (Detoni *et al.*, 2015; Ito *et al.*, 2018; Mendes *et al.*, 2012), transporting organic matter through DSW into the deepest layers of the Bransfield Strait where it may be decomposed. Organic matter decomposition is associated with increases in CT and pCO_2 and reductions in TA, pH_{sws}, and Ω, as noticed in the central basin in the 2010s relative to the 2000s (Figure IV.4). Also, hydrothermal vents and volcanos are found at the bottom of the Bransfield Strait (Almendros *et al.*, 2020), the chemosynthesis processes of which may alter TA and CT by a ratio between CO_2 dissolution and organic matter decomposition, and release of CO_2 through hydrothermal vents may act as a direct CO_2 ingassing process into the water column with no TA change. Thus, several processes are occurring at the same time in the deep layers, holding a TA:CT ratio between organic matter decomposition and close to that expected in the ocean-atmosphere interface (i.e., direct CO_2 injection by the hydrothermal activities plus a rapid filling of the deep basins with DSW properties, Figure IV.5c).

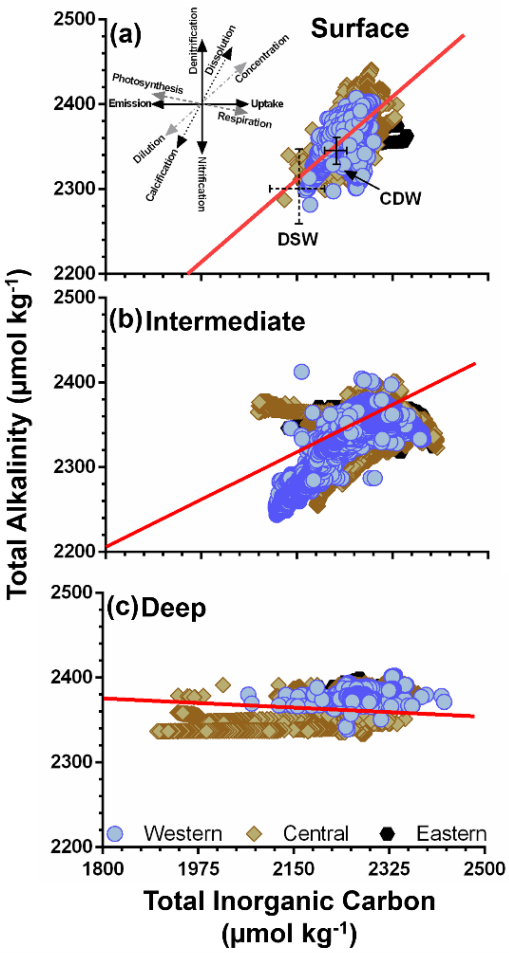

Figure IV.5. Dispersal diagram of the relationship between total inorganic carbon (CT) and total alkalinity (TA) for the (a) surface, (b) intermediate, and (c) deep layers of the Bransfield Strait. The color and symbols differ among basins, as indicated in (c). The inset in (a) presents the standard relation for the TA:CT ratio in the ocean (Zeebe e Wolf-Gladrow, 2001). The red lines show the linear regression between CT and TA in surface (n = 95274; slope: 0.554 ± 0.002; TA = 0.554*CT + 1120; p < 0.001), intermediate (n = 150748; slope = 0.323 ± 0.001; TA = 0.323*CT + 1623; p < 0.001), and deep (n = 99740; slope = – 0.018 ± 0.001; TA = -0.018*CT + 2406; p < 0.001) layers. The TA and CT source water masses end-members were marked by the crosses and selected from Broullón et al. (2019) and Broullón et al. (2020), respectively. The source water masses are Circumpolar Deep Water (CDW) in the open ocean nearby the western Antarctic Peninsula and Dense Shelf Water (DSW) in the north-western Weddell Sea.

Beyond biogeochemical processes, the ice dynamic from the Weddell Sea may affect carbonate system variability, such as noticed for TA changes (e.g., Azaneu et al., 2013; Dotto et al., 2016; Hellmer et al., 2011). Similar to the deep layer of the western basin, the central basin in the 2010s presented TA changes with associated input of ~0.02 units of salinity relative to the 2000s (Figure V.14b) and 0.06 units of salinity relative to

the last 60 years (Dotto *et al.*, 2016). Indeed, this layer in the central basin has been showing increases in salinity during 2010 – 2016 as a consequence of the increased sea ice formation in the western Weddell Sea (Damini *et al.*, 2022), likely providing TA alterations in the deep layer as noticed in the 2010s in the central basin (Figure IV.4a). Another point to take into account is extreme events around the NAP. Heat waves and atmospheric rivers may contribute to favoring meltwater input and iceberg calving along ice shelves around the western Weddell Sea through atmospheric heating, potential runoff, and high exposure of the ice shelf to swells triggered by storms (Massom *et al.*, 2018; Reid e Massom, 2022; Scambos *et al.*, 2000; Wille *et al.*, 2022). Indeed, negative interannual CT anomalies in the deep layer of the central basin (Figure V.10b) covaried alongside the coastal exposure of the Weddell Sea (i.e., low sea ice coverage, Reid & Massom, 2022) and the frequency of atmospheric rivers (Wille *et al.*, 2022) by a correlation of -0.91 and -0.61, respectively. In this case, negative anomalies of CT and, then, positive anomalies of pH_{sws} (Figure V.10d) might be intensified when ice shelves collapse or lose great ice volume. Therefore, sudden events such as the abrupt collapse of the Larsen A and B (Massom *et al.*, 2018; Scambos *et al.*, 2000) also had potential to promote biogeochemical changes as traced into the deep layer of the central basin in the Bransfield Strait.

The deep layers may also be influenced by nitrification and water mass intrusions carrying low anthropogenic signatures. Years marked as periods of SAM- showed changes in TA, but no CT changes below 1000 m in depth (Figure V.16c). The 1:0 relationship of TA:CT may infer nitrification processes (see Wolf-Gladrow et al., 2007) occurring in the central basin, which may be connected to the archaea of the genus *Thaumarchaeota* found in the Southern Ocean, including the Bransfield Strait (Signori

et al., 2014). We hypothesize that SAM- events may improve the contribution of water masses with high ammonium and/or nitrite ion concentrations into these deepest layers. The source area of that water mass is likely the continental shelves of the Weddell Sea. With respect to another process contributing to carbonate system variability, Gordon et al. (2000) and von Gyldenfeldt et al. (2002) pointed out that water mass contribution from the Ronne-Filchner ice shelf overflows by a sill nearby the Powell Basin into the deep layer of the eastern basin of the Bransfield Strait. Due to its low temperature (Frölicher *et al.*, 2015; Hellmer *et al.*, 2017) and anthropogenic carbon content (Pardo *et al.*, 2014), this water mass may minimize the effects of anthropogenic carbon carried on by DSW in the deep layer, which may promote increases of pH_{sws} values as a thermal effect. However, the eastern basin has been a challenging area for both hydrographic and biogeochemical assessments, resulting in no investigations until now.

IV.7.2. Acidification process and carbon dioxide saturation in the Bransfield Strait

Spatial and temporal variability of carbonate system parameters in the Bransfield Strait weighs changes in pH_{sws} and Ω, which vary in trend and magnitude among basins (Table IV.2, Figure V.7, V.10, and V.11). The western basin may be associated with the strongest negative trends (Table IV.2, Figure V.7d) because of frequent intrusions of CDW (Figure V.14a), highlighting a contribution of a natural process to pH trends. For instance, the surface layer of the western basin has trends (-0.003 ± 0.002 pH_{sws} units yr^{-1}, Table IV.2) similar to those of the deep layer of the northern Gerlache Strait (-0.003 ± 0.001 pH_{sws} units yr^{-1}, Lencina-Avila et al., 2018), central western Antarctic Peninsula (0.002 ± 0.002 pH_T units yr^{-1}, Hauri et al., 2015), and the surface layer of the

Southern Ocean (-0.002 ± 0.0003 pH_T units yr^{-1}, Midorikawa et al., 2012). However, these trends observed surrounding the Antarctic Peninsula are smaller than those found in other sensitive regions that have a high Revelle factor (Jiang *et al.*, 2019; Sabine *et al.*, 2004), such as the North Sea (Blackford e Gilbert, 2007). Adding up the trends of other areas of the Southern Ocean, such as the south of the Polar Front (-0.0022 ± 0.0004 pH_T units yr^{-1}, Midorikawa et al. (2012); -0.0043 ± 0.0016 to -0.0009 ± 0.0007 pH_T units yr^{-1}, Leseurre et al. (2022)), reveals that these trends in the western basin are one (deep layer) order of magnitude higher than any area in the coastal zone and surrounding ocean. Additionally, the entire Southern Ocean holds a pH trend at -0.0020 ± 0.0002 pH_T units yr^{-1} (Lauvset *et al.*, 2015), which is similar to those surrounding the Antarctic Peninsula, but smaller than estimated here in the western basin of the Bransfield Strait. Conversely, the central basin presented interannually swinging, but undefined, trends (Table IV.2, Figure V.10d) over the 30 years investigated because of the dominance of DSW contributions (Figure V.14b). Furthermore, the intense well-mixed water column in the eastern basin may be the reason for the lower trend in the present study (Table IV.2, Figure V.11).

Hence, we suggest that three possible processes may be driving the pH_{sws} trends in the western basin: (i) intensified intrusions of CDW over the continental shelf of the western and NAP due to the increased frequency of years marked by SAM+ phase (Henley *et al.*, 2020; Jones *et al.*, 2017); (ii) vertical mixture transports meltwater signal throughout the water column with its carbon content (Monteiro *et al.*, 2020) in more intense wind-stress in SAM+ and ENSO- events and; (iii) increased mixture between modified-CDW and DSW – while the former is rich in organic matter decomposition products, the latter is also enriched with anthropogenic carbon. The latter point is

associated with its increased contribution to the Bransfield Strait in the 2010s (Damini *et al.*, 2022; Dotto *et al.*, 2016; Ruiz Barlett *et al.*, 2018), which may yield the sharpest negative trends observed in the deep layer in the western basin as also noticed for the Gerlache Strait (Lencina-Avila *et al.*, 2018). Indeed, the source area of DSW at the western Weddell Sea presented a reduction of 0.02 pH_T units from 1992 to 2008 (Hauck *et al.*, 2010), and its signature may be carried into the Bransfield Strait. However, other processes may be acting throughout the water column and this signature may be damped, such as the organic matter decomposition in the central basin (see Figure IV.5b and c). Yet, since DSW is ventilated before flowing into the deepest layers of the Bransfield Strait (Caspel, van *et al.*, 2018; Dotto *et al.*, 2016), the signature of atmospheric CO_2 increase may be absorbed by DSW and transported through advection (see Figure IV.5c).

The pH_{sws} trends respond to the CO_2 increment into the water column of the Bransfield Strait. This is corroborated by the decadal rising Revelle factor for the western and central basins throughout the water column (Figure IV.6a and b), reaching values close to those observed in the eastern basin (Figure IV.6c). However, decadal changes in the central basin were more intense than those in the western basin because of the contribution of anthropogenic processes, such as the signature of atmospheric CO_2 increase due to the recent human footprint on the carbon cycle (i.e.,

anthropogenic carbon) and then, its transport through DSW advection into the Bransfield Strait. Since a high signature of modified-CDW is detected in the western

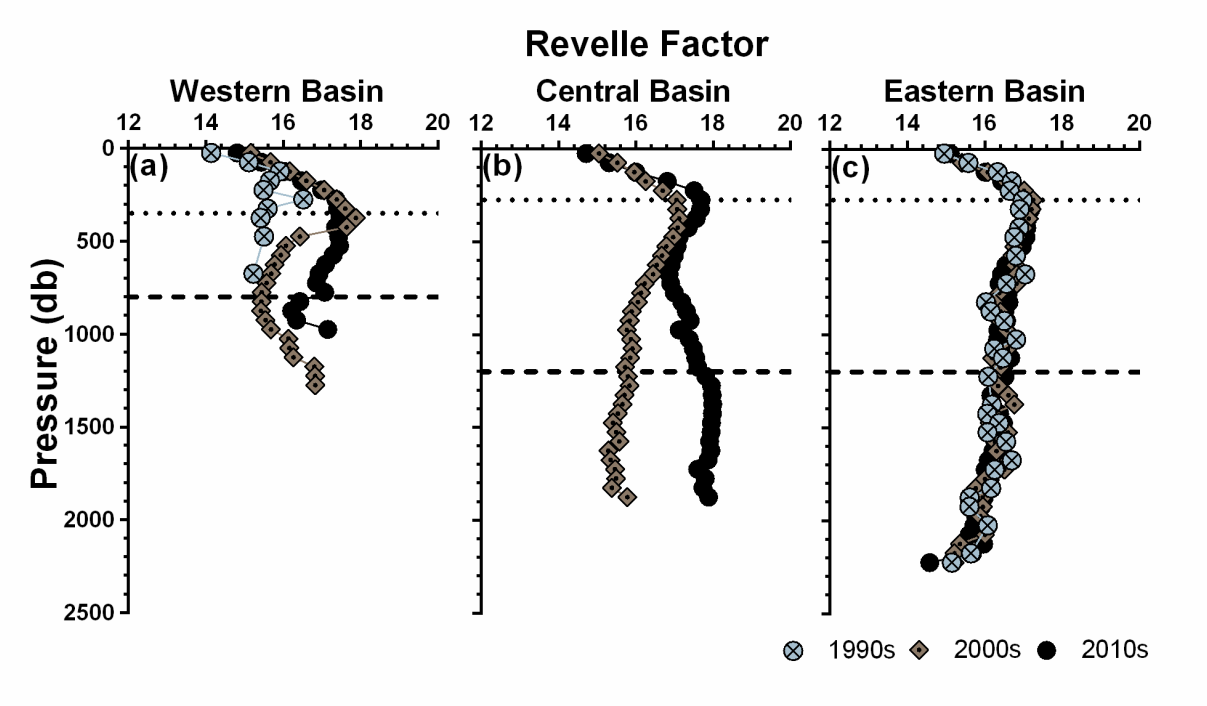

Figure IV.6. Vertical distribution of the Revelle factor over three decades in the Bransfield Strait for (a) western, (b) central, and (c) eastern basins. Plotter data is the average (± standard error) at each 50 m depth. The black horizontal dotted and dashed lines in the panels represent the average value of the neutral density levels of 28.00 kg m^{-3} and 28.27 kg m^{-3}, respectively.

basin, the pH_{sws} decreases in the region have major influence related to the old and acidified water mass carrying naturally products of organic matter decomposition. However, most frequently CDW intrusions respond to changes in modes of climate variability, as a consequence of anthropogenic activities. Furthermore, the eastern basin has less influence on both water masses, reflecting a more mixed water mass structure in the region even with a Revelle factor indicating that the basin has already been near CO_2 saturation since the 1990s (Figure IV.6c). Although this acidification process is minimal, the complexity of the eastern basin needs further investigation to clarify the reasons for its particular effects on hydrography and biogeochemistry.

Overall, the Bransfield Strait demonstrated being close to reaching CO_2 saturation and may represent an issue for much more intense pH_{sws} negative trends with impacts on calcified structures of marine organisms in the water column, such as pteropods, and on the seafloor, such as echinoderms and bryozoans (Acqua *et al.*, 2019; Figuerola *et al.*, 2020; Henley *et al.*, 2020).

IV.8. Conclusions

Changes in marine carbonate chemistry in the Bransfield Strait evidence the key role played by hydrography and its variability and responses to climate patterns over space and time. Such variability is mainly controlled by the link between ENSO and SAM. Furthermore, biogeochemical processes, such as organic matter decomposition and anthropogenic carbon inputs, may also influence the variability of marine carbonate chemistry. Their combined effects tend to promote a distinct response in the strait: while the western basin is mostly influenced by CDW intrusions at intermediate levels, the central basin is impacted by DSW at deeper levels. In addition, the eastern basin has a peculiar and challenging water mass structure that indicated a region where the mixing of different water masses plays a major role. The eastern basin itself has demonstrated to be a particular area for which investigations about its natural behavior are needed. Overall, the strait is heading towards a condition of CO_2 saturation, primarily in the central basin because of the anthropogenic carbon transported by DSW into the deep basin. However, other investigations are needed to explore the role that biogeochemical processes, such as nitrification and hydrothermal vents, have in influencing carbonate system variability in the region. A summary of identified and

inferred hydrographic and biogeochemical processes that may contribute to this carbonate chemistry variability is provided in the schematic of Figure IV.7.

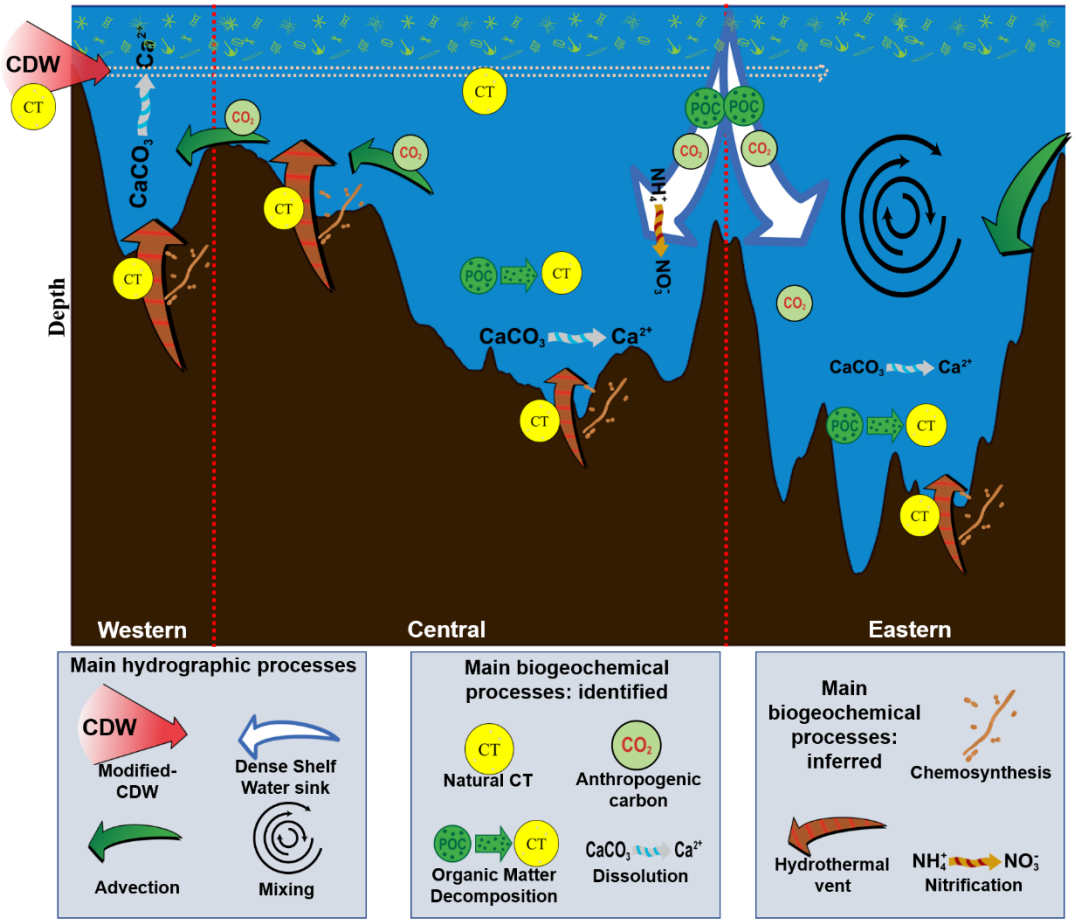

Figure IV.7. Summary of the main processes affecting CO_2-carbonate system variability over 30 years in the Bransfield Strait. The highlighted section crosses from southearstern (left) to north-eastern (right). Red-dashed lines indicate bounds by sills between basins.

Like many other coastal zones surrounding the Antarctic Peninsula, the Bransfield Strait revealed that direct and indirect anthropogenic effects, such as anthropogenic carbon inputs and intensification of westerlies associated with the SAM+ phase, may be significant in altering the chemical system that controls ocean pH and carbonate concentration. Indeed, the strait acts as a sentinel for biogeochemical changes occurring in the sensitive area around the Antarctic Peninsula. As a transitional zone connecting subpolar systems, the Bransfield Strait draws attention to the critical state

of the influence of open ocean areas into the coastal zones around the Antarctic Peninsula. As part of the Southern Ocean, the strait may be crucial to countering the effect of atmospheric CO_2 increase, since its CO_2 saturation is almost reached. On a larger scale, comprehending the biogeochemical processes responding to climate change may introduce new approaches to stimulate the inclusion of Antarctica in the sustainable plans for the Ocean Decade. This is true since the continent, and the roles it plays over climate control and ecological processes, are crucial to trigger suitable actions concerning sustainable development goals such as climate action (SDG 13) and life below water (SGD 14).

IV.9. Acknowledgments

This study is part of the activities of the Brazilian High Latitude Oceanography Group (GOAL) within the Brazilian Antarctic Program (PROANTAR). GOAL has been funded by and/or has received logistical support from the Brazilian Ministry of the Environment (MMA); the Brazilian Ministry of Science, Technology, and Innovation (MCTI); the Council for Research and Scientific Development of Brazil (CNPq); the Brazilian Navy; the Inter-ministerial Secretariat for Sea Resources (SECIRM); the National Institute of Science and Technology of the Cryosphere (INCT CRIOSFERA; CNPq grant n° 573720/2008–8 and 465680/2014–3); and the Research Support Foundation of the State of Rio Grande do Sul (FAPERGS grant nº 17/2551-000518-0). This study was conducted within the activities of GOAL projects (CNPq grant nº 550370/2002–1, 520189/2006–0, 556848/2009–8, 565040/ 2010–3, 405869/2013–4, 407889/2013–2, 442628/2018–8 and 442637/2018–7). Financial support was also

received from Coordination for the Improvement of Higher Education Personnel (CAPES) through the project CAPES “Ciências do Mar” (grant nº 23038.001421/2014–30). CAPES also provided free access to many relevant journals through the portal “Periódicos CAPES” and the activities of the Graduate Program in Oceanology. Rodrigo Kerr and Mauricio M. Mata are granted with researcher fellowships from CNPq grant nº 304937/2018–5 and 306896/2015–0, respectively. Mauricio Santos-Andrade acknowledges financial support from CNPq scholarship grant nº 132983/2020-6. The authors thank the officers and crew of the polar vessels Ary Rongel and Almirante Maximiano of the Brazilian Navy, and the several scientists and technicians participating in the cruises, for their valuable help during data sampling and data processing. We thank all scientists and research groups for making their data available. All data sets used and respective websites are indicated in the manuscript.

IV.10. Author Contributions

Conceptualization: M. Santos-Andrade, R. Kerr

Data curation: M. Santos-Andrade

Formal analysis: M. Santos-Andrade

Validation: M. Santos-Andrade

Investigation: M. Santos-Andrade, R. Kerr

Supervision: R. Kerr

Funding acquisition: R. Kerr, M. M. Mata

Writing - original draft: M. Santos-Andrade, R. Kerr

Writing – review & editing: I. B. M. Orselli, T. Monteiro, M. M. Mata, C. Goyet

IV.11. Declaration of competing interest

The authors declare that they have no known competing financial interests or personal relationships that could have appeared to influence the work reported in this paper.

IV.12. References

ABBAS, F.; HAMMAD, H. M.; FAHAD, S.; CERDÀ, A.; RIZWAN, M.; FARHAD, W.; EHSAN, S.; BAKHAT, H. F. Agroforestry: a sustainable environmental practice for carbon sequestration under the climate change scenarios—a review. **Environmental Science and Pollution Research**, v. 24, n. 12, p. 11177–11191, 2017.

ABERNATHEY, R. P.; CEROVECKI, I.; HOLLAND, P. R.; NEWSOM, E.; MAZLOFF, M.; TALLEY, L. D. Water-mass transformation by sea ice in the upper branch of the Southern Ocean overturning. **Nature Geoscience**, v. 9, n. 8, p. 596–601, 2016.

ACQUA, O. D.; FERRANDO, S.; CHIANTORE, M.; ASNAGHI, V. The impact of ocean acidification on the gonads of three key Antarctic benthic macroinvertebrates. **Aquatic Toxicology**, v. 210, n. September 2018, p. 19–29, 2019.

ALMENDROS, J. *et al.* BRAVOSEIS: Geophysical investigation of rifting and volcanism in the Bransfield strait, Antarctica. **Journal of South American Earth Sciences**, v. 104, n. September, 2020.

ÁLVAREZ-VALERO, A. M.; GISBERT, G.; AULINAS, M.; GEYER, A.; KERESZTURI, G.; POLO-SÁNCHEZ, A.; NÚÑEZ-GUERRERO, E.; SUMINO, H.; BORRAJO, J. δD and δ18O variations of the

magmatic system beneath Deception Island volcano (Antarctica): Implications for magma ascent and eruption forecasting. **Chemical Geology**, v. 542, n. March, p. 1–15, jun. 2020.

ALVAREZ, M.; AIDA, F. R.; ROS, G. Spatio-temporal variability of air-sea fluxes of carbon dioxide and oxygen in the Bransfield and Gerlache Straits during Austral summer 1995-96. **Deep-Sea Research Part II**, v. 49, p. 643–662, 2002.

ANADÓN, R.; ESTRADA, M. The FRUELA cruises. A carbon flux study in productive areas of the Antarctic Peninsula (December 1995-February 1996). **Deep-Sea Research Part II: Topical Studies in Oceanography**, v. 49, n. 4–5, p. 567–583, 2002.

ANDERSON, L. G.; HOLBY, O.; LINDEGREN, R.; OHLSON, M. The transport of anthropogenic carbon dioxide into the Weddell Sea. **Journal of Geophysical Research**, v. 96, n. C9, 1991.

ARRIGO, K. R.; PABI, S.; DIJKEN, G. L. VAN; MASLOWSKI, W. Air-sea flux of CO2 in the Arctic Ocean, 1998-2003. **Journal of Geophysical Research: Biogeosciences**, v. 115, n. 4, p. 1998–2003, 2010.

AVELINA, R.; CUNHA, L. C. DA; FARIAS, C. DE O.; HAMACHER, C.; KERR, R.; MATA, M. M. Contrasting dissolved organic carbon concentrations in the Bransfield Strait, Northern Antarctic Peninsula: insights into ENSO and SAM effects. **Journal of Marine Systems**, v. 212, p. 103457, 2020.

AZANEU, M.; KERR, R.; MATA, M. M. Assessment of the representation of Antarctic Bottom Water properties in the ECCO2 reanalysis. **Ocean Science**, v. 10, n. 6, p. 923–946, 2014.

AZANEU, M.; KERR, R.; MATA, M. M.; GARCIA, C. A. E. E. Trends in the deep Southern Ocean (1958-2010): Implications for Antarctic Bottom Water properties and volume export. **Journal of Geophysical Research: Oceans**, v. 118, n. 9, p. 4213–4227, set. 2013.

BELLERBY, R. G. J.; TURNER, D. R.; ROBERTSON, J. E. Surface pH and pC02 distributions in the Bellingshausen Sea, Southern Ocean, during the early Austral summer. **Deep-Sea Research Part II**, v. 42, n. 4–5, p. 1093–1107, 1995.

BLACKFORD, J. C.; GILBERT, F. J. pH variability and CO2 induced acidification in the North Sea.

Journal of Marine Systems, v. 64, n. 1–4, p. 229–241, 2007.

BOYER, T. P. *et al.* NOAA Atlas NESDIS 87. World Ocean Database 2018. p. 1–207, 2018.

BROULLÓN, D. *et al.* A global monthly climatology of total alkalinity: A neural network approach. **Earth System Science Data**, v. 11, n. 3, p. 1109–1127, 2019.

BROULLÓN, D.; PÉREZ, F. F.; VELO, A.; HOPPEMA, M.; OLSEN, A.; TAKAHASHI, T.; KEY, R. M.; TANHUA, T.; SANTANA-CASIANO, J. M.; KOZYR, A. A global monthly climatology of oceanic total dissolved inorganic carbon: a neural network approach. **Earth System Science Data**, v. 12, n. 3, p. 1725–1743, 5 ago. 2020.

BROWN, M. S.; MUNRO, D. R.; FEEHAN, C. J.; SWEENEY, C.; DUCKLOW, H. W.; SCHOFIELD, O. M. Enhanced oceanic CO2 uptake along the rapidly changing West Antarctic Peninsula. **Nature Climate Change**, v. 9, n. 9, p. 678–683, 2019.

CAO, L.; CALDEIRA, K.; JAIN, A. K. Effects of carbon dioxide and climate change on ocean acidification and carbonate mineral saturation. **Geophysical Research Letters**, v. 34, n. 5, p. 1–5, mar. 2007.

CASPEL, M. VAN; HELLMER, H. H.; MATA, M. M. On the ventilation of Bransfield Strait deep basins. **Deep-Sea Research Part II: Topical Studies in Oceanography**, v. 149, n. September 2017, p. 25–30, 2018.

CASPEL, M. VAN; HELLMER, H. H.; MATA, M. M.; CASPEL, M. VAN; HELLMER, H. H.; MATA, M. M. On the ventilation of Bransfield Strait deep basins. **Deep-Sea Research Part II: Topical Studies in Oceanography**, v. 149, n. September 2017, p. 25–30, 2018.

CASTRO, C. G.; RÍOS, A. F.; DOVAL, M. D.; PÉREZ, F. F. Nutrient utilisation and chlorophyll distribution in the Atlantic sector of the Southern Ocean during Austral summer 1995-96. **Deep-Sea Research Part II: Topical Studies in Oceanography**, v. 49, n. 4–5, p. 623–641, 2002.

CLOWES, A. J. Hydrology of the Bransfield Strait. *In*: **Discovery Reports**. [s.l: s.n.]. p. 1–64.

COOK, A. J.; FOX, A. J.; VAUGHAN, D. G.; FERRIGNO, J. G. Retreating glacier fronts on the Antarctic Peninsula over the past half-century. **Science**, v. 308, n. 5721, p. 541–544, 2005.

COOK, A. J.; HOLLAND, P. R.; MEREDITH, M. P.; MURRAY, T.; LUCKMAN, A.; VAUGHAN, D. G. Ocean forcing of glacier retreat in the western Antarctic Peninsula. **Science**, v. 353, n. 6296, p. 283–286, 2016.

COSTA, R. R.; MENDES, C. R. B.; SOUZA, M. S. D.; TAVANO, V. M.; SECCHI, E. R. Chemotaxonomic characterization of the key genera of diatoms in the Northern Antarctic Peninsula. **Anais da Academia Brasileira de Ciencias**, v. 94, p. e20210584, 2022.

COSTA, R. R.; MENDES, C. R. B.; TAVANO, V. M.; DOTTO, T. S.; KERR, R.; MONTEIRO, T.; ODEBRECHT, C.; SECCHI, E. R. Dynamics of an intense diatom bloom in the Northern Antarctic Peninsula, February 2016. **Limnology and Oceanography**, v. 65, n. 9, p. 1–20, 18 mar. 2020.

DAMINI, B. Y.; KERR, R.; DOTTO, T. S.; MATA, M. M. Long-term changes on the Bransfield Strait deep water masses: Variability, drivers and connections with the northwestern Weddell Sea. **Deep Sea Research Part I: Oceanographic Research Papers**, v. 179, p. 103667, jan. 2022.

DETONI, A. M. S.; SOUZA, M. S. DE; GARCIA, C. A. E.; TAVANO, V. M.; MATA, M. M. Environmental conditions during phytoplankton blooms in the vicinity of James Ross Island, east of the Antarctic Peninsula. **Polar Biology**, v. 38, n. 8, p. 1111–1127, 2015.

DICKSON, A. G. Thermodynamics of the Dissociation of Boric Acid in Potassium Chloride Solutions from 273.15 to 318.15 K. **Journal of Chemical and Engineering Data**, v. 35, n. 3, p. 253–257, 1990.

DICKSON, A. G.; MILLERO, F. J. A comparison of the equilibrium constants for the dissociation of carbonic acid in seawater media. **Deep Sea Research Part A, Oceanographic Research Papers**, v. 34, n. 10, p. 1733–1743, 1987.

DINNIMAN, M. S.; KLINCK, J. M.; HOFMANN, E. E. Sensitivity of circumpolar deep water transport and ice shelf basal melt along the west antarctic peninsula to changes in the winds. **Journal of Climate**, v. 25, n. 14, p. 4799–4816, 2012.

DINNIMAN, M. S.; KLINCK, J. M.; SMITH, W. O. A model study of Circumpolar Deep Water on the West Antarctic Peninsula and Ross Sea continental shelves. **Deep-Sea Research Part II: Topical Studies in Oceanography**, v. 58, n. 13–16, p. 1508–1523, 2011.

DONEY, S. C.; FABRY, V. J.; FEELY, R. A; KLEYPAS, J. A. Ocean acidification: the other CO2 problem. **Annual Rev. Mar. Sci.**, v. 1, p. 169–192, 2009.

DOTTO, T. S.; KERR, R.; MATA, M. M.; GARCIA, C. A. E. Multidecadal freshening and lightening in the deep waters of the Bransfield Strait, Antarctica. **Journal of Geophysical Research: Oceans**, v. 121, n. 6, p. 3741–3756, jun. 2016.

DOTTO, T. S.; MATA, M. M.; KERR, R.; GARCIA, C. A. E. A novel hydrographic gridded data set for the northern Antarctic Peninsula. **Earth System Science Data**, v. 13, n. 2, p. 671–696, 26 fev. 2021.

DOVAL, M. D.; ÁLVAREZ-SALGADO, X. A.; CASTRO, C. G.; PÉREZ, F. F. Dissolved organic carbon distributions in the Bransfield and Gerlache Straits, Antarctica. **Deep-Sea Research Part II: Topical Studies in Oceanography**, v. 49, n. 4–5, p. 663–674, 2002.

DUCKLOW, H. W.; FRASER, W. R.; MEREDITH, M. P.; STAMMERJOHN, S. E.; DONEY, S. C.; MARTINSON, D. G.; SAILLEY, S. F.; SCHOFIELD, O. M.; STEINBERG, D. K.; VENABLES, H. J.; AMSLER, C. D. West Antarctic peninsula: An ice-dependent coastal marine ecosystem in transition. **Oceanography**, v. 26, n. 3, p. 190–203, 2013.

EMERSON, S.; HEDGES, J. **Chemical Oceanography and the Marine Carbon Cycle**. [s.l.] Cambridge University Press, 2008. v. 59

FABRY, V. J. Marine calcifiers in a high-CO2 ocean. **Science**, v. 320, n. May, p. 1020–1022, 2008.

FEELY, R.; DONEY, S.; COOLEY, S. Ocean acidification: Present conditions and future changes in a high-CO2 world. **Oceanography**, v. 22, n. 4, p. 36–47, 1 dez. 2009.

FIGUEROLA, B. *et al.* Predicting potential impacts of ocean acidification on marine calcifiers from the Southern Ocean. n. Lmc, p. 1–36, 2020.

FIGUEROLA, B.; HANCOCK, A. M.; BAX, N.; CUMMINGS, V. J.; DOWNEY, R.; GRIFFITHS, H. J.; SMITH, J.; STARK, J. S. A Review and Meta-Analysis of Potential Impacts of Ocean Acidification on Marine Calcifiers From the Southern Ocean. **Frontiers in Marine Science**, v. 8, n. January, 2021.

FISCHER, G. Stable carbon isotope ratios of plankton carbon and sinking organic matter from the Atlantic sector of the Southern Ocean. **Marine Chemistry**, v. 35, n. 1–4, p. 581–596, 1991.

FISK, M. R. Volcanism in the Bransfield Strait, Antarctica. **Journal of South American Earth Sciences**, v. 3, n. 2–3, p. 91–101, 1990.

FRIEDLINGSTEIN, P. *et al.* Global Carbon Budget 2021. **Earth Syst. Sci. Data Discuss. [preprint]**, n. November, 2021.

FRÖLICHER, T. L.; SARMIENTO, J. L.; PAYNTER, D. J.; DUNNE, J. P.; KRASTING, J. P.; WINTON, M. Dominance of the Southern Ocean in anthropogenic carbon and heat uptake in CMIP5 models. **Journal of Climate**, v. 28, n. 2, p. 862–886, 2015.

GARCÍA, M. A.; CASTRO, C. G.; RÍOS, A. F.; DOVAL, M. D.; ROSÓN, G.; GOMIS, D.; LÓPEZ, O. Water masses and distribution of physico-chemical properties in the Western Bransfield Strait and Gerlache Strait during Austral summer 1995/96. **Deep-Sea Research Part II: Topical Studies in Oceanography**, v. 49, n. 4–5, p. 585–602, 2002.

GILLE, S. T. Decadal-scale temperature trends in the Southern Hemisphere ocean. **Journal of Climate**, v. 21, n. 18, p. 4749–4765, 2008.

GORDON, A. L.; MENSCH, M.; DONG, Z.; SMETHIE, W. M.; BETTENCOURT, J. DE. Deep and bottom water of the Bransfield Strait eastern and central basins. **Journal of Geophysical Research: Oceans**, v. 105, n. C5, p. 11337–11346, 2000.

GOYET, C.; POISSON, A. New determination of carbonic acid dissociation constants in seawater as a function of temperature and salinity. **Deep Sea Research Part A. Oceanographic Research Papers**, v. 36, n. 11, p. 1635–1654, nov. 1989.

GREEN, C.; BYRNE, K. A. Biomass: Impact on Carbon Cycle and Greenhouse Gas Emissions. **Encyclopedia of Energy**, v. 1, p. 223–236, 2004.

GRUBER, N. *et al.* The oceanic sink for anthropogenic CO 2 from 1994 to 2007. **Science**, v. 363, n. 6432, p. 1193–1199, 2019.

GRUBER, N.; LANDSCHÜTZER, P.; LOVENDUSKI, N. S. The Variable Southern Ocean Carbon Sink. **Annual Review of Marine Science**, v. 11, n. 1, p. 159–186, 2019.

GYLDENFELDT, A. B. VON; FAHRBACH, E.; GARCÍA, M. A.; SCHRÖDER, M. Flow variability at the

tip of the Antarctic Peninsula. **Deep-Sea Research Part II: Topical Studies in Oceanography**, v. 49, n. 21, p. 4743–4766, 2002.

HANSSON, I. A new set of acidity constants for carbonic acid and boric acid in sea water. **Deep-Sea Research and Oceanographic Abstracts**, v. 20, n. 5, p. 461–478, 1973.

HAUCK, J.; HOPPEMA, M.; BELLERBY, R. G. J.; VÖLKER, C.; WOLF-GLADROW, D. Data-based estimation of anthropogenic carbon and acidification in the Weddell Sea on a decadal timescale. **Journal of Geophysical Research: Oceans**, v. 115, n. 3, p. 1–14, 2010.

HAUMANN, F. A.; GRUBER, N.; MÜNNICH, M.; FRENGER, I.; KERN, S.; ALEXANDER HAUMANN, F.; GRUBER, N.; MÜNNICH, M.; FRENGER, I.; KERN, S. Sea-ice transport driving Southern Ocean salinity and its recent trends. **Nature**, v. 537, n. 7618, p. 89–92, 2016.

HAURI, C.; DONEY, S. C.; TAKAHASHI, T.; ERICKSON, M.; JIANG, G.; DUCKLOW, H. W. Two decades of inorganic carbon dynamics along the West Antarctic Peninsula. **Biogeosciences**, v. 12, n. 22, p. 6761–6779, 2015.

HELLMER, H. H.; HUHN, O.; GOMIS, D.; TIMMERMANN, R. On the freshening of the northwestern Weddell Sea continental shelf. **Ocean Science**, v. 7, n. 3, p. 305–316, 2011.

HELLMER, H. H.; KAUKER, F.; TIMMERMANN, R.; HATTERMANN, T. The fate of the Southern Weddell sea continental shelf in a warming climate. **Journal of Climate**, v. 30, n. 12, p. 4337–4350, jun. 2017.

HENLEY, S. F. *et al.* Variability and change in the west Antarctic Peninsula marine system: Research priorities and opportunities. **Progress in Oceanography**, v. 173, n. March, p. 208–237, abr. 2019.

HENLEY, S. F. *et al.* Changing Biogeochemistry of the Southern Ocean and Its Ecosystem Implications. **Frontiers in Marine Science**, v. 7, n. July, p. 1–31, 31 jul. 2020.

HEUVEN, S. M. A. C. VAN; HOPPEMA, M.; JONES, E. M.; BAAR, H. J. W. DE. Rapid invasion of anthropogenic CO2 into the deep circulation of the Weddell Gyre. **Philosophical Transactions of the Royal Society A: Mathematical, Physical and Engineering Sciences**, v. 372, n. 2019, p. 1–11, 13 jul. 2014.

HOFMANN, E. E.; KLINCK, J. M.; LASCARA, C. M.; SMITH, D. A. Water mass distribution and circulation west of the Antarctic Peninsula and including Bransfield Strait. *In*: **Foundations for Ecological Research West of the Antarctic Peninsula: Antactic Research Series**. [s.l: s.n.]. p. 61–80.

HOUGHTON, R. A. The Contemporary Carbon Cycle. *In*: **Treatise on Geochemistry**. [s.l.] Elsevier, 2003. p. 473–513.

HOUGHTON, R. A. **The Contemporary Carbon Cycle**. 2. ed. [s.l.] Elsevier Ltd., 2013. v. 10

HUNEKE, W. G. C.; HUHN, O.; SCHRÖEDER, M. Water masses in the Bransfield Strait and adjacent seas, austral summer 2013. **Polar Biology**, v. 39, n. 5, p. 789–798, 2016.

INTERGOVERNMENTAL OCEANOGRAPHIC COMMISSION; SCIENTIFIC COMMITTEE ON OCEANIC RESEARCH; INTERNATIONAL ASSOCIATION FOR THE PHYSICAL SCIENCES OF THE OCEANS. The international thermodynamic equation of seawater – 2010: Calculation and use of thermodynamic properties. **Intergovernmental Oceanographic Commission, Manuals and Guides No. 56**, n. June, p. 196, 2010.

IPCC. Summary for Policymakers. *In*: MASSON-DELMOTTE, V. *et al.* (Eds.). . **Global Warming of 1.5°C. An IPCC Special Report on the impacts of global warming of 1.5°C above pre-industrial levels and related global greenhouse gas emission pathways, in the context of strengthening the global response to the threat of climate change,**. Geneva, Switzerland: [s.n.]. v. 18p. 32.

ITO, R. G.; TAVANO, V. M.; MENDES, C. R. B.; GARCIA, C. A. E. Sea-air CO2 fluxes and pCO2 variability in the Northern Antarctic Peninsula during three summer periods (2008–2010). **Deep-Sea Research Part II: Topical Studies in Oceanography**, v. 149, n. September 2017, p. 84–98, 2018.

ITO, T.; WOLOSZYN, M.; MAZLOFF, M. Anthropogenic carbon dioxide transport in the Southern Ocean driven by Ekman flow. **Nature**, v. 463, n. 7277, p. 80–83, 2010.

JIANG, L. Q.; CARTER, B. R.; FEELY, R. A.; LAUVSET, S. K.; OLSEN, A. Surface ocean pH and buffer capacity: past, present and future. **Scientific Reports**, v. 9, n. 1, p. 1–11, 2019.

JONES, E. M.; FENTON, M.; MEREDITH, M. P.; CLARGO, N. M.; OSSEBAAR, S.; DUCKLOW, H.

W.; VENABLES, H. J.; BAAR, H. J. W. DE. Ocean acidification and calcium carbonate saturation states in the coastal zone of the West Antarctic Peninsula. **Deep-Sea Research Part II: Topical Studies in Oceanography**, v. 139, n. January, p. 181–194, 2017.

KAPSENBERG, L.; KELLEY, A. L.; SHAW, E. C.; MARTZ, T. R.; HOFMANN, G. E. Near-shore Antarctic pH variability has implications for the design of ocean acidification experiments. **Scientific Reports**, v. 5, n. 1, p. 9638, 22 set. 2015.

KARL, D. M.; TILBROOK, B.; TIEN, G. Seasonal coupling of organic matter production and particle flux in the western Bransfield Strait, Antarctica. **Deep-Sea Research**, v. 38, p. 1097–1126, 1990.

KELLER, R. A.; FISK, M. R.; WHITE, W. M.; BIRKENMAJER, K. Isotopic and trace element constraints on mixing and melting models of marginal basin volcanism, Bransfield Strait, Antarctica. **Earth and Planetary Science Letters**, v. 111, n. 2–4, p. 287–303, 1992.

KERR, R.; GOYET, C.; CUNHA, L. C. DA; ORSELLI, I. B. M.; LENCINA-AVILA, J. M.; MENDES, C. R. B.; CARVALHO-BORGES, M.; MATA, M. M.; TAVANO, V. M. Carbonate system properties in the Gerlache Strait, Northern Antarctic Peninsula (February 2015): II. Anthropogenic CO2 and seawater acidification. **Deep-Sea Research Part II: Topical Studies in Oceanography**, v. 149, n. July 2017, p. 182–192, 2018.

KERR, R.; MATA, M. M.; MENDES, C. R. B.; SECCHI, E. R. Northern Antarctic Peninsula: a marine climate hotspot of rapid changes on ecosystems and ocean dynamics. **Deep-Sea Research Part II: Topical Studies in Oceanography**, v. 149, p. 4–9, 2018.

KERR, R.; ORSELLI, I. B. M.; LENCINA-AVILA, J. M.; EIDT, R. T.; MENDES, C. R. B.; CUNHA, L. C. DA; GOYET, C.; MATA, M. M.; TAVANO, V. M. Carbonate system properties in the Gerlache Strait, Northern Antarctic Peninsula (February 2015): I. Sea–Air CO2 fluxes. **Deep-Sea Research Part II: Topical Studies in Oceanography**, v. 149, n. February 2017, p. 171–181, 2018.

LAIKA, H. E.; GOYET, C.; VOUVE, F.; POISSON, A.; TOURATIER, F. Interannual properties of the CO2 system in the Southern Ocean south of Australia. **Antarctic Science**, v. 21, n. 6, p. 663–680, 2009.

LAUVSET, S. K.; CARTER, B. R.; PEREZ, F. F.; JIANG, L. Q.; FEELY, R. A.; VELO, A.; OLSEN, A. Processes Driving Global Interior Ocean pH Distribution. **Global Biogeochemical Cycles**, v. 34, n. 1, p. 1–17, 2020.

LAUVSET, S. K.; GRUBER, N.; LANDSCHÜTZER, P.; OLSEN, A.; TJIPUTRA, J. Trends and drivers in global surface ocean pH over the past 3 decades. **Biogeosciences**, v. 12, n. 5, p. 1285–1298, 2015.

LEE, K.; TONG, L. T.; MILLERO, F. J.; SABINE, C. L.; DICKSON, A. G.; GOYET, C.; PARK, G. H.; WANNINKHOF, R.; FEELY, R. A.; KEY, R. M. Global relationships of total alkalinity with salinity and temperature in surface waters of the world's oceans. **Geophysical Research Letters**, v. 33, n. 19, 2006.

LEGGE, O. J.; BAKKER, D. C. E.; MEREDITH, M. P.; VENABLES, H. J.; BROWN, P. J.; JONES, E. M.; JOHNSON, M. T. The seasonal cycle of carbonate system processes in Ryder Bay, West Antarctic Peninsula. **Deep Sea Research Part II: Topical Studies in Oceanography**, v. 139, n. November 2016, p. 167–180, maio 2017.

LENCINA-AVILA, J. M.; GOYET, C.; KERR, R.; ORSELLI, I. B. M.; MATA, M. M.; TOURATIER, F. Past and future evolution of the marine carbonate system in a coastal zone of the Northern Antarctic Peninsula. **Deep-Sea Research Part II: Topical Studies in Oceanography**, v. 149, n. December 2017, p. 193–205, 2018.

LESEURRE, C.; MONACO, C. LO; REVERDIN, G.; METZL, N.; FIN, J.; MIGNON, C.; BENITO, L. Trends and driversof sea surface fCO2 and pH changes observed in Southern Indian Ocean over the last two decades. **Biogeosciences**, v. 19, n. 10, p. 2599–2625, 2022.

LEWIS, E.; WALLACE, D. **Program developed for CO2 system calculationsOrnl/Cdiac-105**Oak Ridge, TennCarbon Dioxide Information Analysis Center, , 1998. Disponível em: <http://cdiac.esd.ornl.gov/oceans/co2rprtnbk.html>

LOEB, V. J.; HOFMANN, E. E.; KLINCK, J. M.; HOLM-HANSEN, O.; WHITE, W. B. ENSO and variability of the antarctic peninsula pelagic marine ecosystem. **Antarctic Science**, v. 21, n. 2, p. 135–148, 2009.

LOPEZ, O.; GARCIA, M. A.; GOMIS, D.; ROJAS, P.; SOSPEDRA, J.; ARCILLA-SÁNCHEZ, A. Hydrographic and hydrodynamic characteristics a of the eastern basin of the Bransfiled Strait. **Deep Sea Research Part I: Oceanographic Research Papers**, v. 46, p. 1755–1778, 1999.

LUEKER, T. J.; DICKSON, A. G.; KEELING, C. D. Ocean pCO2 calculated from dissolved inorganic carbon, alkalinity, and equations for K1 and K2: Validation based on laboratory measurements of CO2 in gas and seawater at equilibrium. **Marine Chemistry**, v. 70, n. 1–3, p. 105–119, 2000.

MARSHALL, G. J.; ORR, A.; LIPZIG, N. P. M. VAN; KING, J. C. The impact of a changing Southern Hemisphere Annular Mode on Antarctic Peninsula summer temperatures. **Journal of Climate**, v. 19, n. 20, p. 5388–5404, 2006.

MASQUÉ, P.; ISLA, E.; SANCHEZ-CABEZA, J. A.; PALANQUES, A.; BRUACH, J. M.; PUIG, P.; GUILLÉN, J. Sediment accumulation rates and carbon fluxes to bottom sediments at the western Bransfield Strait (Antarctica). **Deep-Sea Research Part II: Topical Studies in Oceanography**, v. 49, n. 4–5, p. 921–933, 2002.

MASSOM, R. A.; SCAMBOS, T. A.; BENNETTS, L. G.; REID, P.; SQUIRE, V. A.; STAMMERJOHN, S. E. Antarctic ice shelf disintegration triggered by sea ice loss and ocean swell. **Nature**, v. 558, n. 7710, p. 383–389, 2018.

MATA, M. M.; TAVANO, V. M.; GARCIA, C. A. E. 15 years sailing with the Brazilian High Latitude Oceanography Group (GOAL). **Deep-Sea Research Part II: Topical Studies in Oceanography**, v. 149, p. 1–3, mar. 2018.

MCNEIL, B. I.; MATEAR, R. J. Southern Ocean acidification: A tipping point at 450-ppm atmospheric CO2. **Proceedings of the National Academy of Sciences of the United States of America**, v. 105, n. 48, p. 18860–18864, 2008.

MEHRBACH, C.; CULBERSON, C. H.; HAWLEY, J. E.; PYTKOWICX, R. M. Measurement of the Apparent Dissociation Constants of Carbonic Acid in Seawater At Atmospheric Pressure. **Limnology and Oceanography**, v. 18, n. 6, p. 897–907, 1973.

MENDES, C. R. B.; SOUZA, M. S. DE; GARCIA, V. M. T.; LEAL, M. C.; BROTAS, V.; GARCIA, C. A.

E. Dynamics of phytoplankton communities during late summer around the tip of the Antarctic Peninsula. **Deep-Sea Research Part I: Oceanographic Research Papers**, v. 65, p. 1–14, 2012.

MEREDITH, M. P.; BRANDON, M. A.; WALLACE, M. I.; CLARKE, A.; LENG, M. J.; RENFREW, I. A.; LIPZIG, N. P. M. VAN; KING, J. C. Variability in the freshwater balance of northern Marguerite Bay, Antarctic Peninsula: Results from δ18O. **Deep-Sea Research Part II: Topical Studies in Oceanography**, v. 55, n. 3–4, p. 309–322, 2008.

MEREDITH, M. P.; JULLION, L.; BROWN, P. J.; GARABATO, A. C. N.; COULDREY, M. P. Dense waters of the Weddell and Scotia seas: Recent changes in properties and circulation. **Philosophical Transactions of the Royal Society A: Mathematical, Physical and Engineering Sciences**, v. 372, n. 2019, p. 1–11, 2014.

MEREDITH, M. P.; KING, J. C. Rapid climate change in the ocean west of the Antarctic Peninsula during the second half of the 20th century. **Geophysical Research Letters**, v. 32, n. 19, p. 1–5, 2005.

MIDORIKAWA, T.; INOUE, H. Y.; ISHII, M.; SASANO, D.; KOSUGI, N.; HASHIDA, G.; NAKAOKA, S. ICHIRO; SUZUKI, T. Decreasing pH trend estimated from 35-year time series of carbonate parameters in the Pacific sector of the Southern Ocean in summer. **Deep-Sea Research Part I: Oceanographic Research Papers**, v. 61, p. 131–139, 2012.

MILLERO, F. J. The Marine Inorganic Carbon Cycle. **Chemical Reviews**, v. 107, n. 2, p. 308–341, fev. 2007.

MILLERO, F. J. **Chemical Oceanography**. [s.l.] CRC Press, 2016. v. 30

MILLERO, F. J.; GRAHAM, T. B.; HUANG, F.; BUSTOS-SERRANO, H.; PIERROT, D. Dissociation constants of carbonic acid in seawater as a function of salinity and temperature. **Marine Chemistry**, v. 100, n. 1–2, p. 80–94, 2006.

MILLERO, F. J.; LEE, K.; ROCHE, M. Distribution of alkalinity in the surface waters of the major oceans. **Marine Chemistry**, v. 60, n. 1–2, p. 111–130, 1998.

MILLERO, F. J.; PIERROT, D.; LEE, K.; WANNINKHOF, R.; FEELY, R.; SABINE, C. L.; KEY, R. M.; TAKAHASHI, T. Dissociation constants for carbonic acid determined from field measurements. **Deep-**

Sea Research Part I: Oceanographic Research Papers, v. 49, n. 10, p. 1705–1723, 2002.

MOFFAT, C.; MEREDITH, M. Shelf-ocean exchange and hydrography west of the Antarctic Peninsula: A review. **Philosophical Transactions of the Royal Society A: Mathematical, Physical and Engineering Sciences**, v. 376, n. 2122, 2018.

MOFFAT, C.; OWENS, B.; BEARDSLEY, R. C. On the characteristics of Circumpolar Deep Water intrusions to the west Antarctic Peninsula Continental Shelf. **Journal of Geophysical Research: Oceans**, v. 114, n. 5, p. 1–16, 2009.

MONTEIRO, T.; KERR, R.; MACHADO, E. DA C. Seasonal variability of net sea-air CO2 fluxes in a coastal region of the northern Antarctic Peninsula. **Scientific Reports**, v. 10, n. 1, p. 14875, 10 dez. 2020.

MONTEIRO, T.; KERR, R.; ORSELLI, I. B. M.; LENCINA-AVILA, J. M. Towards an intensified summer CO2 sink behaviour in the Southern Ocean coastal regions. **Progress in Oceanography**, v. 183, n. January, p. 1–13, 2020.

ORR, J. C. *et al.* Anthropogenic ocean acidification over the twenty-first century and its impact on calcifying organisms. **Nature**, v. 437, n. 7059, p. 681–686, 2005.

ORR, J. C.; EPITALON, J. M.; DICKSON, A. G.; GATTUSO, J. P. Routine uncertainty propagation for the marine carbon dioxide system. **Marine Chemistry**, v. 207, n. June, p. 84–107, 2018.

ORSELLI, I. B. M.; CARVALHO, A. C. O.; MONTEIRO, T.; DAMINI, B. Y.; CARVALHO-BORGES, M. DE; ALBUQUERQUE, C.; KERR, R. The marine carbonate system along the northern Antarctic Peninsula: current knowledge and future perspectives. **Anais da Academia Brasileira de Ciências**, v. 94, n. suppl 1, 2022.

PARDO, P. C.; PÉREZ, F. F.; KHATIWALA, S.; RÍOS, A. F. Anthropogenic CO2 estimates in the Southern Ocean: Storage partitioning in the different water masses. **Progress in Oceanography**, v. 120, p. 230–242, 2014.

RAVEN, J.; CALDEIRA, K.; ELDERFIELD, H.; HOEGH-GULDBERG, O.; LISS, P.; RIEBESELL, U.; SHEPHERD, J.; TURLEY, C.; WATSON, A. **Ocean acidification due to increasing atmospheric**

carbon dioxideCoral Reefs. [s.l: s.n.]. Disponível em: <http://eprints.ifm-geomar.de/7878/1/965_Raven_2005_OceanAcidificationDueToIncreasing_Monogr_pubid13120.pdf>.

REID, P. A.; MASSOM, R. A. Change and variability in Antarctic coastal exposure, 1979–2020. **Nature Communications**, v. 13, n. 1164, p. 1–11, 2022.

RENFORTH, P.; HENDERSON, G. Assessing ocean alkalinity for carbon sequestration. **Reviews of Geophysics**, v. 55, n. 3, p. 636–674, 2017.

RENNER, A. H. H.; THORPE, S. E.; HEYWOOD, K. J.; MURPHY, E. J.; WATKINS, J. L.; MEREDITH, M. P. Advective pathways near the tip of the Antarctic Peninsula: Trends, variability and ecosystem implications. **Deep-Sea Research Part I: Oceanographic Research Papers**, v. 63, p. 91–101, 2012.

RIGNOT, E.; MOUGINOT, J.; SCHEUCHL, B.; BROEKE, M. VAN DEN; WESSEM, M. J. VAN; MORLIGHEM, M. Four decades of Antarctic ice sheet mass balance from 1979–2017. **Proceedings of the National Academy of Sciences of the United States of America**, v. 116, n. 4, p. 1095–1103, 2019.

RIVARO, P.; MESSA, R.; IANNI, C.; MAGI, E.; BUDILLON, G. Distribution of total alkalinity and pH in the Ross Sea (Antarctica) waters during austral summer 2008. **Polar Research**, v. 33, n. 2014, 2014.

RODEN, N. P.; SHADWICK, E. H.; TILBROOK, B.; TRULL, T. W. Annual cycle of carbonate chemistry and decadal change in coastal. **Marine Chemistry**, v. 155, p. 135–147, 2013.

ROY, R. N.; ROY, L. N.; VOGEL, K. M.; PORTER-MOORE, C.; PEARSON, T.; GOOD, C. E.; MILLERO, F. J.; CAMPBELL, D. M. The dissociation constants of carbonic acid in seawater at salinities 5 to 45 and temperatures 0 to 45°C. **Marine Chemistry**, v. 44, n. 2–4, p. 249–267, 1993.

RUIZ BARLETT, E. M.; TOSONOTTO, G. V.; PIOLA, A. R.; SIERRA, M. E.; MATA, M. M. On the temporal variability of intermediate and deep waters in the Western Basin of the Bransfield Strait. **Deep-Sea Research Part II: Topical Studies in Oceanography**, v. 149, n. December 2017, p. 31–46, 2018.

SABINE, C. L. *et al.* The Oceanic Sink for Anthropogenic CO2. **Science**, v. 305, n. 5682, p. 367–371, 16 jul. 2004.

SABINE, C. L.; FEELY, R. A.; MILLERO, F. J.; DICKSON, A. G.; LANGDON, C.; MECKING, S.; GREELEY, D. Decadal changes in Pacific carbon. **Journal of Geophysical Research: Oceans**, v. 113, n. 7, p. 1–12, 2008.

SANDRINI, S.; AIT-AMEUR, N.; RIVARO, P.; MASSOLO, S.; TOURATIER, F.; TOSITTI, L.; GOYET, C. Anthropogenic carbon distribution in the Ross Sea, Antarctica. **Antarctic Science**, v. 19, n. 3, p. 395–407, 2007.

SANGRÀ, P.; GORDO, C.; HERNÁNDEZ-ARENCIBIA, M.; MARRERO-DÍAZ, A.; RODRÍGUEZ-SANTANA, A.; STEGNER, A.; MARTÍNEZ-MARRERO, A.; PELEGRÍ, J. L.; PICHON, T. The Bransfield current system. **Deep-Sea Research Part I: Oceanographic Research Papers**, v. 58, n. 4, p. 390–402, 2011.

SANGRÀ, P.; STEGNER, A.; HERNÁNDEZ-ARENCIBIA, M.; MARRERO-DÍAZ, Á.; SALINAS, C.; AGUIAR-GONZÁLEZ, B.; HENRÍQUEZ-PASTENE, C.; MOURIÑO-CARBALLIDO, B. The Bransfield Gravity Current. **Deep-Sea Research Part I: Oceanographic Research Papers**, v. 119, n. November 2016, p. 1–15, jan. 2017.

SCAMBOS, T. A.; HULBE, C.; FAHNESTOCK, M.; BOHLANDER, J. The link between climate warming and break-up of ice shelves in the Antarctic Peninsula. **Journal of Glaciology**, v. 46, n. 154, p. 516–530, 2000.

SHEPHERD, A. *et al.* Mass balance of the Antarctic Ice Sheet from 1992 to 2017. **Nature**, v. 558, n. 7709, p. 219–222, 13 jun. 2018.

SHEPHERD, A.; WINGHAM, D.; RIGNOT, E. Warm ocean is eroding West Antarctic Ice Sheet. **Geophysical Research Letters**, v. 31, n. 23, p. 1–4, 2004.

SIEGERT, M. *et al.* The Antarctic Peninsula under a 1.5°C global warming scenario. **Frontiers in Environmental Science**, v. 7, n. JUN, p. 1–7, 2019.

SIGNORI, C. N.; THOMAS, F.; ENRICH-PRAST, A.; POLLERY, R. C. G.; SIEVERT, S. M. Microbial diversity and community structure across environmental gradients in Bransfield Strait, Western Antarctic Peninsula. **Frontiers in Microbiology**, v. 5, n. DEC, p. 1–12, 2014.

STIPS, A.; BOLDING, K.; MACIAS, D.; BRUGGEMAN, J.; COUGHLAN, C. **Scoping report on the potential impact of on-board desulphurisation on the water quality in SOx Emission Control Areas 2016**. [s.l: s.n.].

TAKAHASHI, T.; SUTHERLAND, S. C.; CHIPMAN, D. W.; GODDARD, J. G.; HO, C. Climatological distributions of pH, pCO2, total CO2, alkalinity, and CaCO3 saturation in the global surface ocean, and temporal changes at selected locations. **Marine Chemistry**, v. 164, p. 95–125, 2014.

THOMPSON, D. W. J.; SOLOMON, S. Interpretation of recent Southern Hemisphere climate change. **Science**, v. 296, n. 5569, p. 895–899, 2002.

TORRES-LASSO, J. C. **Acidificação oceânica e variação interanual de CO2 antropogênico no estreito de Bransfield, Antártica**. [s.l.] Universidade Federal do Rio Grande, 2019.

TORRES PARRA, R. R.; CAICEDO LAURIDO, A. L.; IRIARTE SÁNCHEZ, J. D. Hydrographic conditions during two austral summer situations (2015 and 2017) in the Gerlache and Bismarck straits, northern Antarctic Peninsula. **Deep-Sea Research Part I: Oceanographic Research Papers**, v. 161, n. April, 2020.

TOURATIER, F.; AZOUZI, L.; GOYET, C. CFC-11, Δ14C and 3H tracers as a means to assess anthropogenic CO2 concentrations in the ocean. **Tellus, Series B: Chemical and Physical Meteorology**, v. 59, n. 2, p. 318–325, 2007.

TOURATIER, F.; GOYET, C. Definition, properties, and Atlantic Ocean distribution of the new tracer TrOCA. **Journal of Marine Systems**, v. 46, n. 1–4, p. 169–179, 2004a.

___. Applying the new TrOCA approach to assess the distribution of anthropogenic CO2 in the Atlantic Ocean. **Journal of Marine Systems**, v. 46, n. 1–4, p. 181–197, 2004b.

TURLEY, C.; FINDLAY, H. S. **Ocean Acidification**. Second Edi ed. [s.l.] Elsevier B.V., 2016. v. 1

TURNER, S.; TONARINI, S.; BINDEMAN, I.; LEEMAN, W. P.; SCHAEFER, B. F. Boron and oxygen isotope evidence for recycling of subducted components over the past 2.5 Gyr. **Nature**, v. 447, n. 7145, p. 702–705, 2007.

TYNAN, E.; CLARKE, J. S.; HUMPHREYS, M. P.; RIBAS-RIBAS, M.; ESPOSITO, M.; RÉROLLE, V.

M. C.; SCHLOSSER, C.; THORPE, S. E.; TYRRELL, T.; ACHTERBERG, E. P. Physical and biogeochemical controls on the variability in surface pH and calcium carbonate saturation states in the Atlantic sectors of the Arctic and Southern Oceans. **Deep Sea Research Part II: Topical Studies in Oceanography**, v. 127, p. 7–27, maio 2016.

UPPSTRÖM, L. R. The boron/chlorinity ratio of deep-sea water from the Pacific Ocean. **Deep-Sea Research and Oceanographic Abstracts**, v. 21, n. 2, p. 161–162, 1974.

WANG, X.; MOFFAT, C.; DINNIMAN, M. S.; KLINCK, J. M.; SUTHERLAND, D. A.; AGUIAR-GONZÁLEZ, B. Variability and Dynamics of Along-Shore Exchange on the West Antarctic Peninsula (WAP) Continental Shelf. **Journal of Geophysical Research: Oceans**, v. 127, n. 2, 2022.

WANNINKHOF, R.; LEWIS, E.; FEELY, R. A.; MILLERO, F. J. The optimal carbonate dissociation constants for determining surface water pCO2 from alkalinity and total inorganic carbon. **Marine Chemistry**, v. 65, n. 3–4, p. 291–301, 1999.

WATSON, A. J.; SCHUSTER, U.; SHUTLER, J. D.; HOLDING, T.; ASHTON, I. G. C.; LANDSCHÜTZER, P.; WOOLF, D. K.; GODDIJN-MURPHY, L. Revised estimates of ocean-atmosphere CO2 flux are consistent with ocean carbon inventory. **Nature Communications**, v. 11, n. 1, p. 1–6, 2020.

WILLE, J. D. *et al.* Intense atmospheric rivers can weaken ice shelf stability at the Antarctic Peninsula. **Communications Earth & Environment**, v. 3, n. 90, p. 1–14, 2022.

WILSON, C.; KLINKHAMMER, G. P.; CHIN, C. S. Hydrography within the central and east basins of the Bransfield Strait, Antarctica. **Journal of Physical Oceanography**, v. 29, n. 3, p. 465–479, 1999.

WOLF-GLADROW, D. A.; ZEEBE, R. E.; KLAAS, C.; KÖRTZINGER, A.; DICKSON, A. G. Total alkalinity: The explicit conservative expression and its application to biogeochemical processes. **Marine Chemistry**, v. 106, n. 1- 2 SPEC. ISS., p. 287–300, 2007.

YANJUN, W.; LI, X.; SONG, J.; LI, X.; ZHONG, G.; ZHANG, B. Carbon Sinks and Variations of pCO2 in the Southern Ocean from 1998 to 2018 Based on a Deep Learning Approach. **IEEE Journal of Selected Topics in Applied Earth Observations and Remote Sensing**, n. March, p. 1–1, 2021.

ZEEBE, R. E. History of seawater carbonate chemistry, atmospheric CO 2, and ocean acidification. **Annual Review of Earth and Planetary Sciences**, v. 40, p. 141–165, 2012.

ZEEBE, R. E.; WOLF-GLADROW, D. A. **CO2 in Seawater: Equilibrium, Kinetics, Isotopes**. Second pri ed. [s.l.] Elsevier, 2001.

ZHOU, M.; NIILER, P. P.; ZHU, Y.; DORLAND, R. D. The western boundary current in the Bransfield Strait, Antarctica. **Deep-Sea Research Part I: Oceanographic Research Papers**, v. 53, n. 7, p. 1244–1252, 2006.

Capítulo V

Este capítulo apresenta o material suplementar do artigo científico apresentado no capítulo IV.

SUPPLEMENTARY MATERIAL

Drivers of Marine CO_2-Carbonate Chemistry in the Northern Antarctic Peninsula

Maurício Santos-Andrade[1,2], Rodrigo Kerr[1,2], Iole B. M. Orselli[1,2], Thiago Monteiro[1,2], Mauricio M. Mata[1,2], and Catherine Goyet[3,4]

[1]Laboratório de Estudos dos Oceanos e Clima, Instituto de Oceanografia, Universidade Federal do Rio Grande – FURG, Rio Grande, RS, 96203-900, Brazil.
[2]Programa de Pós-Graduação em Oceanologia, Instituto de Oceanografia, Universidade Federal do Rio Grande – FURG, Rio Grande, RS, 96203-900, Brazil.
[3]IMAGES_ESPACE-DEV, Université de Perpignan Via Domitia, 52 ave. Paul Alduy, 66860 Cedex Perpignan, France.
[4]ESPACE-DEV UMR UG UA UM IRD, Maison de la télédétection, 500 rue Jean-François Breton, 34093 Montpellier Cedex 5, France.

Corresponding authors: Mauricio Santos-Andrade (mauriciosa@furg.br) and Rodrigo Kerr (rodrigokerr@furg.br)

Supplementary information.

This file contains:

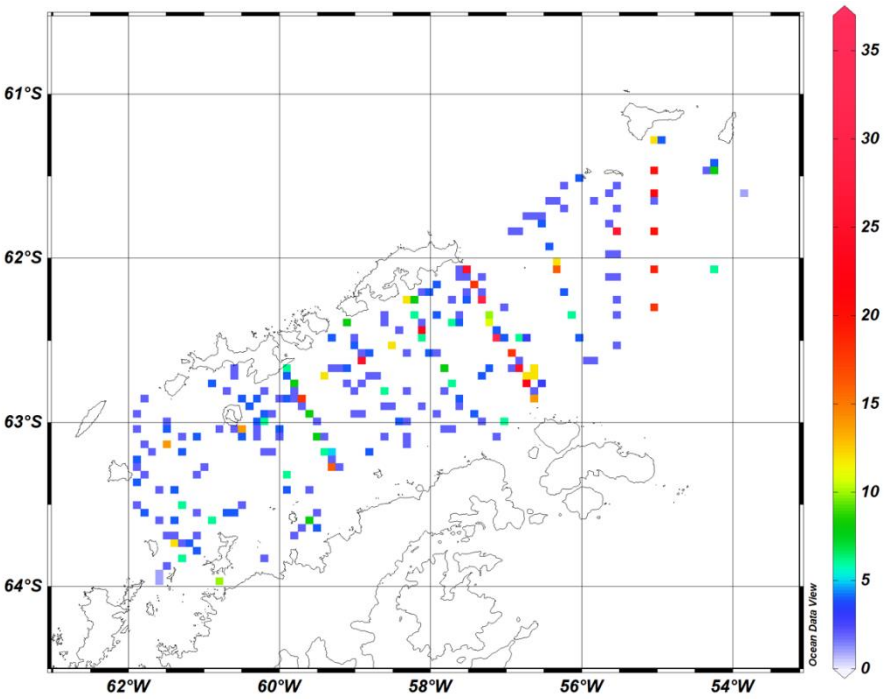

Figure V.1. Station counts over the 30 years of data used in this study.

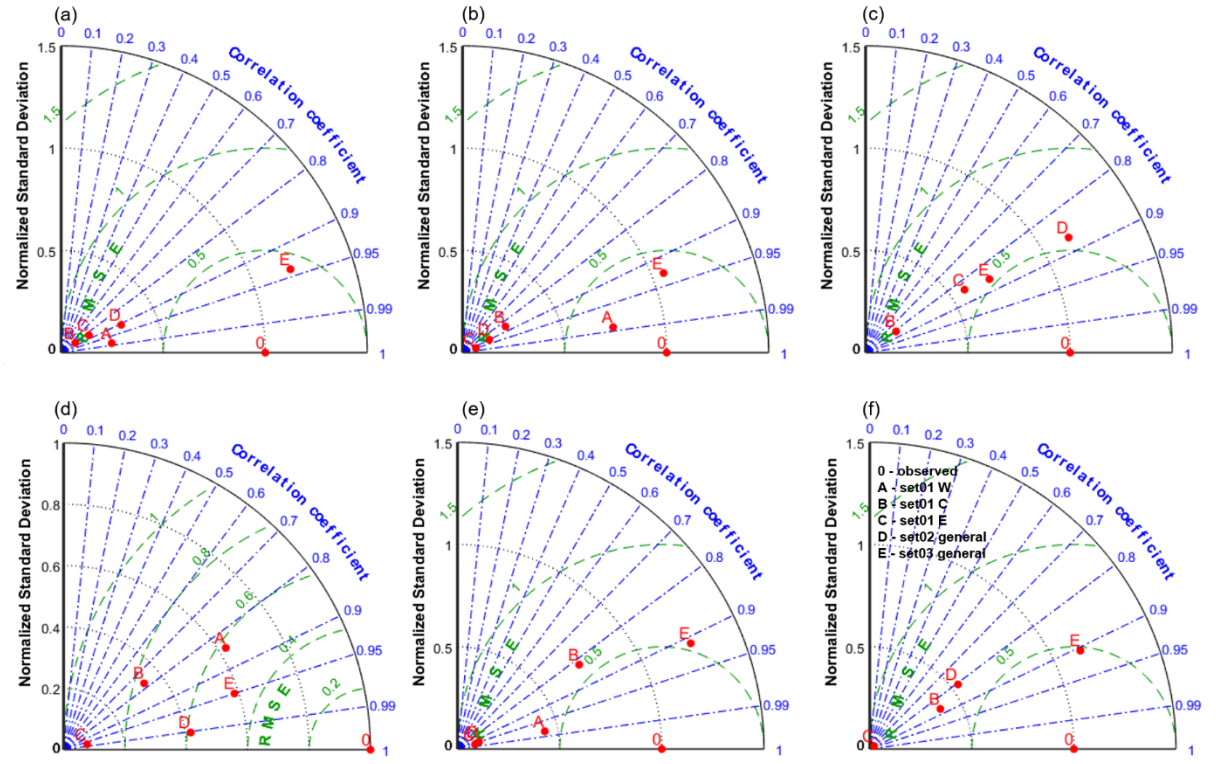

Figure V.2. Taylor diagram comparing the best-fitted equations from several trials performed along this study for total alkalinity - TA (upper line) and total inorganic carbon - CT (lower line) for (a and d) surface, (b and e) intermediate, and (c and f) deep layers. The set01 represents those equations applicable for each layer (i.e., surface, intermediate, and deep) of each basin (i.e., western, central, and eastern) from the Bransfield Strait. The set02 and set03 are more general, applicable to each respective layer from the whole strait. The difference between both sets is the input data: set02 used specific years as input data whereas set03 used random data along the available data. For all sets, validation was determined through the data did not used on reconstruction.

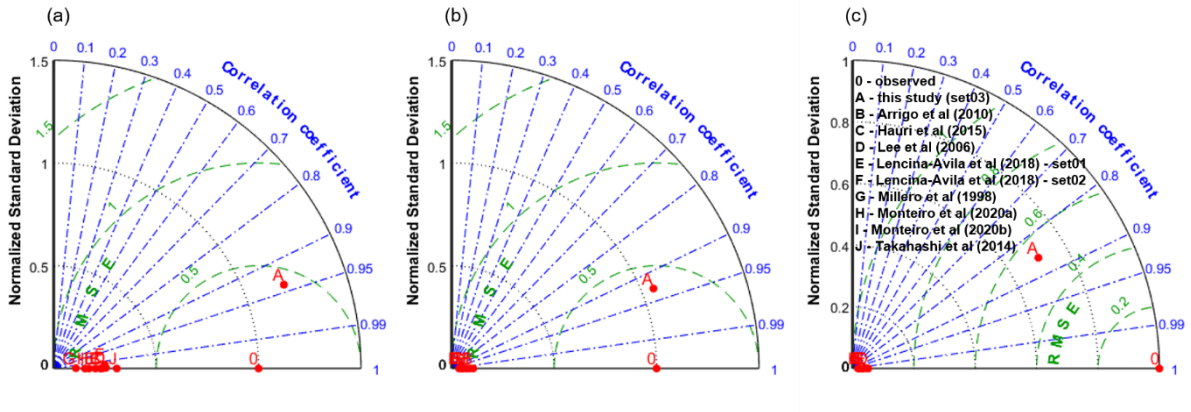

Figure V.3. Taylor diagram presenting different equations set for total alkalinity - TA in the (a) surface, (b) intermediate, and (c) deep layers developed by this study and other authors. This comparison is based on those equations which used temperature and salinity in order to estimate TA. Equations for regional (Lee *et al.*, 2006; Millero, Lee e Roche, 1998; Takahashi *et al.*, 2014), local, around the Antarctic Peninsula (Hauri *et al.*, 2015; Lencina-Avila *et al.*, 2018; Monteiro *et al.*, 2020; Monteiro, Kerr e Machado, 2020), and one from the Arctic Ocean (Arrigo *et al.*, 2010) were chosen and applied in our *in situ* data. Once most of them are suitable for surface waters, we tested their effects on reconstruction throughout the water column. Lencina-Avila et al. (2018) created another set for deep layers in the Gerlache Strait, in both southern (mentioned by set01 following its author) and northern (mentioned by set02 following its author) Gerlache area. Thereby, we assessed both equation sets where those related to mixed layers were considered suitable for the whole water column assuming it is well-homogenized.

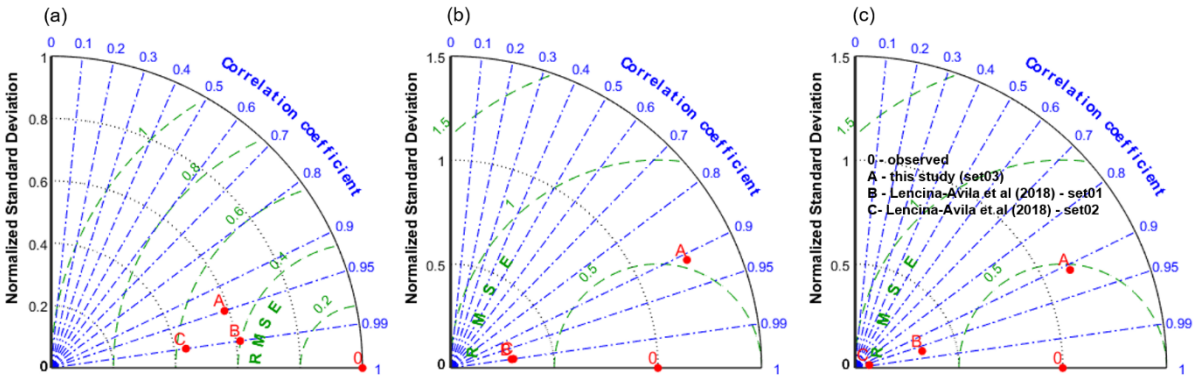

Figure V.4. Taylor diagram presenting different equations set for total inorganic carbon - CT in the (a) surface, (b) intermediate, and (c) deep layers developed by this study and other authors. This comparison is based on those equations which used temperature, salinity and dissolved oxygen in order to estimate CT. The same criterion used on Figure V.2 is valid here.

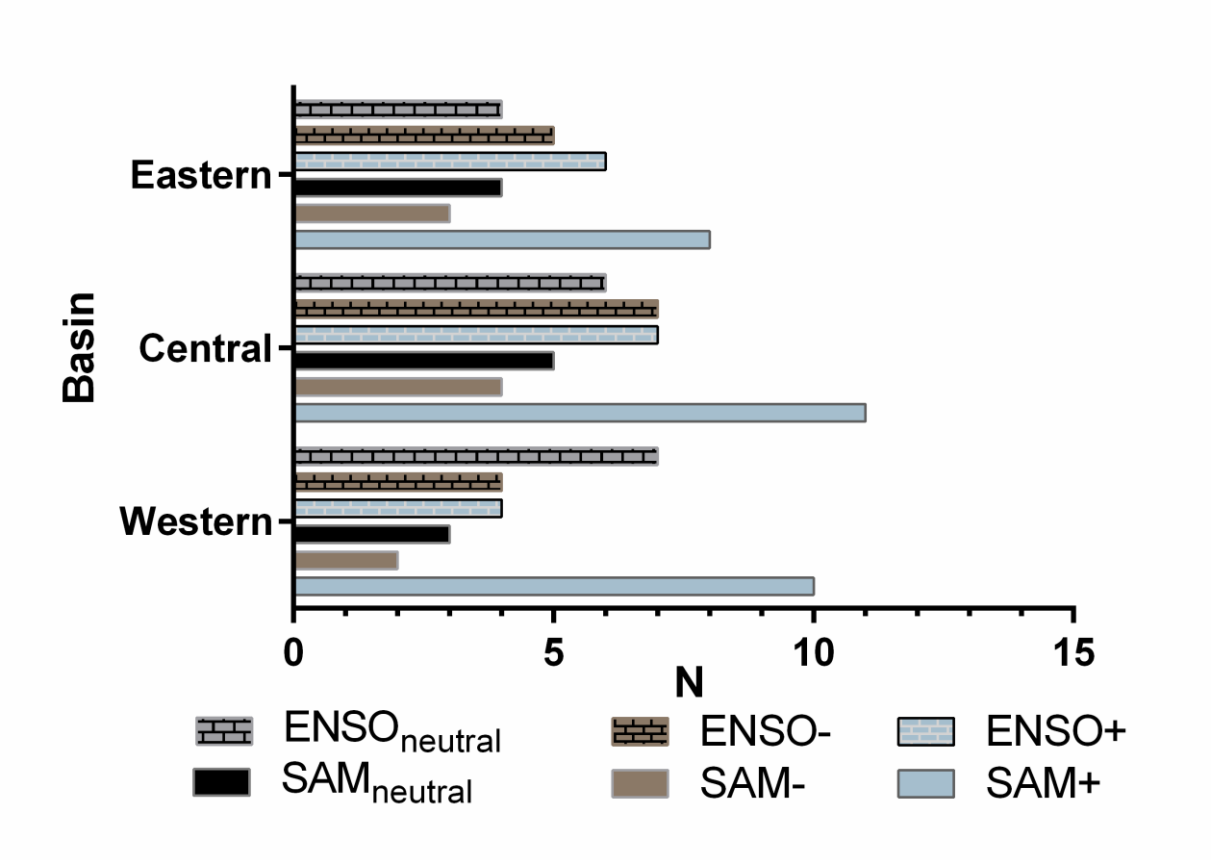

Figure V.5. Number of years used on each phase of the mode of climate variability by index composited in this study, considering the El Niño – Southern Oscillation – ENSO (as Oceanic Niño Index) and Southern Annular Mode – SAM. The number of years is presented by each basin of the Bransfield Strait based on the summer average of ENSO and SAM indexes, which were obtained at the websites: https://origin.cpc.ncep.noaa.gov/products/analysis_monitoring/ensostuff/ONI_v5.php and http://www.nerc-bas.ac.uk/icd/gjma/sam.html, respectively.

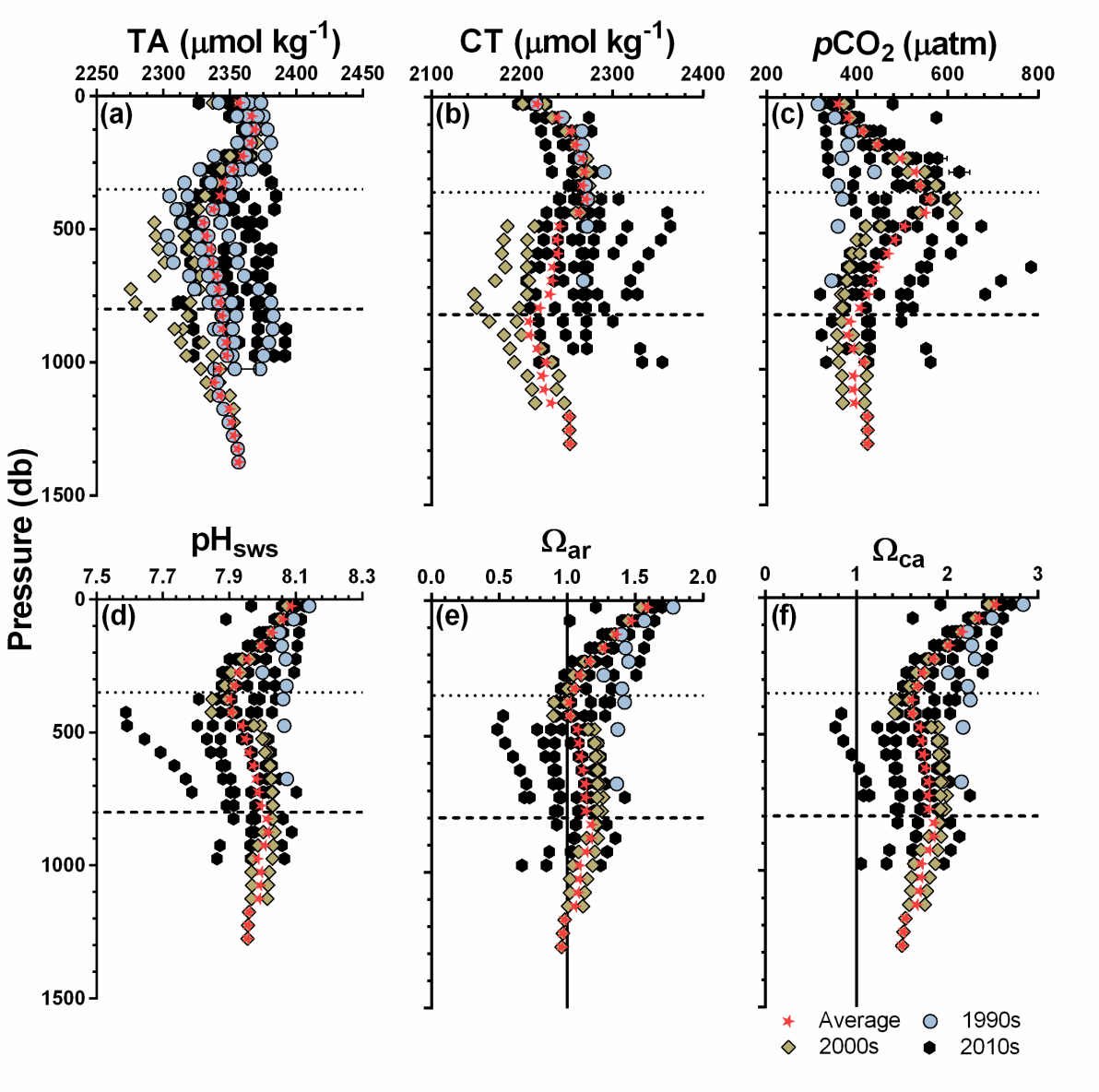

Figure V.6. Annual and total (average of the whole dataset) vertical profiles of the carbonate system in the western basin. Data plotted are (a) total alkalinity (TA), (b) total inorganic carbon (CT), (c) partial pressure of carbon dioxide (pCO_2), (d) pH_{sws} (seawater scale), calcium carbonate state for (e) aragonite (Ω_{ar}) and (f) calcite (Ω_{ca}) for 1990s (blue circles), 2000s (brown diamonds), and 2010s (black hexagons). Vertical profile marked as red star is the total average relative to the whole annual vertical profiles. Dotted and dashed lines highlight the boundary of surface-intermediate (i.e., γ^n = 28.00 kg m^{-3}) and intermediate-deep (i.e., γ^n = 28.27 kg m^{-3}) layers.

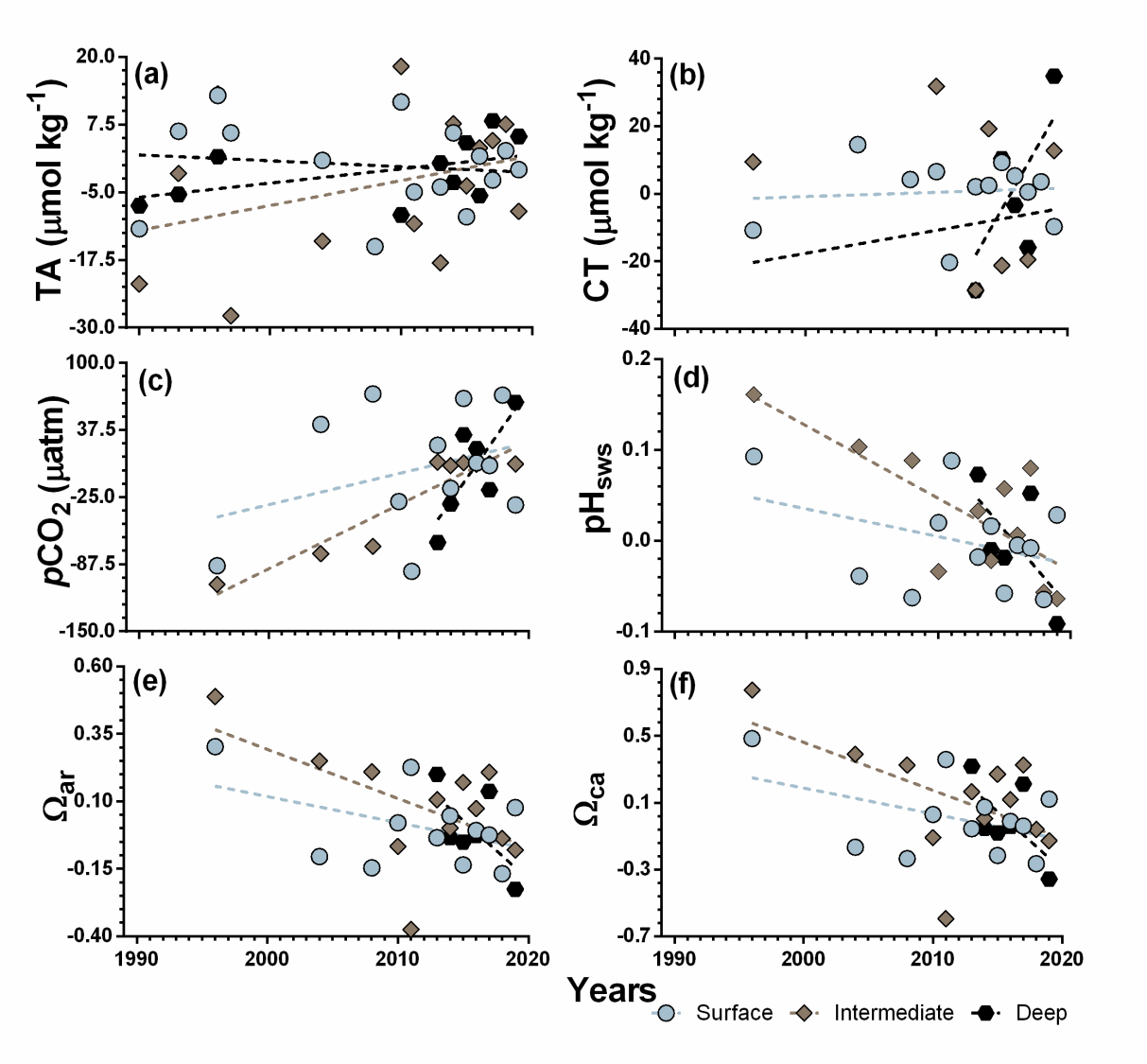

Figure V.7. Time series of carbonate system parameters throughout the 30 years used in this study for the western basin and water mass layers in the Bransfield Strait. Plotted data are annual anomalies for (a) total alkalinity – TA, (b) total inorganic carbon – CT, (c) partial pressure of carbon dioxide – pCO_2, (d) pH_{sws} (seawater scale), (e) aragonite saturation state – Ω_{ar}, and (f) calcite saturation state – Ω_{ca}. Trend line for each layer is showed as a dashed line based on anomaly data (see legend for details with regard to colours and their respective layers), which values are described in Table IV.2.

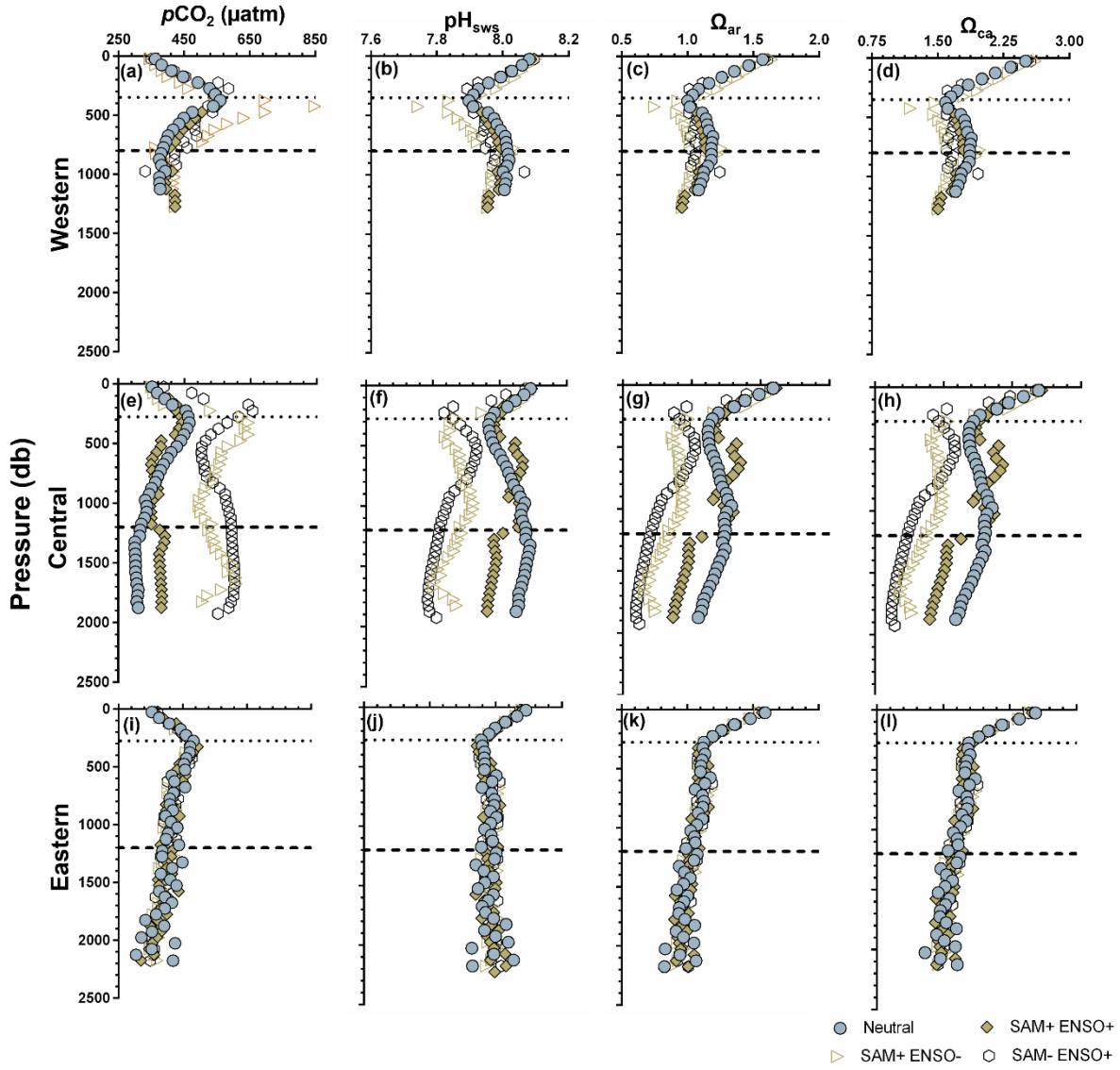

Figure V.8. Vertical distribution of other carbonate system parameters (a, e, and i - partial pressure of carbon dioxide - pCO_2; b, f, and j - pH_{sws}; c, g, and k - saturation state of aragonite - Ω_{ar}; d, h, and l - saturation state of calcite - Ω_{ca}) composited for years considering the phases of the climate modes El Niño – Southern Oscillation (ENSO) and Southern Annular Mode (SAM). Averaged carbonate system parameters profiles at the western (first arrow; a, b, c, and d), central (second arrow; e, f, g, and h), and eastern (third arrow; i, j, k, and l) basins of the Bransfield Strait with respect to different coupled interactions between ENSO and SAM phases. The years related to each composition are presented in Table V.7. The neutral profile for the western basin was estimated by the mean of the vertical profiles for neutral of SAM and ENSO, which we found a standard deviation about 0.03 for pH, 7.6 µatm for pCO_2, 0.03 for Ω_{ar}, and 0.05 for Ω_{ca}.

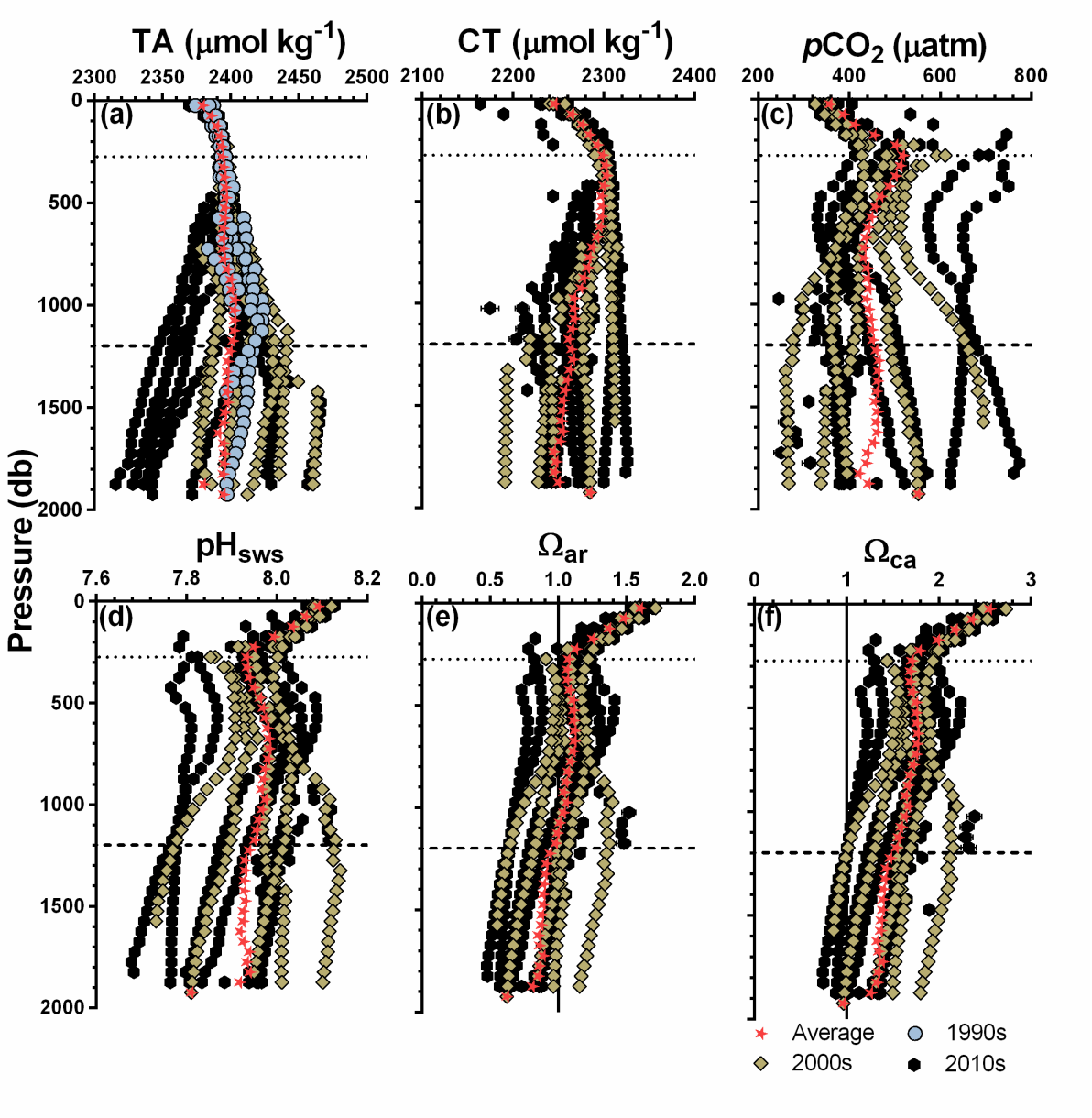

Figure V.9. Annual and total (average of the whole dataset) vertical profiles of the carbonate system in the central basin. Data plotted are (a) total alkalinity (TA), (b) total inorganic carbon (CT), (c) partial pressure of carbon dioxide (pCO_2), (d) pH_{sws} (seawater scale), calcium carbonate state for (e) aragonite (Ω_{ar}) and (f) calcite (Ω_{ca}) for 1990s (blue circles), 2000s (brown diamonds), and 2010s (black hexagons). Vertical profile marked as red star is the total average relative to the whole annual vertical profiles. Dotted and dashed lines highlight the boundary of surface-intermediate (i.e., γ^n = 28.00 kg m^{-3}) and intermediate-deep (i.e., γ^n = 28.27 kg m^{-3}) layers.

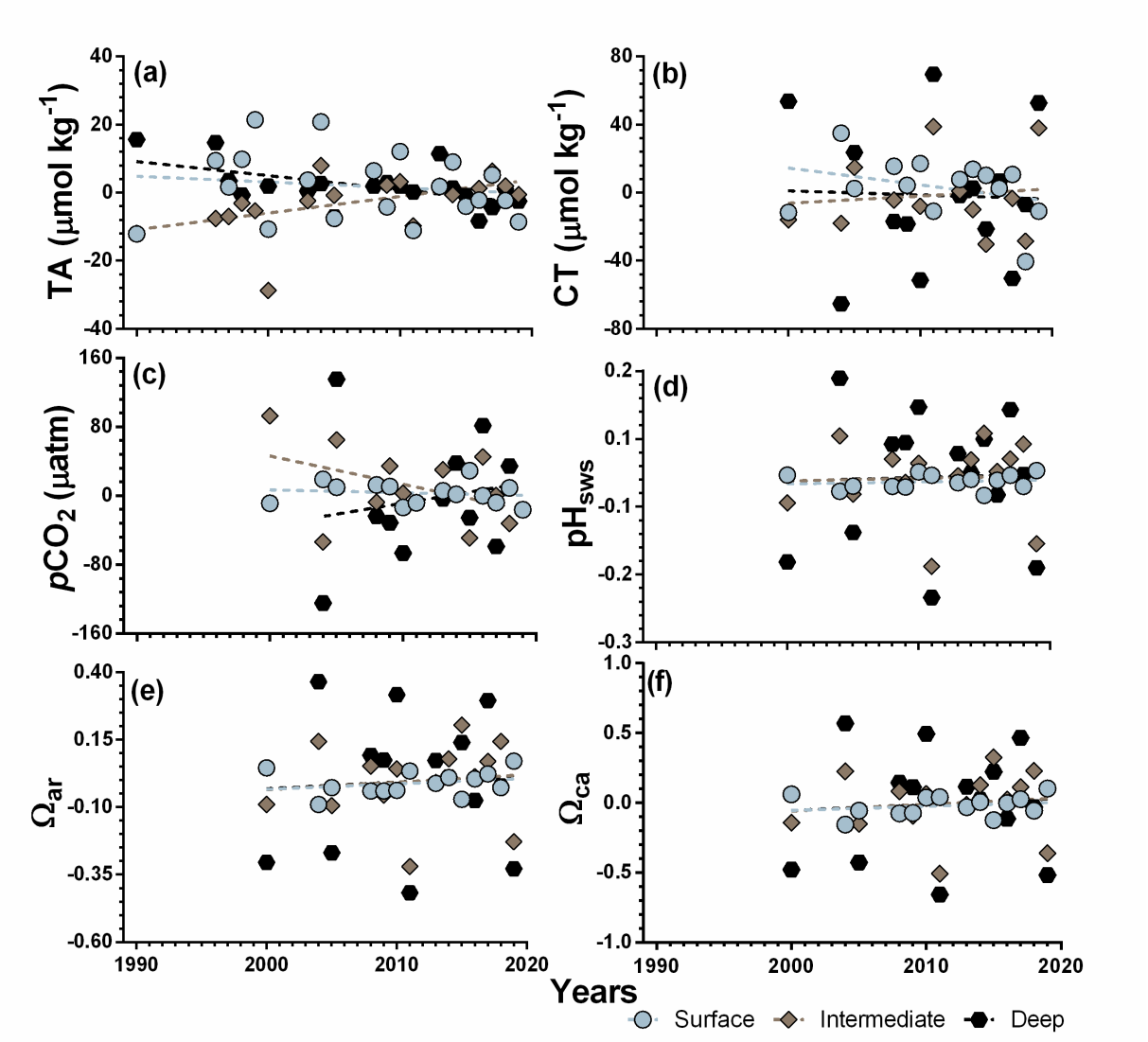

Figure V.10. Time series of carbonate system parameters throughout the 30 years used in this study for the central basin and water mass layers in the Bransfield Strait. Plotted data are annual anomalies for (a) total alkalinity – TA, (b) total inorganic carbon – CT, (c) partial pressure of carbon dioxide – pCO_2, (d) pH_{sws} (seawater scale), (e) aragonite saturation state – Ω_{ar}, and (f) calcite saturation state – Ω_{ca}. Trend line for each layer is showed as a dashed line based on anomaly data (see legend for details with regard to colours and their respective layers), which values are described in Table IV.2.

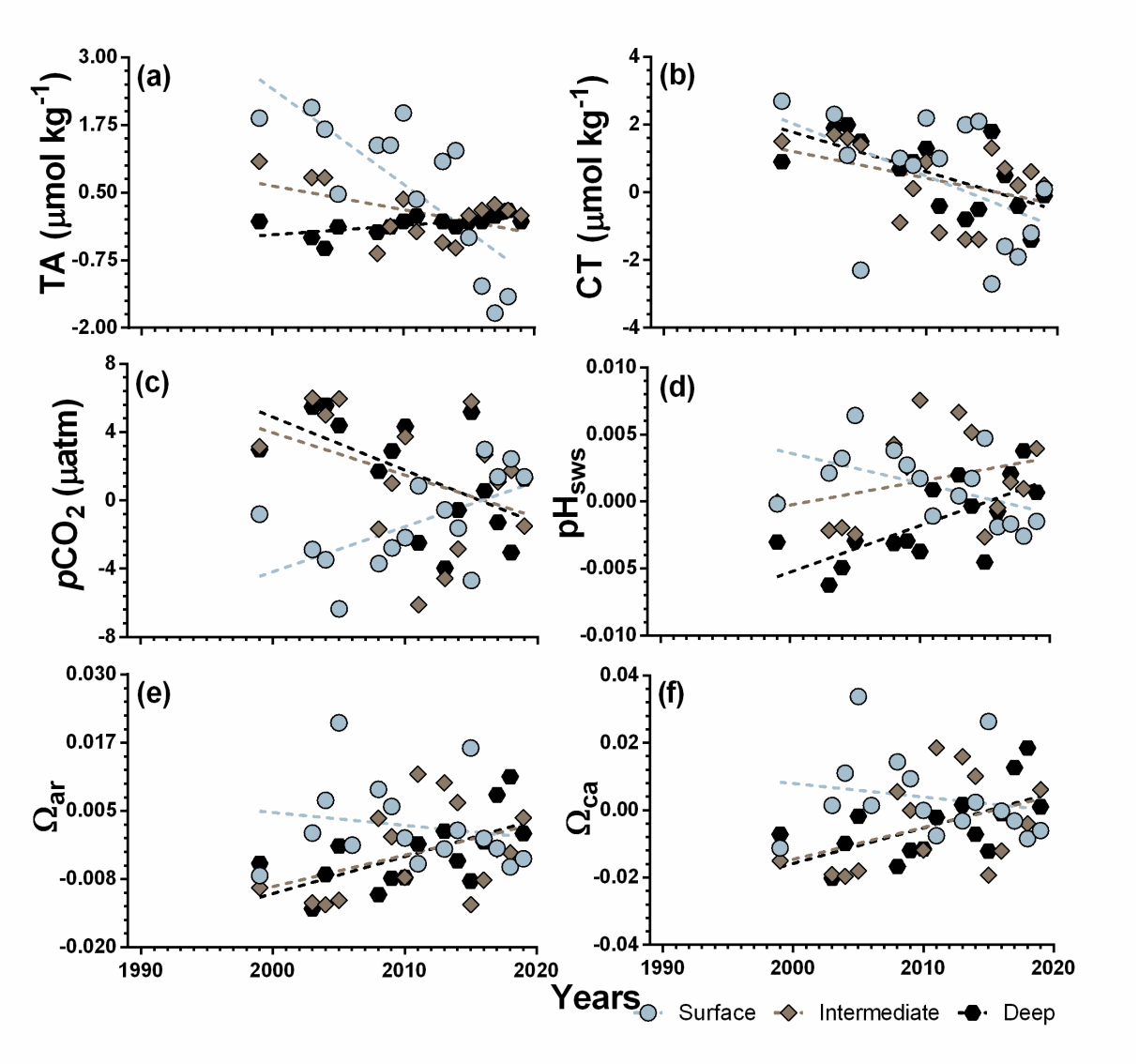

Figure V.11. Time series of carbonate system parameters throughout the 20 years used in this study for the eastern basin and water mass layers in the Bransfield Strait. Plotted data are annual anomalies for (a) total alkalinity – TA, (b) total inorganic carbon – CT, (c) partial pressure of carbon dioxide – pCO_2, (d) pH_{sws} (seawater scale), (e) aragonite saturation state – Ω_{ar}, and (f) calcite saturation state – Ω_{ca}. Trend line for each layer is showed as a dashed line based on anomaly data (see legend for details with regard to colours and their respective layers), which values are described in Table IV.2.

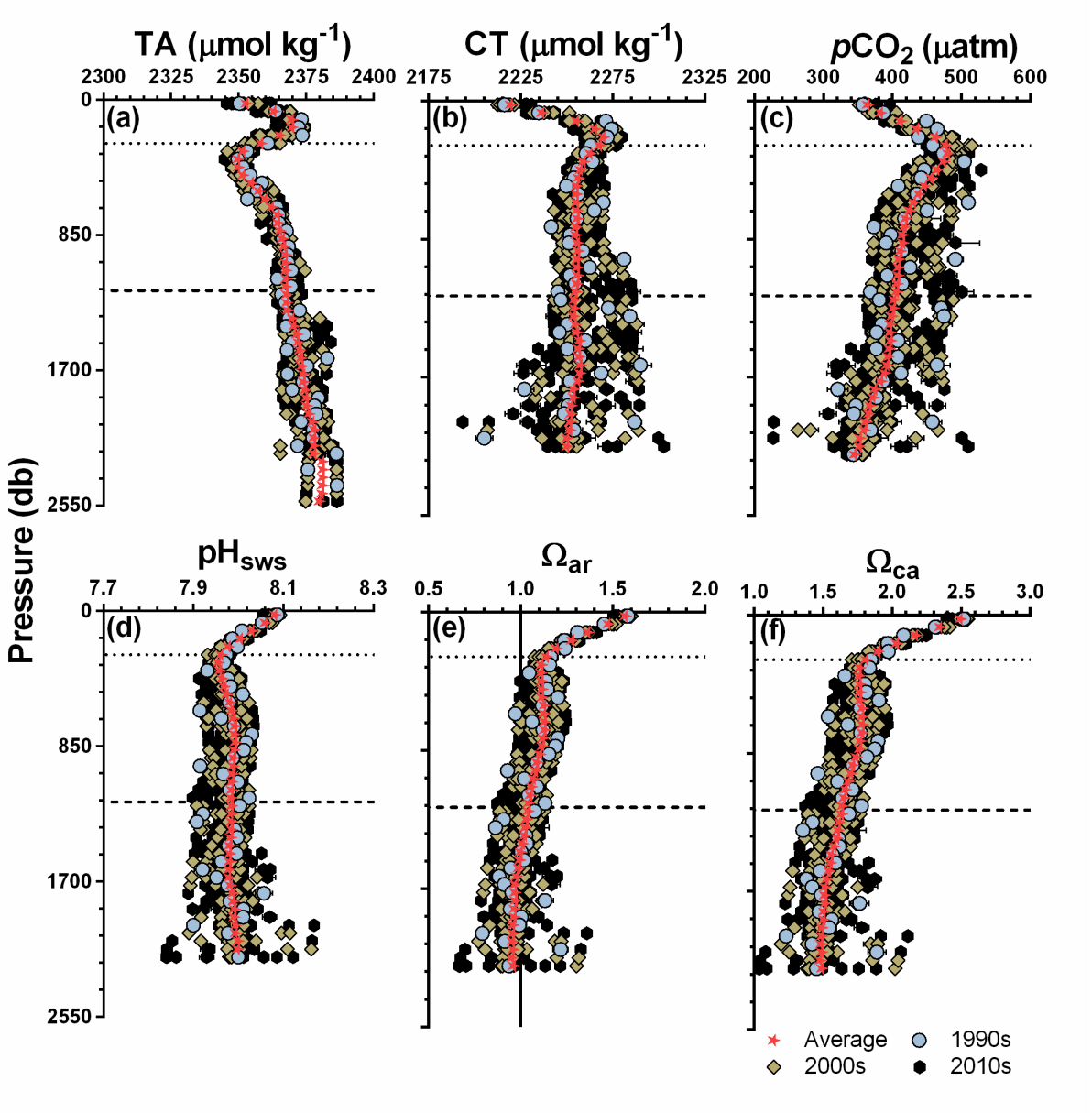

Figure V.12. Annual and total (average of the whole dataset) vertical profiles of the carbonate system in the eastern basin. Data plotted are (a) total alkalinity (TA), (b) total inorganic carbon (CT), (c) partial pressure of carbon dioxide (pCO_2), (d) pH_{sws} (seawater scale), calcium carbonate state for (e) aragonite (Ω_{ar}) and (f) calcite (Ω_{ca}) for 1990s (blue circles), 2000s (brown diamonds), and 2010s (black hexagons). Vertical profile marked as red star is the total average relative to the whole annual vertical profiles. Dotted and dashed lines highlight the boundary of surface-intermediate (i.e., γ^n = 28.00 kg m^{-3}) and intermediate-deep (i.e., γ^n = 28.27 kg m^{-3}) layers.

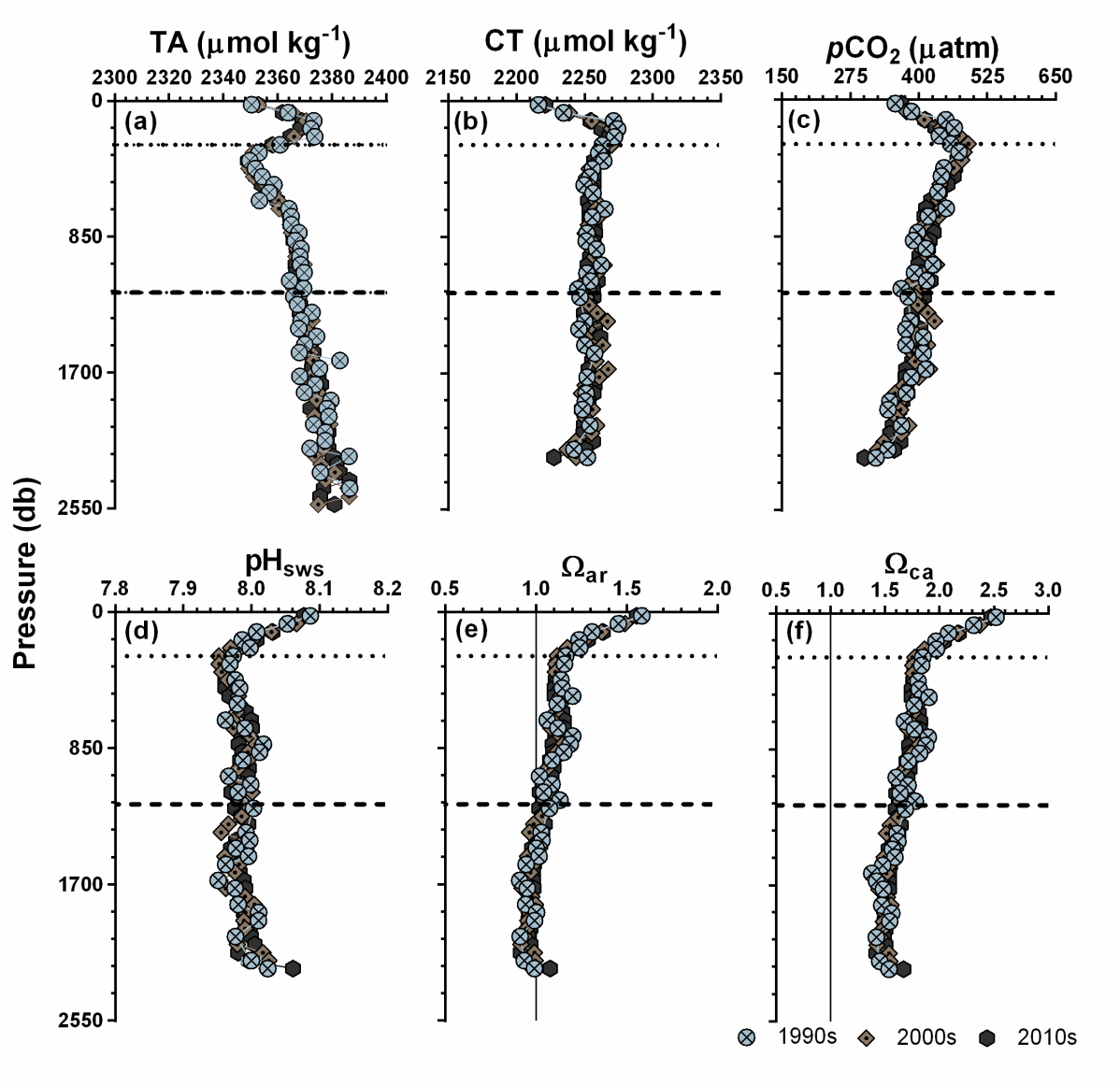

Figure V.13. Vertical profiles of decadal average of the carbonate system properties in the eastern basin of the Bransfield Strait during 1999 – 2019 for all parameters. Data plotted are (a) total alkalinity – TA, (b) total inorganic carbon – CT, (c) partial pressure of carbon dioxide – pCO_2, (d) pH_{sws} (seawater scale), (e) aragonite saturation state – Ω_{ar}, and (f) calcite saturation state – Ω_{ca}. Data for 1990s, then, is determined by only one year (i.e., 1999). The standard errors are < 1.6 µmol kg^{-1} for TA, < 3.4 µmol kg^{-1} for CT, < 11.9 µatm for pCO_2, < 0.01 pH_{sws} units, and < 0.05 for both Ω. The vertical solid line in panels (e) and (f) indicate the threshold for $\Omega_{ar} > 1$ and $\Omega_{ca} > 1$, respectively. The vertical solid line in panels (e) and (f) indicate the $\Omega_{ar} = 1$ and $\Omega_{ca} = 1$, respectively, the values below 1 refers to undersaturation of calcium carbonate.

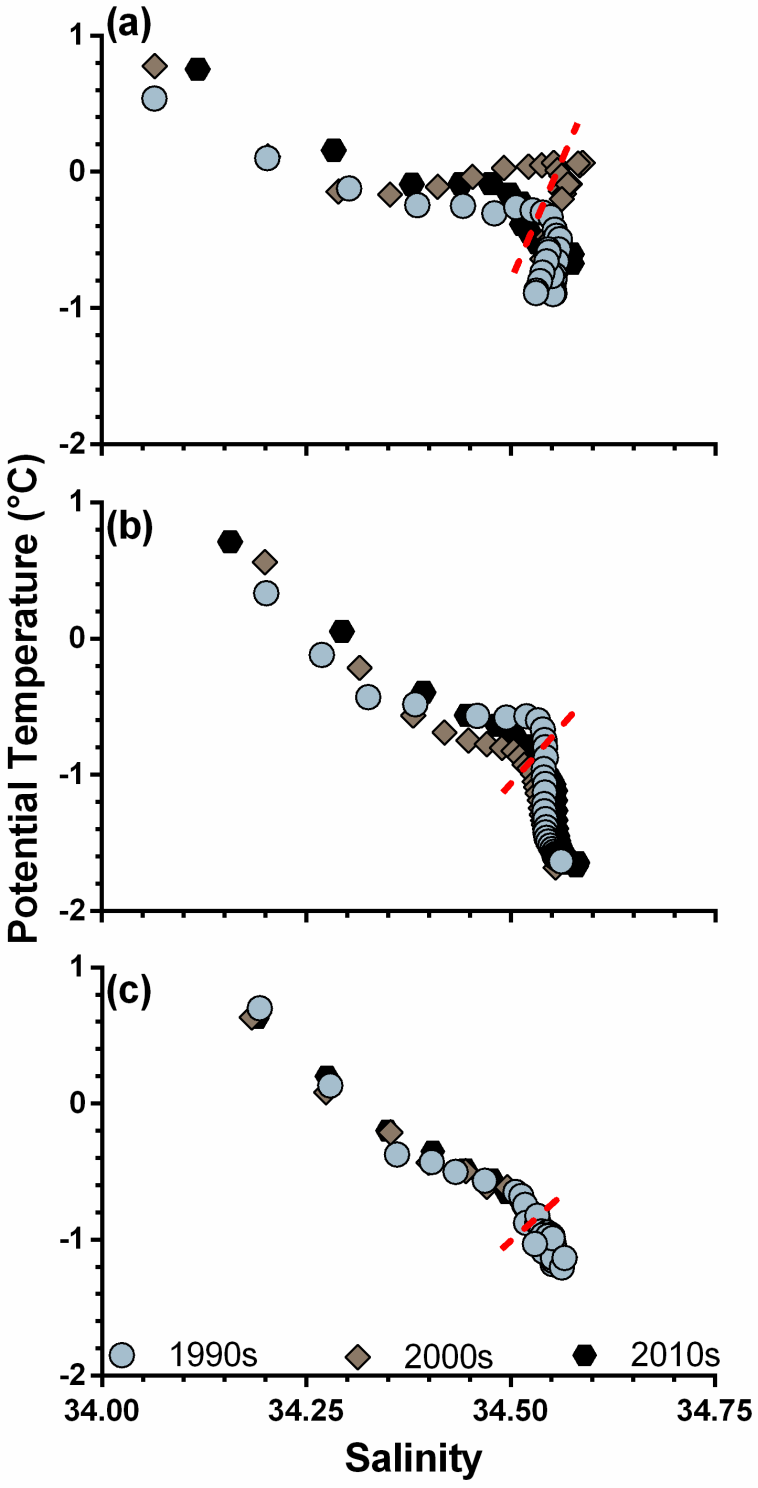

Figure V.14. Decadal potential temperature – salinity diagram for the (a) western, (b) central, and (c) eastern basins of the Bransfield Strait. Values were depth-averaged for each 50 m. The red dashed line indicates the depth of ~500 m.

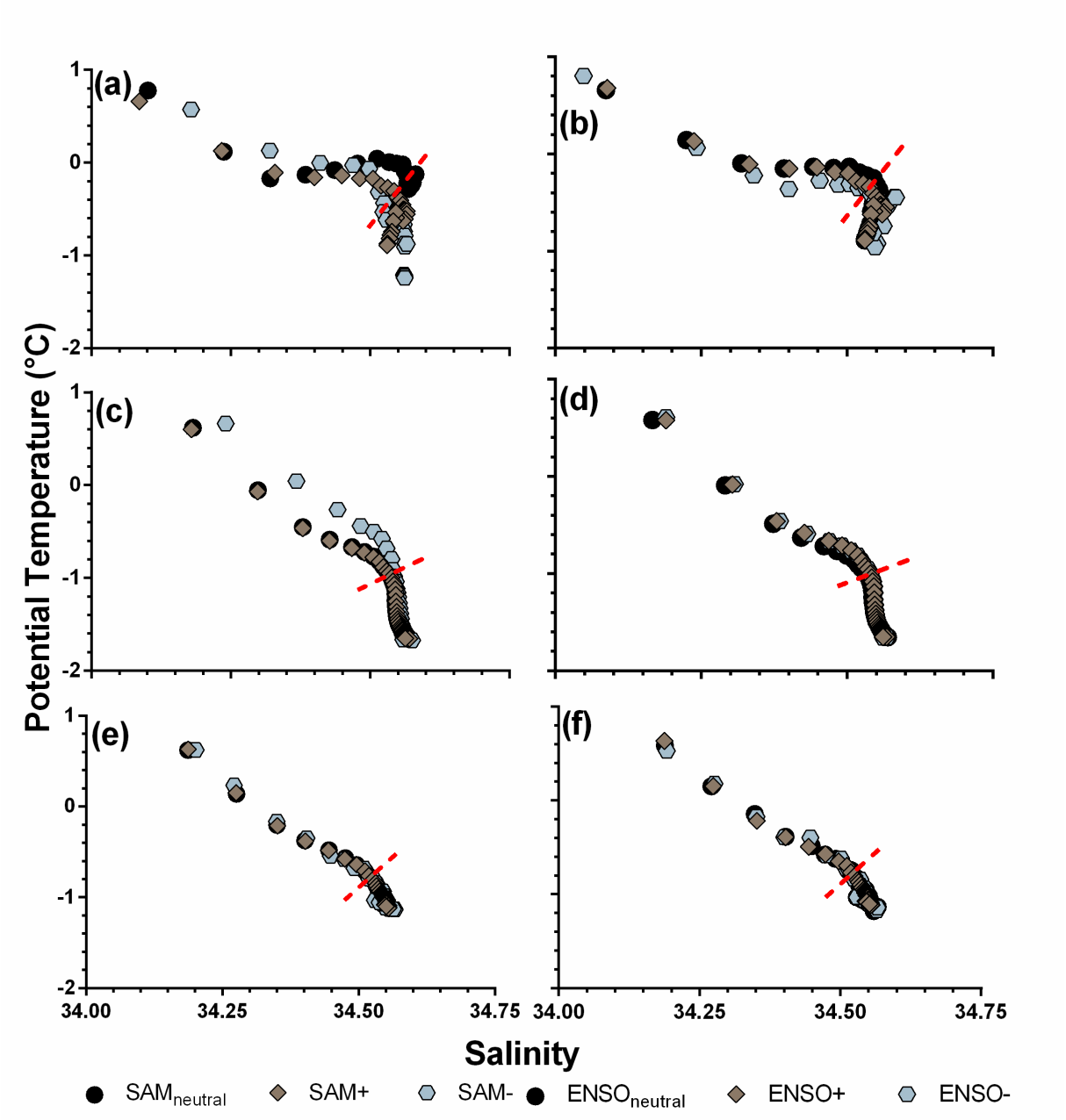

Figure V.15. Potential temperature – salinity diagram for the vertical profiles of modes of climate variability and its impact on hydrographic properties on (a, b) western, (c, d) central, and (e, f) eastern basin. The first column represents the SAM while the second one, ENSO. Depth intervals were each 50 m. The red dashed line indicates the depth ~500 m.

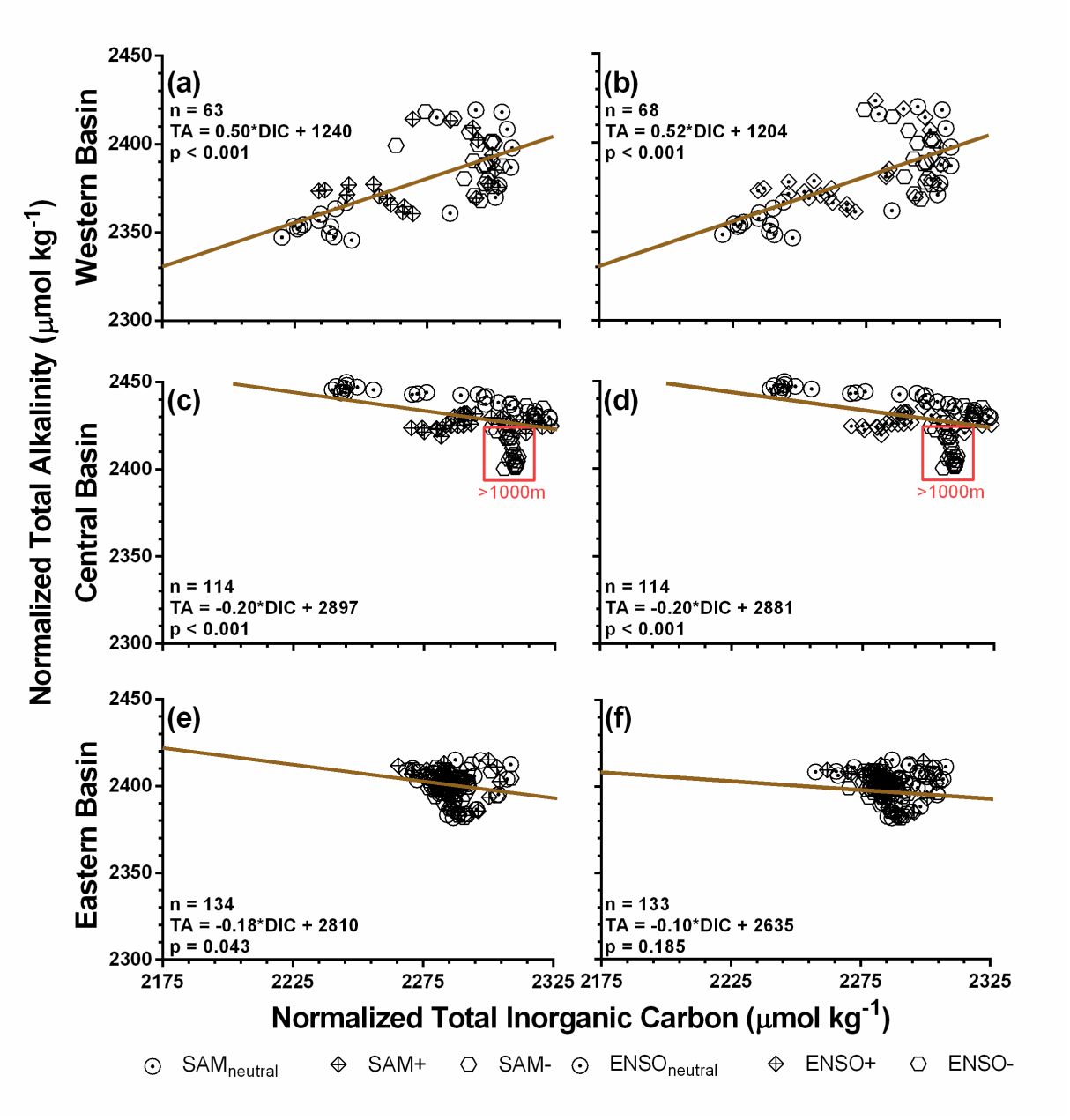

Figure V.16. Salinity-normalized total alkalinity (TA) and total inorganic carbon (CT) diagram considering the climate mode composited periods for the (a and b) western, (c and d) central, and (e and f) eastern basins of the Bransfield Strait. Normalization was performed considering the annual mean salinity in correspondent CT and TA averages plotted. Brown lines show the linear regression between CT and TA in the western, central, and eastern basins. The red rectangle at the panel (c) and (d) highlights the deep layer > 1000 m at the central basin of the Bransfield Strait.

Table V.1. Precision of *in situ* data available (total alkalinity – TA and total inorganic carbon – CT) in the database accessed here. Associated errors to our reconstruction are presented in Table IV.1. Not available precision on previous papers or their database is highlighted as not available (NA).

Year **Parameter**	**1996**	**2006**	**2010**	**2015**	**2016**	**2017**	**2018**	**2019**
TA µmol kg^{-1}	1.4 Alvarez et al., 2002	NA	NA	3.0 Kerr et al., 2018	3.4	2.8	5.5	2.9
					LEOC/GOAL			
CT µmol kg^{-1}	4.0 Alvarez et al., 2002	NA	NA	5.0 Kerr et al., 2018	4.4	2.9	3.4	4.5
					LEOC/GOAL			

Table V.2. Sensitive test for the output data for the western basin from CO2Sys v2.1 via comparison among the best K1 and K2 set identified here (Goyet e Poisson, 1989) and the others available in the script. Sensitivity was determined by the parameter's value estimated by Goyet & Poisson (1989) constants minus the others determined by different constant set.

a) Surface

K1 and K2 set	pH_{sws}	pCO_2 (µatm)	Ω_{ca}	Ω_{ar}
Roy et al. (1993)	0.0044	0.12	-0.0095	-0.0060
Hansson (1973)	0.0231	-28.84	-0.0921	-0.0579
Mehrbach et al. (1973)	-0 .0011	0.33	0.0029	0.0018
Dickson and Millero (1987)	0.0075	-7.17	-0.0269	-0.0169
Lueker et al. (2000)	-0.0003	-2.23	-0.0027	-0.0017
Millero et al. (2002)	-0.0191	-4.10	0.0367	0.0231
Millero et al. (2006)	0.0040	-9.18	-0.0223	-0.0140

b) Intermediate

K1 and K2 set	pH_{sws}	pCO_2 (µatm)	Ω_{ca}	Ω_{ar}
Roy et al. (1993)	0.0043	0.15	-0.0079	-0.0050
Hansson (1973)	0.0227	-31.41	-0.0857	-0.0542
Mehrbach et al. (1973)	-0.0011	-1.28	0.0002	0.0001
Dickson and Millero (1987)	0.0075	-7.87	-0.0250	-0.0158
Lueker et al. (2000)	-0.0003	-4.14	-0.0054	-0.0034
Millero et al. (2002)	-0.0187	-5.71	0.0278	0.0176
Millero et al. (2006)	0.0041	-11.42	-0.0236	-0.0149

c) Deep

K1 and K2 set	pH_{sws}	pCO_2 (µatm)	Ω_{ca}	Ω_{ar}
Roy et al. (1993)	0.0042	0.13	-0.0086	-0.0054
Hansson (1973)	0.0272	-30.28	-0.0967	-0.0612
Mehrbach et al. (1973)	-0.0007	-2.61	-0.0022	-0.0014
Dickson and Millero (1987)	0.0086	-7.63	-0.0282	-0.0179

Lueker et al. (2000)	0.0006	-5.41	-0.0087	-0.0055
Millero et al. (2002)	-0.0183	-6.33	0.0297	0.0188
Millero et al. (2006)	0.0059	-12.11	-0.0288	-0.0182

Table V.3. Sensitive test for the output data for central basin from CO2Sys v2.1 via comparison among the best K1 and K2 set identified here (Goyet e Poisson, 1989) and the others available in the script. Sensitivity was determined by the parameter's value estimated by Goyet & Poisson (1989) constants minus the others determined by different constant set.

a) Surface

K1 and K2 set	pH_{sws}	pCO_2 (µatm)	Ω_{ca}	Ω_{ar}
Roy et al. (1993)	0.0044	0.11	-0.0102	-0.0064
Hansson (1973)	0.0252	-27.77	-0.0997	-0.0627
Mehrbach et al. (1973)	-0.0011	-0.51	0.0019	0.0012
Dickson and Millero (1987)	0.0080	-6.93	-0.0292	-0.0184
Lueker et al. (2000)	-0.0007	-3.00	-0.0043	-0.0027
Millero et al. (2002)	-0.0191	-4.48	0.0395	0.0248
Millero et al. (2006)	0.0047	-9.49	-0.0251	-0.0158

b) Intermediate

K1 and K2 set	pH_{sws}	pCO_2 (µatm)	Ω_{ca}	Ω_{ar}
Roy et al. (1993)	0.0042	0.16	-0.0075	-0.0048
Hansson (1973)	0.0243	-33.78	-0.0917	-0.0579
Mehrbach et al. (1973)	-0.0009	-2.59	-0.0020	-0.0013
Dickson and Millero (1987)	0.0078	-8.52	-0.0264	-0.0167
Lueker et al. (2000)	0.0001	-5.70	-0.0083	-0.0053
Millero et al. (2002)	-0.0188	-6.92	0.0251	0.0159
Millero et al. (2006)	0.0047	-13.25	-0.0275	-0.0174

c) Deep

K1 and K2 set	pH_{sws}	pCO_2 (µatm)	Ω_{ca}	Ω_{ar}
Roy et al. (1993)	0.0042	0.18	-0.0073	-0.0046
Hansson (1973)	0.0265	-32.11	-0.0883	-0.0562
Mehrbach et al. (1973)	-0.0008	-3.57	-0.0032	-0.0020
Dickson and Millero (1987)	0.0084	-8.10	-0.0256	-0.0163
Lueker et al. (2000)	0.0005	-6.58	-0.0094	-0.0060

Millero et al. (2002)	-0.0184	-7.47	0.0240	0.0152
Millero et al. (2006)	0.0056	-13.52	-0.0275	-0.0175

Table V.4. Sensitive test for the output data for eastern basin from CO2Sys v2.1 via comparison among the best K1 and K2 set identified here (Goyet e Poisson, 1989) and the others available in the script. Sensitivity was determined by the parameter's value estimated by Goyet & Poisson (1989) constants minus the others determined by different constant set.

a) Surface

K1 and K2 set	pH_{sws}	pCO_2 (µatm)	Ω_{ca}	Ω_{ar}
Roy et al. (1993)	0.0044	0.12	-0.0099	-0.0063
Hansson (1973)	0.0243	-28.24	-0.0964	-0.0606
Mehrbach et al. (1973)	-0.0012	-0.23	0.0024	0.0015
Dickson and Millero (1987)	0.0078	-7.04	-0.0282	-0.0178
Lueker et al. (2000)	-0.0002	-2.75	-0.0036	-0.0023
Millero et al. (2002)	-0.0192	-4.37	0.0384	0.0242
Millero et al. (2006)	0.0044	-9.42	-0.0239	-0.0150

b) Intermediate

K1 and K2 set	pH_{sws}	pCO_2 (µatm)	Ω_{ca}	Ω_{ar}
Roy et al. (1993)	0.0043	0.16	-0.0077	-0.0049
Hansson (1973)	0.0250	-31.71	-0.0879	-0.0557
Mehrbach et al. (1973)	-0.0008	-2.17	-0.0013	-0.0008
Dickson and Millero (1987)	0.0080	-7.98	-0.0255	-0.0162
Lueker et al. (2000)	0.0002	-5.08	-0.0072	-0.0046
Millero et al. (2002)	-0.0185	-6.39	0.0265	0.0168
Millero et al. (2006)	0.0050	-12.24	-0.0256	-0.0162

c) Deep

K1 and K2 set	pH_{sws}	pCO_2 (µatm)	Ω_{ca}	Ω_{ar}
Roy et al. (1993)	0.0042	0.15	-0.0078	-0.0050
Hansson (1973)	0.0277	-28.16	-0.0851	-0.0543
Mehrbach et al. (1973)	-0.0006	-2.46	-0.0017	-0.0011
Dickson and Millero (1987)	0.0087	-7.08	-0.0250	-0.0159

Lueker et al. (2000)	0.0007	-5.07	-0.0074	-0.0047
Millero et al. (2002)	-0.0180	-6.07	0.0277	0.0177
Millero et al. (2006)	0.0061	-11.30	-0.0250	-0.0160

Table V.5. Propagated errors of outputs from the CO2Sys v2.1 following Orr et al. (2018). pH_{sws} was evaluated by $[H^+]$ (nmol kg^{-1}).

(a) Western basin

Parameter	Surface	Intermediate	Deep
pCO_2 (µatm)	91.3 ± 22.0	14.1 ± 4.6	100.4 ± 26.5
$[H^+]$ (nmol kg^{-1})	1.56 ± 0.40	0.24 ± 0.08	1.71 ± 0.44
Ω_{ca}	0.136 ± 0.014	0.016 ± 0.002	0.143 ± 0.012
Ω_{ar}	0.085 ± 0.008	0.010 ± 0.001	0.090 ± 0.008

(b) Central basin

Parameter	Surface	Intermediate	Deep
pCO_2 (µatm)	79.7 ± 12.1	14.7 ± 3.9	115.0 ± 39.3
$[H^+]$ (nmol kg^{-1})	1.36 ± 0.20	0.25 ± 0.07	1.97 ± 0.67
Ω_{ca}	0.140 ± 0.005	0.056 ± 0.002	0.124 ± 0.020
Ω_{ar}	0.090 ± 0.005	0.001 ± 0.001	0.079 ± 0.013

(c) Eastern basin

Parameter	Surface	Intermediate	Deep
pCO_2 (µatm)	83.5 ± 12.2	13.2 ± 2.8	91.9 ± 25.6
$[H^+]$ (nmol kg^{-1})	1.42 ± 0.20	0.23 ± 0.05	1.57 ± 0.43
Ω_{ca}	0.141 ± 0.008	0.015 ± 0.002	0.124 ± 0.015
Ω_{ar}	0.088 ± 0.005	0.010 ± 0.001	0.079 ± 0.010

Table V.6. Distribution of the number of years per layer in the different basins of the Bransfield Strait. TA had much more years of data reconstructed in our time series so that years indicated are related to TA data. Years with CT data are highlighted with *. Other CO_2-carbonate system parameters followed CT temporal distribution. ** basin in which TA and CT had the same temporal distribution in the eastern basin.

Layer	Western	Central	Eastern**
Surface	1990, 1993, 1996*, 1997, 2004*, 2008*, 2010*, 2011*, 2013*, 2014*, 2015*, 2016*, 2017*, 2018*, 2019*	1990, 1996, 1997, 1998, 1999, 2000*, 2003, 2004*, 2005*, 2008*, 2009*, 2010*, 2011*, 2013*, 2014*, 2015*, 2016*, 2017*, 2018*, 2019*	1999, 2003, 2004, 2005, 2008, 2009, 2010, 2011, 2013, 2014, 2015, 2016, 2017, 2018, 2019
Intermediate	1990, 1993, 1996*, 1997, 2004*, 2008*, 2010*, 2011, 2013*, 2014*, 2015*, 2016*, 2017*, 2018, 2019*	1990, 1996, 1997, 1998, 1999, 2000*, 2003, 2004*, 2005*, 2008*, 2009*, 2010*, 2011*, 2013*, 2014*, 2015*, 2016*, 2017*, 2018*, 2019*	1999, 2003, 2004, 2008, 2009, 2010, 2011, 2013, 2014, 2015, 2016, 2017, 2018, 2019
Deep	1990, 1993, 1996, 2010, 2013*, 2014*, 2015*, 2016*, 2017*, 2018, 2019*	1990, 1996, 1997, 1998, 2000*, 2003, 2004*, 2005*, 2008*, 2009*, 2010*, 2011*, 2013*, 2014*, 2015*, 2016*, 2017*, 2018*, 2019*	1999, 2003, 2004, 2005, 2008, 2009, 2010, 2011, 2013, 2014, 2015, 2016, 2017, 2018, 2019

Table V.7. Year sets used on our composite analysis split per basin. Our composition only included data for those years for which reconstructed data were available.

Basin	Compositions			
	SAM and ENSO neutral	**SAM+ ENSO+**	**SAM+ ENSO-**	**SAM- ENSO+**
Western	1990, 2004, 2013	2010, 2015	1996, 2008, 2011, 2018	2016, 2019
Central	1990, 2004, 2013	1998, 2010, 2015	1996, 1999, 2008, 2011	2005, 2016, 2019
Eastern	2004, 2013	2010, 2015	1999, 2008, 2011, 2018	2005, 2016, 2019

Table V.8. Significance level for Mann-Whitney test (confidence level 95%, $p < 0.05$) for decadal mean in each depth interval of 50 m throughout the water column in the western basin of the Bransfield Strait for (a) total alkalinity – TA and (b) total inorganic carbon – CT. Values with no statistical significance are blank in the table. Not determined *p*-values are highlighted by ND due to the lack of data for these depths.

a) TA

Depth (m)	1990s-2000s	1990s-2010s	2000s-2010s
25	< 0.0001	< 0.0001	0.0013
75	0.0109	< 0.0001	< 0.0001
125		< 0.0001	< 0.0001
175		< 0.0001	< 0.0001
225		< 0.0001	< 0.0001
275	0.0169	< 0.0001	< 0.0001
325	< 0.0001	0.0019	< 0.0001
375	0.0021		0.0001
425		< 0.0001	0.0225
475	< 0.0001	< 0.0001	< 0.0001
525	< 0.0001	< 0.0001	< 0.0001
575	< 0.0001	< 0.0001	< 0.0001
625	< 0.0001	< 0.0001	< 0.0001
675	< 0.0001	< 0.0001	< 0.0001
725	< 0.0001		< 0.0001
775	< 0.0001	< 0.0001	< 0.0001
825	< 0.0001	< 0.0001	< 0.0001
875	< 0.0001	0.0063	< 0.0001
925	< 0.0001	0.0233	< 0.0001
975	< 0.0001		< 0.0001
1025	< 0.0001	ND	ND
1075		ND	ND
1125		ND	ND
1175	< 0.0001	ND	ND
1225	< 0.0001	ND	ND
1275	< 0.0001	ND	ND

b) CT

Depth (m)	1990s-2000s	1990s-2010s	2000s-2010s

25	0.0209		< 0.0001
75		0.0017	< 0.0001
125		0.0347	< 0.0001
175		0.0209	< 0.0001
225			< 0.0001
275			< 0.0001
325	ND	ND	< 0.0001
375			< 0.0001
425			
475			< 0.0001
525	ND	ND	< 0.0001
575	ND	ND	< 0.0001
625	ND	ND	< 0.0001
675	ND	ND	< 0.0001
725	ND	ND	< 0.0001
775	ND	ND	< 0.0001
825	ND	ND	< 0.0001
875	ND	ND	< 0.0001
925	ND	ND	< 0.0001
975	ND	ND	< 0.0001
1025	ND	ND	ND
1075	ND	ND	ND
1125	ND	ND	ND
1175	ND	ND	ND
1225	ND	ND	ND
1275	ND	ND	ND

Table V.9. Significance level for Mann-Whitney test (confidence level 95%, $p < 0.05$) for decadal mean in each interval of 50 m throughout the water column in the central basin for (a) total alkalinity - TA and (b) total inorganic carbon - CT. Values with no statistical significance are not filled up in the table. Not determined *p* values are highlighted by ND due to the lack of data for these depths.

a) TA

Depth (m)	1990s-2000s	1990s-2010s	2000s-2010s
25		< 0.0001	< 0.0001
75	< 0.0001	< 0.0001	< 0.0001
125	0.0050	< 0.0001	< 0.0001
175	< 0.0001	< 0.0001	< 0.0001
225	< 0.0001	< 0.0001	< 0.0001
275	< 0.0001	< 0.0001	< 0.0001
325	< 0.0001	< 0.0001	< 0.0001
375	< 0.0001		< 0.0001
425	< 0.0001		< 0.0001
475	< 0.0001		< 0.0001
525	< 0.0001		< 0.0001
575	< 0.0001	0.0088	< 0.0001
625	< 0.0001	< 0.0001	< 0.0001
675	< 0.0001	< 0.0001	< 0.0001
725	< 0.0001	< 0.0001	0.0189
775	< 0.0001	< 0.0001	< 0.0001
825	< 0.0001	< 0.0001	< 0.0001
875	< 0.0001	< 0.0001	< 0.0001
925	< 0.0001	< 0.0001	< 0.0001
975	< 0.0001	< 0.0001	< 0.0001
1025	< 0.0001	< 0.0001	< 0.0001
1075	< 0.0001	< 0.0001	< 0.0001
1125	< 0.0001	< 0.0001	< 0.0001
1175	< 0.0001	< 0.0001	< 0.0001
1225	< 0.0001	< 0.0001	< 0.0001
1275	0.0222	< 0.0001	< 0.0001
1325		< 0.0001	< 0.0001
1375	0.0458	< 0.0001	< 0.0001
1425	0.0147	< 0.0001	< 0.0001
1475	0.0355	< 0.0001	< 0.0001

1525		< 0.0001	< 0.0001
1575		< 0.0001	< 0.0001
1625		< 0.0001	< 0.0001
1675		< 0.0001	< 0.0001
1725		< 0.0001	< 0.0001
1775		< 0.0001	< 0.0001
1825	< 0.0001	< 0.0001	< 0.0001
1875	< 0.0001	< 0.0001	< 0.0001
1925	< 0.0001	< 0.0001	< 0.0001

b) CT

Depth (m)	1990s-2000s	1990s-2010s	2000s-2010s
25	ND	ND	0.0002
75	ND	ND	
125	ND	ND	< 0.0001
175	ND	ND	< 0.0001
225	ND	ND	< 0.0001
275	ND	ND	< 0.0001
325	ND	ND	< 0.0001
375	ND	ND	< 0.0001
425	ND	ND	< 0.0001
475	ND	ND	< 0.0001
525	ND	ND	< 0.0001
575	ND	ND	< 0.0001
625	ND	ND	< 0.0001
675	ND	ND	
725	ND	ND	< 0.0001
775	ND	ND	< 0.0001
825	ND	ND	0.0021
875	ND	ND	0.0082
925	ND	ND	0.0056
975	ND	ND	< 0.0001
1025	ND	ND	0.0001
1075	ND	ND	< 0.0001
1125	ND	ND	< 0.0001
1175	ND	ND	< 0.0001
1225	ND	ND	< 0.0001
1275	ND	ND	< 0.0001

1325	ND	ND	< 0.0001
1375	ND	ND	< 0.0001
1425	ND	ND	< 0.0001
1475	ND	ND	< 0.0001
1525	ND	ND	< 0.0001
1575	ND	ND	< 0.0001
1625	ND	ND	< 0.0001
1675	ND	ND	< 0.0001
1725	ND	ND	< 0.0001
1775	ND	ND	< 0.0001
1825	ND	ND	< 0.0001
1875	ND	ND	< 0.0001
1925	ND	ND	< 0.0001

Table V.10. Significance level for Mann-Whitney test (confidence level 95%, $p < 0.05$) for decadal mean in each interval of 50 m throughout the water column in the eastern basin for (a) total alkalinity - TA and (b) total inorganic carbon - CT. Values with no statistical significance are not filled up in the table. Not determined *p* values are highlighted by ND due to the lack of data for these depths.

a) TA

Depth (m)	1990s-2000s	1990s-2010s	2000s-2010s
25			
75			< 0.0001
125		0.0005	< 0.0001
175			< 0.0001
225	< 0.0001	< 0.0001	
275		0.0357	
325			0.0264
375			0.0060
425			
475	0.0206	0.0220	
525	0.0200	0.0010	0.0449
575			
625	< 0.0001	< 0.0001	
675	0.0101		< 0.0001
725			
775			
825	0.0130	0.0361	
875			0.0012
925			
975			< 0.0001
1025			< 0.0001
1075		0.0354	< 0.0001
1125	0.0067		
1175	< 0.0001		< 0.0001
1225		0.0463	
1275			
1325	0.0013	0.0003	
1375	< 0.0001		< 0.0001
1425		0.0175	0.0173
1475	0.0017		< 0.0001

1525	0.0235	0.0082	
1575	0.0006	< 0.0001	
1625	< 0.0001	< 0.0001	
1675			< 0.0001
1725	< 0.0001	< 0.0001	< 0.0001
1775			< 0.0001
1825			< 0.0001
1875		0.0001	
1925	0.0420	0.0001	< 0.0001
1975	< 0.0001	< 0.0001	
2025	0.0011		< 0.0001
2075			0.0184
2125			
2175	0.0036	0.0004	0.0386
2225		< 0.0001	< 0.0001
2275	ND	ND	
2325	< 0.0001	0.0037	< 0.0001
2375	ND	ND	< 0.0001
2425		< 0.0001	< 0.0001
2475	ND	ND	< 0.0001
2525	ND	ND	< 0.0001

b) CT

Depth (m)	1990s-2000s	1990s-2010s	2000s-2010s
25			< 0.0001
75			< 0.0001
125	< 0.0001	< 0.0001	0.0005
175	0.0051	< 0.0001	< 0.0001
225		< 0.0001	< 0.0001
275	0.0002	< 0.0001	< 0.0001
325			
375	0.0314	< 0.0001	< 0.0001
425			0.0004
475		0.0377	< 0.0001
525	0.0002	< 0.0001	
575			
625	< 0.0001	< 0.0001	< 0.0001
675	0.0049	< 0.0001	< 0.0001

725	0.0001		< 0.0001
775	< 0.0001	< 0.0001	0.0215
825		0.0008	< 0.0001
875	0.0383	0.0003	0.0466
925	0.0258		0.0125
975	< 0.0001	< 0.0001	0.0009
1025	0.0001	< 0.0001	< 0.0001
1075	< 0.0001	0.0410	< 0.0001
1125		0.0396	< 0.0001
1175		0.0080	< 0.0001
1225		0.0014	0.0028
1275	0.0003	< 0.0001	
1325	< 0.0001	< 0.0001	< 0.0001
1375	< 0.0001		< 0.0001
1425	< 0.0001	0.0031	< 0.0001
1475			< 0.0001
1525	0.0013		0.0001
1575			
1625	0.0013	< 0.0001	0.0014
1675		0.0003	< 0.0001
1725	< 0.0001	0.0300	< 0.0001
1775		0.0285	0.0003
1825			0.0208
1875			0.0434
1925			
1975	< 0.0001	< 0.0001	
2025		0.0270	0.0001
2075	< 0.0001	< 0.0001	0.0029
2125	ND	ND	< 0.0001
2175			0.0241
2225		0.0028	
2275	ND	ND	ND
2325	ND	ND	< 0.0001
2375	ND	ND	
2425			0.0063
2475	ND	ND	< 0.0001
2525	ND	ND	< 0.0001

Table V.11. *P* values for composition analyses of the coupled interactions of the modes of climate variability in the Bransfield Strait for western basin for (a) total alkalinity - TA and (b) total inorganic carbon - CT.

a) TA

Depth (m)	Non-event vs SAM+ ENSO+	Non-event vs SAM+ ENSO-	Non-event vs SAM- ENSO+	SAM+ ENSO+ vs SAM+ ENSO-	SAM+ ENSO+ vs SAM- ENSO+	SAM+ ENSO- vs SAM- ENSO+
25	< 0.0001	< 0.0001	< 0.0001	0.0002	0.0323	
75	< 0.0001	< 0.0001	< 0.0001	< 0.0001	< 0.0001	< 0.0001
125	< 0.0001	< 0.0001	0.0235	< 0.0001	< 0.0001	< 0.0001
175	< 0.0001	< 0.0001	0.0437	< 0.0001	< 0.0001	< 0.0001
225	< 0.0001	< 0.0001	< 0.0001	< 0.0001	< 0.0001	< 0.0001
275	< 0.0001	< 0.0001	0.0270	0.0007	< 0.0001	< 0.0001
325	< 0.0001	< 0.0001	< 0.0001		< 0.0001	< 0.0001
375	< 0.0001	< 0.0001	< 0.0001			
425	< 0.0001	< 0.0001	< 0.0001		< 0.0001	< 0.0001
475	< 0.0001	< 0.0001	< 0.0001	0.0155	< 0.0001	< 0.0001
525	0.0180	0.0003	< 0.0001	0.0070	< 0.0001	< 0.0001
575	0.0122	0.0008	< 0.0001		< 0.0001	< 0.0001
625		0.0006	< 0.0001	0.0011	< 0.0001	< 0.0001
675	0.0201	0.0004	< 0.0001	0.0234	< 0.0001	< 0.0001
725		0.0071	< 0.0001	0.0045	< 0.0001	< 0.0001
775			< 0.0001	0.0083	< 0.0001	0.0436
825			< 0.0001		< 0.0001	0.0001
875		< 0.0001	< 0.0001	< 0.0001	< 0.0001	0.0427
925		< 0.0001	< 0.0001	< 0.0001	< 0.0001	
975		< 0.0001	< 0.0001	< 0.0001	< 0.0001	
1025			< 0.0001	ND	ND	ND
1075	ND	ND	ND	< 0.0001	ND	ND
1125	ND	ND	ND	< 0.0001	ND	ND

1175	ND	ND	ND	< 0.0001	ND	ND
1225	ND	ND	ND	< 0.0001	ND	ND
1275	ND	ND	ND	0.0002	ND	ND

b) CT

Depth (m)	Non-event vs SAM+ ENSO+	Non-event vs SAM+ ENSO-	Non-event vs SAM- ENSO+	SAM+ ENSO+ vs SAM+ ENSO-	SAM+ ENSO+ vs SAM- ENSO+	SAM+ ENSO- vs SAM- ENSO+
25	< 0.0001	< 0.0001	< 0.0001	< 0.0001		< 0.0001
75	< 0.0001	< 0.0001	< 0.0001	< 0.0001	< 0.0001	< 0.0001
125	< 0.0001	< 0.0001	< 0.0001	< 0.0001	< 0.0001	< 0.0001
175	< 0.0001	< 0.0001	< 0.0001	< 0.0001	< 0.0001	< 0.0001
225	< 0.0001	< 0.0001	0.0231	< 0.0001		< 0.0001
275	0.0002	< 0.0001	< 0.0001	< 0.0001	< 0.0001	0.0442
325	0.0045	0.0018	< 0.0001		0.0024	
375		< 0.0001		< 0.0001		< 0.0001
425	< 0.0001	< 0.0001	< 0.0001	< 0.0001		< 0.0001
475	< 0.0001	< 0.0001	< 0.0001	0.0016	< 0.0001	
525	< 0.0001	< 0.0001	< 0.0001	0.0296	< 0.0001	
575	< 0.0001	< 0.0001	< 0.0001		< 0.0001	0.0004
625	< 0.0001	< 0.0001	< 0.0001		< 0.0001	< 0.0001
675	< 0.0001	< 0.0001	< 0.0001		< 0.0001	< 0.0001
725	< 0.0001	0.0014	< 0.0001		< 0.0001	< 0.0001
775	< 0.0001	< 0.0001	< 0.0001	< 0.0001	< 0.0001	< 0.0001
825	0.0262	< 0.0001	< 0.0001	< 0.0001	< 0.0001	< 0.0001
875	< 0.0001		< 0.0001	0.0443	< 0.0001	< 0.0001
925	< 0.0001	< 0.0001	< 0.0001		< 0.0001	< 0.0001
975	< 0.0001	< 0.0001	< 0.0001			0.0008
1025	< 0.0001	< 0.0001	ND	< 0.0001	ND	ND
1075	< 0.0001	< 0.0001	ND	< 0.0001	ND	ND
1125	< 0.0001	< 0.0001	ND	< 0.0001	ND	ND
1175	ND	ND	ND		ND	ND

1225	ND	ND	ND		ND	ND
1275	ND	ND	ND		ND	ND

Table V.12. *P* values for composition analyses of the coupled interactions of the modes of climate variability in the Bransfield Strait for central basin for (a) total alkalinity and (b) total inorganic carbon - CT.

a) TA

Depth (m)	Non-event vs SAM+ ENSO+	Non-event vs SAM+ ENSO-	Non-event vs SAM- ENSO+	SAM+ ENSO+ vs SAM+ ENSO-	SAM+ ENSO+ vs SAM- ENSO+	SAM+ ENSO- vs SAM- ENSO+
25	< 0.0001	< 0.0001	< 0.0001	< 0.0001	< 0.0001	0.0056
75	< 0.0001	< 0.0001	< 0.0001	< 0.0001	< 0.0001	< 0.0001
125	< 0.0001	< 0.0001	< 0.0001	< 0.0001	< 0.0001	< 0.0001
175	< 0.0001	< 0.0001	< 0.0001	< 0.0001	< 0.0001	< 0.0001
225	< 0.0001	< 0.0001	< 0.0001	< 0.0001	< 0.0001	< 0.0001
275	< 0.0001	< 0.0001	< 0.0001	< 0.0001	< 0.0001	< 0.0001
325	< 0.0001	< 0.0001	< 0.0001	0.0062	< 0.0001	< 0.0001
375	< 0.0001	< 0.0001	< 0.0001		< 0.0001	< 0.0001
425	0.0140	< 0.0001	< 0.0001	< 0.0001	< 0.0001	< 0.0001
475	< 0.0001	< 0.0001	< 0.0001	< 0.0001	< 0.0001	< 0.0001
525	< 0.0001	< 0.0001	< 0.0001	< 0.0001	< 0.0001	< 0.0001
575	< 0.0001	< 0.0001	< 0.0001	< 0.0001	< 0.0001	
625	< 0.0001	< 0.0001	0.0066	< 0.0001	< 0.0001	< 0.0001
675	< 0.0001	< 0.0001	< 0.0001	< 0.0001	< 0.0001	< 0.0001
725	< 0.0001	< 0.0001		< 0.0001	< 0.0001	< 0.0001
775	< 0.0001	< 0.0001	0.0015	< 0.0001	< 0.0001	< 0.0001
825	< 0.0001	< 0.0001	< 0.0001	< 0.0001	< 0.0001	< 0.0001
875	< 0.0001	< 0.0001	< 0.0001	< 0.0001	< 0.0001	< 0.0001
925	< 0.0001		< 0.0001	< 0.0001	< 0.0001	< 0.0001
975	< 0.0001		< 0.0001	< 0.0001	0.0020	< 0.0001
1025	< 0.0001	0.0111	< 0.0001	< 0.0001		< 0.0001
1075	< 0.0001	< 0.0001	< 0.0001	< 0.0001		< 0.0001
1125	< 0.0001	< 0.0001	< 0.0001	< 0.0001		< 0.0001

1175	< 0.0001	< 0.0001	< 0.0001	< 0.0001		< 0.0001
1225	< 0.0001	< 0.0001	< 0.0001	< 0.0001		< 0.0001
1275	< 0.0001	< 0.0001	< 0.0001	< 0.0001		< 0.0001
1325	< 0.0001	< 0.0001	< 0.0001	< 0.0001		< 0.0001
1375	< 0.0001	< 0.0001	< 0.0001	< 0.0001	0.0023	< 0.0001
1425	< 0.0001	< 0.0001	< 0.0001	< 0.0001	< 0.0001	< 0.0001
1475	< 0.0001	< 0.0001	< 0.0001	< 0.0001	< 0.0001	< 0.0001
1525	< 0.0001	< 0.0001	< 0.0001	< 0.0001	< 0.0001	< 0.0001
1575	< 0.0001	< 0.0001	< 0.0001	< 0.0001	< 0.0001	< 0.0001
1625	< 0.0001	< 0.0001	< 0.0001	< 0.0001	< 0.0001	< 0.0001
1675	< 0.0001	< 0.0001	< 0.0001	< 0.0001	< 0.0001	< 0.0001
1725	< 0.0001	< 0.0001	< 0.0001	< 0.0001	< 0.0001	< 0.0001
1775	< 0.0001	< 0.0001	< 0.0001	< 0.0001	< 0.0001	< 0.0001
1825	0.0060	< 0.0001	< 0.0001	0.0119	< 0.0001	< 0.0001
1875	< 0.0001	ND	< 0.0001	ND	< 0.0001	ND
1925	ND	ND	ND	ND		ND

b) CT

Depth (m)	**Non-event vs SAM+ ENSO+**	**Non-event vs SAM+ ENSO-**	**Non-event vs SAM- ENSO+**	**SAM+ ENSO+ vs SAM+ ENSO-**	**SAM+ ENSO+ vs SAM- ENSO+**	**SAM+ ENSO- vs SAM- ENSO+**
25		< 0.0001	< 0.0001	< 0.0001	< 0.0001	0.0002
75		< 0.0001	< 0.0001	< 0.0001	< 0.0001	< 0.0001
125	< 0.0001	< 0.0001	< 0.0001	< 0.0001	< 0.0001	< 0.0001
175		< 0.0001	< 0.0001	< 0.0001	< 0.0001	< 0.0001
225	< 0.0001	0.0035	< 0.0001	< 0.0001	< 0.0001	< 0.0001
275	< 0.0001	< 0.0001	< 0.0001		< 0.0001	< 0.0001
325	< 0.0001	< 0.0001	< 0.0001	< 0.0001	< 0.0001	< 0.0001
375	< 0.0001	< 0.0001	< 0.0001	< 0.0001	0.0001	< 0.0001
425	< 0.0001	< 0.0001	< 0.0001	< 0.0001		< 0.0001

475	< 0.0001	< 0.0001	< 0.0001	< 0.0001	< 0.0001	< 0.0001
525	< 0.0001	< 0.0001	< 0.0001	< 0.0001	< 0.0001	< 0.0001
575	< 0.0001	< 0.0001	< 0.0001	< 0.0001	< 0.0001	< 0.0001
625	< 0.0001	0.0313	0.0014	< 0.0001	< 0.0001	0.0001
675	< 0.0001	< 0.0001	0.0069	< 0.0001	< 0.0001	0.0004
725	< 0.0001	< 0.0001		< 0.0001	< 0.0001	< 0.0001
775	< 0.0001	< 0.0001		< 0.0001	< 0.0001	< 0.0001
825	< 0.0001	< 0.0001	< 0.0001	< 0.0001	< 0.0001	< 0.0001
875	< 0.0001	< 0.0001	< 0.0001	< 0.0001	< 0.0001	0.0133
925	< 0.0001	< 0.0001	< 0.0001	< 0.0001	< 0.0001	0.0412
975	< 0.0001	< 0.0001	< 0.0001	< 0.0001	< 0.0001	< 0.0001
1025	< 0.0001	< 0.0001	< 0.0001	< 0.0001	< 0.0001	0.0003
1075	< 0.0001	< 0.0001	< 0.0001	< 0.0001	< 0.0001	< 0.0001
1125	< 0.0001	< 0.0001	< 0.0001	< 0.0001	< 0.0001	< 0.0001
1175	< 0.0001	< 0.0001	< 0.0001	< 0.0001	< 0.0001	< 0.0001
1225	0.0080	< 0.0001	< 0.0001	< 0.0001	< 0.0001	< 0.0001
1275	< 0.0001	< 0.0001	< 0.0001	< 0.0001	< 0.0001	< 0.0001
1325	< 0.0001	< 0.0001	< 0.0001	< 0.0001	< 0.0001	< 0.0001
1375	< 0.0001	< 0.0001	< 0.0001	< 0.0001	< 0.0001	< 0.0001
1425	< 0.0001	< 0.0001	< 0.0001	< 0.0001	< 0.0001	< 0.0001
1475	< 0.0001	< 0.0001	< 0.0001	< 0.0001	< 0.0001	0.0156
1525	< 0.0001	< 0.0001	< 0.0001	< 0.0001	< 0.0001	
1575	< 0.0001	< 0.0001	< 0.0001	< 0.0001	< 0.0001	0.0035
1625	< 0.0001	< 0.0001	< 0.0001	< 0.0001	< 0.0001	
1675	< 0.0001	< 0.0001	< 0.0001	< 0.0001	< 0.0001	
1725	< 0.0001	< 0.0001	< 0.0001	< 0.0001	< 0.0001	< 0.0001
1775	< 0.0001	< 0.0001	< 0.0001	< 0.0001	< 0.0001	< 0.0001
1825	< 0.0001	< 0.0001	< 0.0001	< 0.0001	< 0.0001	< 0.0001
1875	< 0.0001	ND	< 0.0001	ND	< 0.0001	ND
1925	ND	ND	ND	ND	ND	ND

Table V.13. *P* values for composition analyses of the coupled interactions of the modes of climate variability in the Bransfield Strait for eastern basin for (a) total alkalinity - TA and (b) total inorganic carbon - CT.

a) TA

Depth (m)	Non-event vs SAM+ ENSO+	Non-event vs SAM+ ENSO-	Non-event vs SAM- ENSO+	SAM+ ENSO+ vs SAM+ ENSO-	SAM+ ENSO+ vs SAM- ENSO+	SAM+ ENSO- vs SAM- ENSO+
25	< 0.0001		0.0034	< 0.0001	< 0.0001	0.0005
75		0.0017	< 0.0001		0.0002	
125	< 0.0001			< 0.0001	< 0.0001	
175	0.0417		< 0.0001	< 0.0001	< 0.0001	0.0015
225	0.0003	< 0.0001		< 0.0001	< 0.0001	< 0.0001
275	< 0.0001			< 0.0001	< 0.0001	
325	< 0.0001	< 0.0001			0.0032	0.0094
375	0.0302		0.0173	0.0147		0.0080
425	< 0.0001		0.0173	< 0.0001	0.0019	0.0008
475	0.0106	< 0.0001				0.0003
525						
575	< 0.0001	< 0.0001	< 0.0001		< 0.0001	< 0.0001
625			< 0.0001		< 0.0001	0.0007
675	< 0.0001	< 0.0001	0.0040			
725				0.0005		0.0335
775	0.0374	0.0324			0.0180	0.0161
825				0.0193	0.0003	
875				0.0427	0.0001	
925				0.0377	0.0251	
975			0.0198		< 0.0001	
1025	< 0.0001	0.0027	< 0.0001			0.0017
1075		0.0016		< 0.0001		< 0.0001
1125				0.0011		0.0070
1175	0.0343	0.0164	0.0001		0.0319	

1225	< 0.0001		0.0005	< 0.0001		0.0258
1275	0.0019			0.0128	0.0080	
1325				0.0373		0.0020
1375						
1425	< 0.0001		< 0.0001	< 0.0001	0.0014	< 0.0001
1475	0.0130	0.0362	< 0.0001		0.0002	0.0002
1525	< 0.0001	0.0403		0.0001	< 0.0001	
1575	0.0002			0.0292	0.0102	
1625	< 0.0001				0.0262	
1675	< 0.0001	< 0.0001	< 0.0001		0.0086	
1725			0.0007			0.0060
1775	0.0049	0.0026		< 0.0001	0.0001	
1825	0.0075	0.0217	0.0257	< 0.0001		< 0.0001
1875	< 0.0001			< 0.0001	< 0.0001	
1925			< 0.0001		< 0.0001	
1975		< 0.0001		< 0.0001	0.0014	< 0.0001
2025	< 0.0001		0.0307	< 0.0001	< 0.0001	
2075						
2125		< 0.0001		< 0.0001		< 0.0001
2175		< 0.0001		< 0.0001		< 0.0001
2225	< 0.0001	< 0.0001	< 0.0001		0.0050	< 0.0001
2275	< 0.0001			< 0.0001	< 0.0001	
2325	0.0034			0.0002	0.0308	
2375	0.0401	ND	< 0.0001	ND	< 0.0001	ND
2425	0.0246	< 0.0001		< 0.0001		< 0.0001
2475		ND	0.0008	ND		ND

b) CT

Depth (m)	**Non-event vs SAM+ ENSO+**	**Non-event vs SAM+ ENSO-**	**Non-event vs SAM- ENSO+**	**SAM+ ENSO+ vs SAM+ ENSO-**	**SAM+ ENSO+ vs SAM- ENSO+**	**SAM+ ENSO- vs SAM- ENSO+**

25	< 0.0001	0.0195		< 0.0001	< 0.0001	
75	0.0266	0.0005	< 0.0001		0.0042	0.0452
125	< 0.0001	< 0.0001		< 0.0001	< 0.0001	< 0.0001
175		< 0.0001	< 0.0001	< 0.0001	< 0.0001	
225		< 0.0001		< 0.0001		< 0.0001
275	< 0.0001			< 0.0001	< 0.0001	0.0115
325		0.0399	0.0230			
375	< 0.0001	< 0.0001	< 0.0001			
425	0.0006		< 0.0001	0.0002		< 0.0001
475		0.0006	0.0078	0.0006	0.0074	
525	0.0001		0.0204	< 0.0001		0.0212
575	< 0.0001			0.0019	< 0.0001	
625	< 0.0001	0.0136	0.0008	0.0043	< 0.0001	< 0.0001
675		< 0.0001	< 0.0001	< 0.0001	0.0016	< 0.0001
725		0.0007			0.0464	0.0001
775			< 0.0001	0.0157	0.0001	< 0.0001
825	0.0017	0.0001	0.0023	< 0.0001	< 0.0001	
875	0.0139	0.0086		< 0.0001		0.0003
925	< 0.0001	0.0003		0.0001	< 0.0001	< 0.0001
975	0.0055		< 0.0001	0.0002	< 0.0001	0.0032
1025	< 0.0001	< 0.0001	< 0.0001	0.0008		0.0041
1075		0.0022	0.0235		0.0271	< 0.0001
1125		0.0178	< 0.0001		< 0.0001	< 0.0001
1175	< 0.0001		0.0081	< 0.0001	< 0.0001	0.0027
1225	0.0017	0.0360				
1275	< 0.0001	< 0.0001		0.0204	< 0.0001	< 0.0001
1325	< 0.0001	< 0.0001	< 0.0001	0.0097	0.0038	
1375	0.0141	< 0.0001	0.0449	< 0.0001		< 0.0001
1425	< 0.0001	0.0011	< 0.0001	0.0049		0.0001
1475	< 0.0001			< 0.0001	< 0.0001	
1525	< 0.0001	0.0022	< 0.0001	< 0.0001	< 0.0001	
1575	< 0.0001			< 0.0001	< 0.0001	
1625	0.0006		< 0.0001	0.0028	< 0.0001	0.0012

1675	< 0.0001	< 0.0001	0.0024	0.0041		0.0004
1725	0.0063	0.0003			0.0461	0.0263
1775	< 0.0001		< 0.0001	< 0.0001		< 0.0001
1825	< 0.0001	< 0.0001	< 0.0001	< 0.0001		0.0238
1875	< 0.0001	0.0016	< 0.0001	0.0052		0.0081
1925	< 0.0001				< 0.0001	
1975	< 0.0001	< 0.0001	< 0.0001	0.0014	< 0.0001	
2025	< 0.0001	< 0.0001	< 0.0001		0.0012	0.0317
2075	0.0041				0.0036	0.0150
2125		< 0.0001	< 0.0001	0.0048	0.00224	
2175	< 0.0001	0.0011	0.0015	< 0.0001		
2225	ND	ND	ND	0.0005	< 0.0001	0.0217
2275	ND			ND	ND	
2325	ND	0.0067	ND	ND	ND	ND
2375	ND	ND	ND	ND	ND	ND
2425						
2475		ND	0.0003	ND		ND

Capítulo VI:
Considerações Finais

Essa dissertação abordou a variabilidade de longo prazo dos parâmetros do sistema carbonato no estreito de Bransfield. Dessa forma, foi identificado que o maior controlador dessa variabilidade está associado à variabilidade hidrográfica da região. Enquanto a CDW contribui com uma assinatura biogeoquímica rica em produtos naturais de remineralização, ou seja, alta concentração de CT e baixo pH, a DSW transporta uma assinatura com alto carbono assimilado da atmosfera devido à sua recente formação antes de ser advectada para dentro do estreito de Bransfield.

A CDW apresenta suas maiores contribuições para a bacia oeste do estreito de Bransfield. Nesta bacia, os efeitos das interações acopladas entre ENSO e SAM demonstraram controlar as contribuições hidrográficas. Nesse sentido, a década

de 2000 é marcada por eventos de ENSO- e SAM+, o que favoreceu intrusões de CDW. Além dessas propriedades, intrusões de CDW também estão associadas ao transporte de calor, os quais impacta diretamente no derretimento de glaciares costeiros no entorno da Antártica. Esse efeito produz o aporte de água de degelo em superfície e, ao ser advectada para outras regiões, pode ter sua assinatura de diluição de propriedades transportada ao longo da coluna de água, como ocorre na bacia oeste. Essa conjuntura de efeitos marca uma diluição de TA e CT entre 500 e 1000 m de profundidade na década de 2000. Em 2010, no entanto, esse mesmo intervalo de profundidade é marcado por um aumento de concentração de TA e CT, possivelmente pelo aumento da contribuição de DSW (Damini *et al.*, 2022). De um modo geral, as variações da CDW e suas intrusões no estreito atuam como principal controlador da variabilidade dos parâmetros do sistema carbonato nesta bacia.

A CDW apresenta menores contribuições do que a DSW para as bacias central e leste. A dinâmica das correntes no estreito de Bransfield e as configurações geológicas, como as ilhas Shetland Sul restringe intrusões de massas de água oceânicas. Assim, a bacia central apresenta assinaturas hidrográficas dessa massa de água abaixo de 500 m de profundidade, marcando as três características da sua área de formação ao longo do seu fluxo advectivo para o estreito de Bransfield. A primeira característica se associa às propriedades hidrográficas. Incrementos de salinidade são identificadas para a década de 2010 na bacia profunda do estreito de Bransfield, a qual pode estar respondendo a intensificação da formação de gelo no oeste do mar de Weddell identificada recentemente. Assim, alterações de salinidade respondem com alterações de TA, como observado em relação a década de 2010. As duas outras

características recaem no aspecto biogeoquímico do oeste do mar de Weddell, área de formação da DSW. O leste da Península Antártica tem sido caracterizado como uma região altamente produtiva, a qual tem essa assinatura transportada ao longo do fluxo da DSW para oeste através do estreito de Bransfield. Uma vez em águas profundas, a matéria orgânica inicia seu processo de decomposição e, então, alterando os parâmetros do sistema carbonato. Por outro lado, a DSW transporta a assinatura de carbono antropogênico para as suas bacias profundas.

Enquanto isso, a bacia leste apresenta uma minimização de qualquer variabilidade de larga (i.e., decenal) ou curta (i.e., anual) escala, provavelmente devido aos efeitos de homogeneização ao longo de toda a coluna de água. É interessante observar, contudo, que embora apresente as menores tendências interanuais dentre as três bacias, esta tem suas tendências para pH e Ω positivas. No entanto, a bacia leste ainda é um desafio muito grande para as avaliações de aspectos hidrográficos e biogeoquímicos, o que requer maiores esforços para a investigação de processos oceanográficos na região.

De um modo geral, o estreito de Bransfield está próximo da saturação quanto ao CO_2. Enquanto as bacias oeste e central demonstraram incrementos decenais de unidades de fator Revelle nas camadas mais profundas, a bacia leste não demonstrou claras variações decenais, embora já seja uma região quase saturada desde 1990. A bacia central, em particular, apresenta variações interdecenais de 2 unidades de fator Revelle, o dobro da bacia oeste. Esta diferença pode estar associada à fonte de carbono: enquanto a CDW contribui com processos naturais, a DSW transporta assinaturas antropogênicas.

Essa dissertação inovou quanto a apresentar o primeiro estudo de longo prazo ao longo de todo o estreito de Bransfield a investigar a variabilidade dos parâmetros do sistema carbonato. Assim, o estreito de Bransfield foi observado como um ambiente naturalmente sensível que já se encontra em condições críticas de redução de pH, como na bacia oeste. Nesta bacia, as intensas tendências de redução atingem 0,017 unidades de pH_{sws} ano^{-1}, a maior tendência de redução desse parâmetro já identificada em ambiente costeiro e oceânico na Antártica. Uma vez que o estreito pode ser considerado como uma sentinela de alterações hidrográficas ocorrendo no entorno da península, características biogeoquímicas e suas alterações também podem ser traçadas nas suas bacias profundas. Isso pode tornar a região em um laboratório através de seu registro de processo ocorrendo ao longo do *hotspot* climático que é a Península Antártica.

Em um panorama geral, o entendimento das variações espaço-temporais dos parâmetros do sistema carbonato funciona como um importante alerta de condições químicas oceânicas. Isso vale para ambientes costeiros de regiões sensíveis à mudança do clima, como o oceano Austral e a própria Península Antártica, além de sistemas transicionais entre regiões subpolares, como o estreito de Bransfield. Ambientes já sensíveis às alterações do ciclo do CO_2 devido à ação antropogênica, como as altas latitudes, devem ser tratados com atenção a essas variações alarmantes, como as aqui identificadas. Nesse sentido, iniciativas para a compreensão de alterações resultantes da mudança do clima devem promover embasamento sólido para medidas como a criação de um plano de desenvolvimento sustentável do oceano para a década de 2030. Essa perspectiva é oriunda da proposta Década dos Oceanos da Organização

das Nações Unidas. Estudos como esta dissertação contribuem no âmbito das metas associadas ao combate às mudanças do clima (Objetivo de Desenvolvimento Sustentável 13) e à conservação da vida marinha (Objetivo de Desenvolvimento Sustentável 14) que podem ser incluídos na Agenda 2030 dessa organização.

Referências Bibliográficas

ABBAS, F.; HAMMAD, H. M.; FAHAD, S.; CERDÀ, A.; RIZWAN, M.; FARHAD, W.; EHSAN, S.; BAKHAT, H. F. Agroforestry: a sustainable environmental practice for carbon sequestration under the climate change scenarios—a review. **Environmental Science and Pollution Research**, v. 24, n. 12, p. 11177–11191, 2017.

ABERNATHEY, R. P.; CEROVECKI, I.; HOLLAND, P. R.; NEWSOM, E.; MAZLOFF, M.; TALLEY, L. D. Water-mass transformation by sea ice in the upper branch of the Southern Ocean overturning. **Nature Geoscience**, v. 9, n. 8, p. 596–601, 2016.

ACQUA, O. D.; FERRANDO, S.; CHIANTORE, M.; ASNAGHI, V. The impact of

ocean acidification on the gonads of three key Antarctic benthic macroinvertebrates. **Aquatic Toxicology**, v. 210, n. September 2018, p. 19–29, 2019.

ALMENDROS, J. *et al.* BRAVOSEIS: Geophysical investigation of rifting and volcanism in the Bransfield strait, Antarctica. **Journal of South American Earth Sciences**, v. 104, n. September, 2020.

ÁLVAREZ-VALERO, A. M.; GISBERT, G.; AULINAS, M.; GEYER, A.; KERESZTURI, G.; POLO-SÁNCHEZ, A.; NÚÑEZ-GUERRERO, E.; SUMINO, H.; BORRAJO, J. δD and δ18O variations of the magmatic system beneath Deception Island volcano (Antarctica): Implications for magma ascent and eruption forecasting. **Chemical Geology**, v. 542, n. March, p. 1–15, jun. 2020.

ALVAREZ, M.; AIDA, F. R.; ROS, G. Spatio-temporal variability of air-sea fluxes of carbon dioxide and oxygen in the Bransfield and Gerlache Straits during Austral summer 1995-96. **Deep-Sea Research Part II**, v. 49, p. 643–662, 2002.

ANADÓN, R.; ESTRADA, M. The FRUELA cruises. A carbon flux study in productive areas of the Antarctic Peninsula (December 1995-February 1996). **Deep-Sea Research Part II: Topical Studies in Oceanography**, v. 49, n. 4–5, p. 567–583, 2002.

ANDERSON, L. G.; HOLBY, O.; LINDEGREN, R.; OHLSON, M. The transport of anthropogenic carbon dioxide into the Weddell Sea. **Journal of Geophysical Research**, v. 96, n. C9, 1991.

ARRIGO, K. R.; PABI, S.; DIJKEN, G. L. VAN; MASLOWSKI, W. Air-sea flux of CO2 in the Arctic Ocean, 1998-2003. **Journal of Geophysical Research: Biogeosciences**, v. 115, n. 4, p. 1998–2003, 2010.

AVELINA, R.; CUNHA, L. C. DA; FARIAS, C. DE O.; HAMACHER, C.; KERR, R.; MATA, M. M. Contrasting dissolved organic carbon concentrations in the Bransfield Strait, Northern Antarctic Peninsula: insights into ENSO and SAM effects. **Journal of Marine Systems**, v. 212, p. 103457, 2020.

AZANEU, M.; KERR, R.; MATA, M. M. Assessment of the representation of Antarctic Bottom Water properties in the ECCO2 reanalysis. **Ocean Science**, v. 10, n. 6, p. 923–946, 2014.

AZANEU, M.; KERR, R.; MATA, M. M.; GARCIA, C. A. E. E. Trends in the deep Southern Ocean (1958-2010): Implications for Antarctic Bottom Water properties and volume export. **Journal of Geophysical Research: Oceans**, v. 118, n. 9, p. 4213–4227, set. 2013.

BELLERBY, R. G. J.; TURNER, D. R.; ROBERTSON, J. E. Surface pH and pC02 distributions in the Bellingshausen Sea, Southern Ocean, during the early Austral summer. **Deep-Sea Research Part II**, v. 42, n. 4–5, p. 1093–1107, 1995.

BLACKFORD, J. C.; GILBERT, F. J. pH variability and CO2 induced acidification in the North Sea. **Journal of Marine Systems**, v. 64, n. 1–4, p. 229–241, 2007.

BOYER, T. P. *et al.* NOAA Atlas NESDIS 87. World Ocean Database 2018. p. 1–207, 2018.

BROULLÓN, D. *et al.* A global monthly climatology of total alkalinity: A neural network approach. **Earth System Science Data**, v. 11, n. 3, p. 1109–1127, 2019.

BROULLÓN, D.; PÉREZ, F. F.; VELO, A.; HOPPEMA, M.; OLSEN, A.; TAKAHASHI, T.; KEY, R. M.; TANHUA, T.; SANTANA-CASIANO, J. M.; KOZYR, A. A global monthly climatology of oceanic total dissolved inorganic carbon: a neural network approach. **Earth System Science Data**, v. 12, n. 3, p. 1725–1743, 5 ago. 2020.

BROWN, M. S.; MUNRO, D. R.; FEEHAN, C. J.; SWEENEY, C.; DUCKLOW, H. W.; SCHOFIELD, O. M. Enhanced oceanic CO2 uptake along the rapidly changing West Antarctic Peninsula. **Nature Climate Change**, v. 9, n. 9, p. 678–683, 2019.

CAO, L.; CALDEIRA, K.; JAIN, A. K. Effects of carbon dioxide and climate change on ocean acidification and carbonate mineral saturation. **Geophysical Research Letters**, v. 34, n. 5, p. 1–5, mar. 2007.

CASPEL, M. VAN; HELLMER, H. H.; MATA, M. M. On the ventilation of Bransfield Strait deep basins. **Deep-Sea Research Part II: Topical Studies in Oceanography**, v. 149, n. September 2017, p. 25–30, 2018.

CASPEL, M. VAN; HELLMER, H. H.; MATA, M. M.; CASPEL, M. VAN; HELLMER, H. H.; MATA, M. M. On the ventilation of Bransfield Strait deep basins. **Deep-Sea Research Part II: Topical Studies in Oceanography**, v. 149, n. September 2017, p. 25–30, 2018.

CASTRO, C. G.; RÍOS, A. F.; DOVAL, M. D.; PÉREZ, F. F. Nutrient utilisation and chlorophyll distribution in the Atlantic sector of the Southern Ocean during Austral summer 1995-96. **Deep-Sea Research Part II: Topical Studies in Oceanography**, v. 49, n. 4–5, p. 623–641, 2002.

CLOWES, A. J. Hydrology of the Bransfield Strait. *In*: **Discovery Reports**. [s.l:

s.n.]. p. 1–64.

COOK, A. J.; FOX, A. J.; VAUGHAN, D. G.; FERRIGNO, J. G. Retreating glacier fronts on the Antarctic Peninsula over the past half-century. **Science**, v. 308, n. 5721, p. 541–544, 2005.

COOK, A. J.; HOLLAND, P. R.; MEREDITH, M. P.; MURRAY, T.; LUCKMAN, A.; VAUGHAN, D. G. Ocean forcing of glacier retreat in the western Antarctic Peninsula. **Science**, v. 353, n. 6296, p. 283–286, 2016.

COSTA, R. R.; MENDES, C. R. B.; SOUZA, M. S. D.; TAVANO, V. M.; SECCHI, E. R. Chemotaxonomic characterization of the key genera of diatoms in the Northern Antarctic Peninsula. **Anais da Academia Brasileira de Ciencias**, v. 94, p. e20210584, 2022.

COSTA, R. R.; MENDES, C. R. B.; TAVANO, V. M.; DOTTO, T. S.; KERR, R.; MONTEIRO, T.; ODEBRECHT, C.; SECCHI, E. R. Dynamics of an intense diatom bloom in the Northern Antarctic Peninsula, February 2016. **Limnology and Oceanography**, v. 65, n. 9, p. 1–20, 18 mar. 2020.

DAMINI, B. Y.; KERR, R.; DOTTO, T. S.; MATA, M. M. Long-term changes on the Bransfield Strait deep water masses: Variability, drivers and connections with the northwestern Weddell Sea. **Deep Sea Research Part I: Oceanographic Research Papers**, v. 179, p. 103667, jan. 2022.

DETONI, A. M. S.; SOUZA, M. S. DE; GARCIA, C. A. E.; TAVANO, V. M.; MATA, M. M. Environmental conditions during phytoplankton blooms in the vicinity of James Ross Island, east of the Antarctic Peninsula. **Polar Biology**, v. 38, n. 8, p. 1111–1127, 2015.

DICKSON, A. G. Thermodynamics of the Dissociation of Boric Acid in Potassium Chloride Solutions from 273.15 to 318.15 K. **Journal of Chemical and Engineering Data**, v. 35, n. 3, p. 253–257, 1990.

DICKSON, A. G.; MILLERO, F. J. A comparison of the equilibrium constants for the dissociation of carbonic acid in seawater media. **Deep Sea Research Part A, Oceanographic Research Papers**, v. 34, n. 10, p. 1733–1743, 1987.

DINNIMAN, M. S.; KLINCK, J. M.; HOFMANN, E. E. Sensitivity of circumpolar deep water transport and ice shelf basal melt along the west antarctic peninsula to changes in the winds. **Journal of Climate**, v. 25, n. 14, p. 4799–4816, 2012.

DINNIMAN, M. S.; KLINCK, J. M.; SMITH, W. O. A model study of Circumpolar Deep Water on the West Antarctic Peninsula and Ross Sea continental shelves. **Deep-Sea Research Part II: Topical Studies in Oceanography**, v. 58, n. 13–16, p. 1508–1523, 2011.

DONEY, S. C.; FABRY, V. J.; FEELY, R. A; KLEYPAS, J. A. Ocean acidification: the other CO2 problem. **Annual Rev. Mar. Sci.**, v. 1, p. 169–192, 2009.

DOTTO, T. S.; KERR, R.; MATA, M. M.; GARCIA, C. A. E. Multidecadal freshening and lightening in the deep waters of the Bransfield Strait, Antarctica. **Journal of Geophysical Research: Oceans**, v. 121, n. 6, p. 3741–3756, jun. 2016.

DOTTO, T. S.; MATA, M. M.; KERR, R.; GARCIA, C. A. E. A novel hydrographic gridded data set for the northern Antarctic Peninsula. **Earth System Science Data**, v. 13, n. 2, p. 671–696, 26 fev. 2021.

DOVAL, M. D.; ÁLVAREZ-SALGADO, X. A.; CASTRO, C. G.; PÉREZ, F. F. Dissolved organic carbon distributions in the Bransfield and Gerlache Straits, Antarctica. **Deep-Sea Research Part II: Topical Studies in Oceanography**, v. 49, n. 4–5, p. 663–674, 2002.

DUCKLOW, H. W.; FRASER, W. R.; MEREDITH, M. P.; STAMMERJOHN, S. E.; DONEY, S. C.; MARTINSON, D. G.; SAILLEY, S. F.; SCHOFIELD, O. M.; STEINBERG, D. K.; VENABLES, H. J.; AMSLER, C. D. West Antarctic peninsula: An ice-dependent coastal marine ecosystem in transition. **Oceanography**, v. 26, n. 3, p. 190–203, 2013.

EMERSON, S.; HEDGES, J. **Chemical Oceanography and the Marine Carbon Cycle**. [s.l.] Cambridge University Press, 2008. v. 59

FABRY, V. J. Marine calcifiers in a high-CO2 ocean. **Science**, v. 320, n. May, p. 1020–1022, 2008.

FEELY, R.; DONEY, S.; COOLEY, S. Ocean acidification: Present conditions and future changes in a high-CO2 world. **Oceanography**, v. 22, n. 4, p. 36–47, 1 dez. 2009.

FIGUEROLA, B. *et al.* Predicting potential impacts of ocean acidification on marine calcifiers from the Southern Ocean. n. Lmc, p. 1–36, 2020.

FIGUEROLA, B.; HANCOCK, A. M.; BAX, N.; CUMMINGS, V. J.; DOWNEY, R.; GRIFFITHS, H. J.; SMITH, J.; STARK, J. S. A Review and Meta-Analysis of Potential Impacts of Ocean Acidification on Marine Calcifiers From the Southern Ocean. **Frontiers in Marine Science**, v. 8, n. January, 2021.

FISCHER, G. Stable carbon isotope ratios of plankton carbon and sinking

organic matter from the Atlantic sector of the Southern Ocean. **Marine Chemistry**, v. 35, n. 1–4, p. 581–596, 1991.

FISK, M. R. Volcanism in the Bransfield Strait, Antarctica. **Journal of South American Earth Sciences**, v. 3, n. 2–3, p. 91–101, 1990.

FRIEDLINGSTEIN, P. *et al.* Global Carbon Budget 2021. **Earth Syst. Sci. Data Discuss. [preprint]**, n. November, 2021.

FRÖLICHER, T. L.; SARMIENTO, J. L.; PAYNTER, D. J.; DUNNE, J. P.; KRASTING, J. P.; WINTON, M. Dominance of the Southern Ocean in anthropogenic carbon and heat uptake in CMIP5 models. **Journal of Climate**, v. 28, n. 2, p. 862–886, 2015.

GARCÍA, M. A.; CASTRO, C. G.; RÍOS, A. F.; DOVAL, M. D.; ROSÓN, G.; GOMIS, D.; LÓPEZ, O. Water masses and distribution of physico-chemical properties in the Western Bransfield Strait and Gerlache Strait during Austral summer 1995/96. **Deep-Sea Research Part II: Topical Studies in Oceanography**, v. 49, n. 4–5, p. 585–602, 2002.

GILLE, S. T. Decadal-scale temperature trends in the Southern Hemisphere ocean. **Journal of Climate**, v. 21, n. 18, p. 4749–4765, 2008.

GORDON, A. L.; MENSCH, M.; DONG, Z.; SMETHIE, W. M.; BETTENCOURT, J. DE. Deep and bottom water of the Bransfield Strait eastern and central basins. **Journal of Geophysical Research: Oceans**, v. 105, n. C5, p. 11337–11346, 2000.

GOYET, C.; POISSON, A. New determination of carbonic acid dissociation constants in seawater as a function of temperature and salinity. **Deep Sea**

Research Part A. Oceanographic Research Papers, v. 36, n. 11, p. 1635–1654, nov. 1989.

GREEN, C.; BYRNE, K. A. Biomass: Impact on Carbon Cycle and Greenhouse Gas Emissions. **Encyclopedia of Energy**, v. 1, p. 223–236, 2004.

GRUBER, N. *et al.* The oceanic sink for anthropogenic CO 2 from 1994 to 2007. **Science**, v. 363, n. 6432, p. 1193–1199, 2019.

GRUBER, N.; LANDSCHÜTZER, P.; LOVENDUSKI, N. S. The Variable Southern Ocean Carbon Sink. **Annual Review of Marine Science**, v. 11, n. 1, p. 159–186, 2019.

GYLDENFELDT, A. B. VON; FAHRBACH, E.; GARCÍA, M. A.; SCHRÖDER, M. Flow variability at the tip of the Antarctic Peninsula. **Deep-Sea Research Part II: Topical Studies in Oceanography**, v. 49, n. 21, p. 4743–4766, 2002.

HANSSON, I. A new set of acidity constants for carbonic acid and boric acid in sea water. **Deep-Sea Research and Oceanographic Abstracts**, v. 20, n. 5, p. 461–478, 1973.

HAUCK, J.; HOPPEMA, M.; BELLERBY, R. G. J.; VÖLKER, C.; WOLF-GLADROW, D. Data-based estimation of anthropogenic carbon and acidification in the Weddell Sea on a decadal timescale. **Journal of Geophysical Research: Oceans**, v. 115, n. 3, p. 1–14, 2010.

HAUMANN, F. A.; GRUBER, N.; MÜNNICH, M.; FRENGER, I.; KERN, S.; ALEXANDER HAUMANN, F.; GRUBER, N.; MÜNNICH, M.; FRENGER, I.; KERN, S. Sea-ice transport driving Southern Ocean salinity and its recent trends. **Nature**, v. 537, n. 7618, p. 89–92, 2016.

HAURI, C.; DONEY, S. C.; TAKAHASHI, T.; ERICKSON, M.; JIANG, G.; DUCKLOW, H. W. Two decades of inorganic carbon dynamics along the West Antarctic Peninsula. **Biogeosciences**, v. 12, n. 22, p. 6761–6779, 2015.

HELLMER, H. H.; HUHN, O.; GOMIS, D.; TIMMERMANN, R. On the freshening of the northwestern Weddell Sea continental shelf. **Ocean Science**, v. 7, n. 3, p. 305–316, 2011.

HELLMER, H. H.; KAUKER, F.; TIMMERMANN, R.; HATTERMANN, T. The fate of the Southern Weddell sea continental shelf in a warming climate. **Journal of Climate**, v. 30, n. 12, p. 4337–4350, jun. 2017.

HENLEY, S. F. *et al.* Variability and change in the west Antarctic Peninsula marine system: Research priorities and opportunities. **Progress in Oceanography**, v. 173, n. March, p. 208–237, abr. 2019.

HENLEY, S. F. *et al.* Changing Biogeochemistry of the Southern Ocean and Its Ecosystem Implications. **Frontiers in Marine Science**, v. 7, n. July, p. 1–31, 31 jul. 2020.

HEUVEN, S. M. A. C. VAN; HOPPEMA, M.; JONES, E. M.; BAAR, H. J. W. DE. Rapid invasion of anthropogenic CO2 into the deep circulation of the Weddell Gyre. **Philosophical Transactions of the Royal Society A: Mathematical, Physical and Engineering Sciences**, v. 372, n. 2019, p. 1–11, 13 jul. 2014.

HOFMANN, E. E.; KLINCK, J. M.; LASCARA, C. M.; SMITH, D. A. Water mass distribution and circulation west of the Antarctic Peninsula and including Bransfield Strait. *In*: **Foundations for Ecological Research West of the Antarctic Peninsula: Antactic Research Series**. [s.l: s.n.]. p. 61–80.

HOUGHTON, R. A. The Contemporary Carbon Cycle. *In*: **Treatise on Geochemistry**. [s.l.] Elsevier, 2003. p. 473–513.

HOUGHTON, R. A. **The Contemporary Carbon Cycle**. 2. ed. [s.l.] Elsevier Ltd., 2013. v. 10

HUNEKE, W. G. C.; HUHN, O.; SCHRÖEDER, M. Water masses in the Bransfield Strait and adjacent seas, austral summer 2013. **Polar Biology**, v. 39, n. 5, p. 789–798, 2016.

INTERGOVERNMENTAL OCEANOGRAPHIC COMMISSION; SCIENTIFIC COMMITTEE ON OCEANIC RESEARCH; INTERNATIONAL ASSOCIATION FOR THE PHYSICAL SCIENCES OF THE OCEANS. The international thermodynamic equation of seawater – 2010: Calculation and use of thermodynamic properties. **Intergovernmental Oceanographic Commission, Manuals and Guides No. 56**, n. June, p. 196, 2010.

IPCC. Summary for Policymakers. *In*: MASSON-DELMOTTE, V. *et al.* (Eds.). . **Global Warming of 1.5°C. An IPCC Special Report on the impacts of global warming of 1.5°C above pre-industrial levels and related global greenhouse gas emission pathways, in the context of strengthening the global response to the threat of climate change,**. Geneva, Switzerland: [s.n.]. v. 18p. 32.

ITO, R. G.; TAVANO, V. M.; MENDES, C. R. B.; GARCIA, C. A. E. Sea-air CO2 fluxes and pCO2 variability in the Northern Antarctic Peninsula during three summer periods (2008–2010). **Deep-Sea Research Part II: Topical Studies in Oceanography**, v. 149, n. September 2017, p. 84–98, 2018.

ITO, T.; WOLOSZYN, M.; MAZLOFF, M. Anthropogenic carbon dioxide

transport in the Southern Ocean driven by Ekman flow. **Nature**, v. 463, n. 7277, p. 80–83, 2010.

JIANG, L. Q.; CARTER, B. R.; FEELY, R. A.; LAUVSET, S. K.; OLSEN, A. Surface ocean pH and buffer capacity: past, present and future. **Scientific Reports**, v. 9, n. 1, p. 1–11, 2019.

JONES, E. M.; FENTON, M.; MEREDITH, M. P.; CLARGO, N. M.; OSSEBAAR, S.; DUCKLOW, H. W.; VENABLES, H. J.; BAAR, H. J. W. DE. Ocean acidification and calcium carbonate saturation states in the coastal zone of the West Antarctic Peninsula. **Deep-Sea Research Part II: Topical Studies in Oceanography**, v. 139, n. January, p. 181–194, 2017.

KAPSENBERG, L.; KELLEY, A. L.; SHAW, E. C.; MARTZ, T. R.; HOFMANN, G. E. Near-shore Antarctic pH variability has implications for the design of ocean acidification experiments. **Scientific Reports**, v. 5, n. 1, p. 9638, 22 set. 2015.

KARL, D. M.; TILBROOK, B.; TIEN, G. Seasonal coupling of organic matter production and particle flux in the western Bransfield Strait, Antarctica. **Deep-Sea Research**, v. 38, p. 1097–1126, 1990.

KELLER, R. A.; FISK, M. R.; WHITE, W. M.; BIRKENMAJER, K. Isotopic and trace element constraints on mixing and melting models of marginal basin volcanism, Bransfield Strait, Antarctica. **Earth and Planetary Science Letters**, v. 111, n. 2–4, p. 287–303, 1992.

KERR, R.; GOYET, C.; CUNHA, L. C. DA; ORSELLI, I. B. M.; LENCINA-AVILA, J. M.; MENDES, C. R. B.; CARVALHO-BORGES, M.; MATA, M. M.; TAVANO, V. M. Carbonate system properties in the Gerlache Strait, Northern Antarctic

Peninsula (February 2015): II. Anthropogenic CO2 and seawater acidification. **Deep-Sea Research Part II: Topical Studies in Oceanography**, v. 149, n. July 2017, p. 182–192, 2018.

KERR, R.; MATA, M. M.; MENDES, C. R. B.; SECCHI, E. R. Northern Antarctic Peninsula: a marine climate hotspot of rapid changes on ecosystems and ocean dynamics. **Deep-Sea Research Part II: Topical Studies in Oceanography**, v. 149, p. 4–9, 2018.

KERR, R.; ORSELLI, I. B. M.; LENCINA-AVILA, J. M.; EIDT, R. T.; MENDES, C. R. B.; CUNHA, L. C. DA; GOYET, C.; MATA, M. M.; TAVANO, V. M. Carbonate system properties in the Gerlache Strait, Northern Antarctic Peninsula (February 2015): I. Sea–Air CO2 fluxes. **Deep-Sea Research Part II: Topical Studies in Oceanography**, v. 149, n. February 2017, p. 171–181, 2018.

LAIKA, H. E.; GOYET, C.; VOUVE, F.; POISSON, A.; TOURATIER, F. Interannual properties of the CO2 system in the Southern Ocean south of Australia. **Antarctic Science**, v. 21, n. 6, p. 663–680, 2009.

LAUVSET, S. K.; CARTER, B. R.; PEREZ, F. F.; JIANG, L. Q.; FEELY, R. A.; VELO, A.; OLSEN, A. Processes Driving Global Interior Ocean pH Distribution. **Global Biogeochemical Cycles**, v. 34, n. 1, p. 1–17, 2020.

LAUVSET, S. K.; GRUBER, N.; LANDSCHÜTZER, P.; OLSEN, A.; TJIPUTRA, J. Trends and drivers in global surface ocean pH over the past 3 decades. **Biogeosciences**, v. 12, n. 5, p. 1285–1298, 2015.

LEE, K.; TONG, L. T.; MILLERO, F. J.; SABINE, C. L.; DICKSON, A. G.; GOYET, C.; PARK, G. H.; WANNINKHOF, R.; FEELY, R. A.; KEY, R. M. Global

relationships of total alkalinity with salinity and temperature in surface waters of the world's oceans. **Geophysical Research Letters**, v. 33, n. 19, 2006.

LEGGE, O. J.; BAKKER, D. C. E.; MEREDITH, M. P.; VENABLES, H. J.; BROWN, P. J.; JONES, E. M.; JOHNSON, M. T. The seasonal cycle of carbonate system processes in Ryder Bay, West Antarctic Peninsula. **Deep Sea Research Part II: Topical Studies in Oceanography**, v. 139, n. November 2016, p. 167–180, maio 2017.

LENCINA-AVILA, J. M.; GOYET, C.; KERR, R.; ORSELLI, I. B. M.; MATA, M. M.; TOURATIER, F. Past and future evolution of the marine carbonate system in a coastal zone of the Northern Antarctic Peninsula. **Deep-Sea Research Part II: Topical Studies in Oceanography**, v. 149, n. December 2017, p. 193–205, 2018.

LESEURRE, C.; MONACO, C. LO; REVERDIN, G.; METZL, N.; FIN, J.; MIGNON, C.; BENITO, L. Trends and driversof sea surface fCO2 and pH changes observed in Southern Indian Ocean over the last two decades. **Biogeosciences**, v. 19, n. 10, p. 2599–2625, 2022.

LEWIS, E.; WALLACE, D. **Program developed for CO2 system calculationsOrnl/Cdiac-105**Oak Ridge, TennCarbon Dioxide Information Analysis Center, , 1998. Disponível em: <http://cdiac.esd.ornl.gov/oceans/co2rprtnbk.html>

LOEB, V. J.; HOFMANN, E. E.; KLINCK, J. M.; HOLM-HANSEN, O.; WHITE, W. B. ENSO and variability of the antarctic peninsula pelagic marine ecosystem. **Antarctic Science**, v. 21, n. 2, p. 135–148, 2009.

LOPEZ, O.; GARCIA, M. A.; GOMIS, D.; ROJAS, P.; SOSPEDRA, J.;

ARCILLA-SÁNCHEZ, A. Hydrographic and hydrodynamic characteristics a of the eastern basin of the Bransfiled Strait. **Deep Sea Research Part I: Oceanographic Research Papers**, v. 46, p. 1755–1778, 1999.

LUEKER, T. J.; DICKSON, A. G.; KEELING, C. D. Ocean pCO2 calculated from dissolved inorganic carbon, alkalinity, and equations for K1 and K2: Validation based on laboratory measurements of CO2 in gas and seawater at equilibrium. **Marine Chemistry**, v. 70, n. 1–3, p. 105–119, 2000.

MARSHALL, G. J.; ORR, A.; LIPZIG, N. P. M. VAN; KING, J. C. The impact of a changing Southern Hemisphere Annular Mode on Antarctic Peninsula summer temperatures. **Journal of Climate**, v. 19, n. 20, p. 5388–5404, 2006.

MASQUÉ, P.; ISLA, E.; SANCHEZ-CABEZA, J. A.; PALANQUES, A.; BRUACH, J. M.; PUIG, P.; GUILLÉN, J. Sediment accumulation rates and carbon fluxes to bottom sediments at the western Bransfield Strait (Antarctica). **Deep-Sea Research Part II: Topical Studies in Oceanography**, v. 49, n. 4–5, p. 921–933, 2002.

MASSOM, R. A.; SCAMBOS, T. A.; BENNETTS, L. G.; REID, P.; SQUIRE, V. A.; STAMMERJOHN, S. E. Antarctic ice shelf disintegration triggered by sea ice loss and ocean swell. **Nature**, v. 558, n. 7710, p. 383–389, 2018.

MATA, M. M.; TAVANO, V. M.; GARCIA, C. A. E. 15 years sailing with the Brazilian High Latitude Oceanography Group (GOAL). **Deep-Sea Research Part II: Topical Studies in Oceanography**, v. 149, p. 1–3, mar. 2018.

MCNEIL, B. I.; MATEAR, R. J. Southern Ocean acidification: A tipping point at 450-ppm atmospheric CO2. **Proceedings of the National Academy of Sciences of the United States of America**, v. 105, n. 48, p. 18860–18864,

2008.

MEHRBACH, C.; CULBERSON, C. H.; HAWLEY, J. E.; PYTKOWICX, R. M. Measurement of the Apparent Dissociation Constants of Carbonic Acid in Seawater At Atmospheric Pressure. **Limnology and Oceanography**, v. 18, n. 6, p. 897–907, 1973.

MENDES, C. R. B.; SOUZA, M. S. DE; GARCIA, V. M. T.; LEAL, M. C.; BROTAS, V.; GARCIA, C. A. E. Dynamics of phytoplankton communities during late summer around the tip of the Antarctic Peninsula. **Deep-Sea Research Part I: Oceanographic Research Papers**, v. 65, p. 1–14, 2012.

MEREDITH, M. P.; BRANDON, M. A.; WALLACE, M. I.; CLARKE, A.; LENG, M. J.; RENFREW, I. A.; LIPZIG, N. P. M. VAN; KING, J. C. Variability in the freshwater balance of northern Marguerite Bay, Antarctic Peninsula: Results from δ18O. **Deep-Sea Research Part II: Topical Studies in Oceanography**, v. 55, n. 3–4, p. 309–322, 2008.

MEREDITH, M. P.; JULLION, L.; BROWN, P. J.; GARABATO, A. C. N.; COULDREY, M. P. Dense waters of the Weddell and Scotia seas: Recent changes in properties and circulation. **Philosophical Transactions of the Royal Society A: Mathematical, Physical and Engineering Sciences**, v. 372, n. 2019, p. 1–11, 2014.

MEREDITH, M. P.; KING, J. C. Rapid climate change in the ocean west of the Antarctic Peninsula during the second half of the 20th century. **Geophysical Research Letters**, v. 32, n. 19, p. 1–5, 2005.

MIDORIKAWA, T.; INOUE, H. Y.; ISHII, M.; SASANO, D.; KOSUGI, N.; HASHIDA, G.; NAKAOKA, S. ICHIRO; SUZUKI, T. Decreasing pH trend

estimated from 35-year time series of carbonate parameters in the Pacific sector of the Southern Ocean in summer. **Deep-Sea Research Part I: Oceanographic Research Papers**, v. 61, p. 131–139, 2012.

MILLERO, F. J. The Marine Inorganic Carbon Cycle. **Chemical Reviews**, v. 107, n. 2, p. 308–341, fev. 2007.

MILLERO, F. J. **Chemical Oceanography**. [s.l.] CRC Press, 2016. v. 30

MILLERO, F. J.; GRAHAM, T. B.; HUANG, F.; BUSTOS-SERRANO, H.; PIERROT, D. Dissociation constants of carbonic acid in seawater as a function of salinity and temperature. **Marine Chemistry**, v. 100, n. 1–2, p. 80–94, 2006.

MILLERO, F. J.; LEE, K.; ROCHE, M. Distribution of alkalinity in the surface waters of the major oceans. **Marine Chemistry**, v. 60, n. 1–2, p. 111–130, 1998.

MILLERO, F. J.; PIERROT, D.; LEE, K.; WANNINKHOF, R.; FEELY, R.; SABINE, C. L.; KEY, R. M.; TAKAHASHI, T. Dissociation constants for carbonic acid determined from field measurements. **Deep-Sea Research Part I: Oceanographic Research Papers**, v. 49, n. 10, p. 1705–1723, 2002.

MOFFAT, C.; MEREDITH, M. Shelf-ocean exchange and hydrography west of the Antarctic Peninsula: A review. **Philosophical Transactions of the Royal Society A: Mathematical, Physical and Engineering Sciences**, v. 376, n. 2122, 2018.

MOFFAT, C.; OWENS, B.; BEARDSLEY, R. C. On the characteristics of Circumpolar Deep Water intrusions to the west Antarctic Peninsula Continental Shelf. **Journal of Geophysical Research: Oceans**, v. 114, n. 5, p. 1–16, 2009.

MONTEIRO, T.; KERR, R.; MACHADO, E. DA C. Seasonal variability of net sea-air CO2 fluxes in a coastal region of the northern Antarctic Peninsula. **Scientific Reports**, v. 10, n. 1, p. 14875, 10 dez. 2020.

MONTEIRO, T.; KERR, R.; ORSELLI, I. B. M.; LENCINA-AVILA, J. M. Towards an intensified summer CO2 sink behaviour in the Southern Ocean coastal regions. **Progress in Oceanography**, v. 183, n. January, p. 1–13, 2020.

ORR, J. C. *et al.* Anthropogenic ocean acidification over the twenty-first century and its impact on calcifying organisms. **Nature**, v. 437, n. 7059, p. 681–686, 2005.

ORR, J. C.; EPITALON, J. M.; DICKSON, A. G.; GATTUSO, J. P. Routine uncertainty propagation for the marine carbon dioxide system. **Marine Chemistry**, v. 207, n. June, p. 84–107, 2018.

ORSELLI, I. B. M.; CARVALHO, A. C. O.; MONTEIRO, T.; DAMINI, B. Y.; CARVALHO-BORGES, M. DE; ALBUQUERQUE, C.; KERR, R. The marine carbonate system along the northern Antarctic Peninsula: current knowledge and future perspectives. **Anais da Academia Brasileira de Ciências**, v. 94, n. suppl 1, 2022.

PARDO, P. C.; PÉREZ, F. F.; KHATIWALA, S.; RÍOS, A. F. Anthropogenic CO2 estimates in the Southern Ocean: Storage partitioning in the different water masses. **Progress in Oceanography**, v. 120, p. 230–242, 2014.

RAVEN, J.; CALDEIRA, K.; ELDERFIELD, H.; HOEGH-GULDBERG, O.; LISS, P.; RIEBESELL, U.; SHEPHERD, J.; TURLEY, C.; WATSON, A. **Ocean acidification due to increasing atmospheric carbon dioxideCoral Reefs**. [s.l: s.n.]. Disponível em: <http://eprints.ifm-

geomar.de/7878/1/965_Raven_2005_OceanAcidificationDueToIncreasing_Monogr_pubid13120.pdf>.

REID, P. A.; MASSOM, R. A. Change and variability in Antarctic coastal exposure, 1979–2020. **Nature Communications**, v. 13, n. 1164, p. 1–11, 2022.

RENFORTH, P.; HENDERSON, G. Assessing ocean alkalinity for carbon sequestration. **Reviews of Geophysics**, v. 55, n. 3, p. 636–674, 2017.

RENNER, A. H. H.; THORPE, S. E.; HEYWOOD, K. J.; MURPHY, E. J.; WATKINS, J. L.; MEREDITH, M. P. Advective pathways near the tip of the Antarctic Peninsula: Trends, variability and ecosystem implications. **Deep-Sea Research Part I: Oceanographic Research Papers**, v. 63, p. 91–101, 2012.

RIGNOT, E.; MOUGINOT, J.; SCHEUCHL, B.; BROEKE, M. VAN DEN; WESSEM, M. J. VAN; MORLIGHEM, M. Four decades of Antarctic ice sheet mass balance from 1979–2017. **Proceedings of the National Academy of Sciences of the United States of America**, v. 116, n. 4, p. 1095–1103, 2019.

RIVARO, P.; MESSA, R.; IANNI, C.; MAGI, E.; BUDILLON, G. Distribution of total alkalinity and pH in the Ross Sea (Antarctica) waters during austral summer 2008. **Polar Research**, v. 33, n. 2014, 2014.

RODEN, N. P.; SHADWICK, E. H.; TILBROOK, B.; TRULL, T. W. Annual cycle of carbonate chemistry and decadal change in coastal. **Marine Chemistry**, v. 155, p. 135–147, 2013.

ROY, R. N.; ROY, L. N.; VOGEL, K. M.; PORTER-MOORE, C.; PEARSON, T.; GOOD, C. E.; MILLERO, F. J.; CAMPBELL, D. M. The dissociation constants of carbonic acid in seawater at salinities 5 to 45 and temperatures 0 to 45°C.

Marine Chemistry, v. 44, n. 2–4, p. 249–267, 1993.

RUIZ BARLETT, E. M.; TOSONOTTO, G. V.; PIOLA, A. R.; SIERRA, M. E.; MATA, M. M. On the temporal variability of intermediate and deep waters in the Western Basin of the Bransfield Strait. **Deep-Sea Research Part II: Topical Studies in Oceanography**, v. 149, n. December 2017, p. 31–46, 2018.

SABINE, C. L. *et al.* The Oceanic Sink for Anthropogenic CO2. **Science**, v. 305, n. 5682, p. 367–371, 16 jul. 2004.

SABINE, C. L.; FEELY, R. A.; MILLERO, F. J.; DICKSON, A. G.; LANGDON, C.; MECKING, S.; GREELEY, D. Decadal changes in Pacific carbon. **Journal of Geophysical Research: Oceans**, v. 113, n. 7, p. 1–12, 2008.

SANDRINI, S.; AIT-AMEUR, N.; RIVARO, P.; MASSOLO, S.; TOURATIER, F.; TOSITTI, L.; GOYET, C. Anthropogenic carbon distribution in the Ross Sea, Antarctica. **Antarctic Science**, v. 19, n. 3, p. 395–407, 2007.

SANGRÀ, P.; GORDO, C.; HERNÁNDEZ-ARENCIBIA, M.; MARRERO-DÍAZ, A.; RODRÍGUEZ-SANTANA, A.; STEGNER, A.; MARTÍNEZ-MARRERO, A.; PELEGRÍ, J. L.; PICHON, T. The Bransfield current system. **Deep-Sea Research Part I: Oceanographic Research Papers**, v. 58, n. 4, p. 390–402, 2011.

SANGRÀ, P.; STEGNER, A.; HERNÁNDEZ-ARENCIBIA, M.; MARRERO-DÍAZ, Á.; SALINAS, C.; AGUIAR-GONZÁLEZ, B.; HENRÍQUEZ-PASTENE, C.; MOURIÑO-CARBALLIDO, B. The Bransfield Gravity Current. **Deep-Sea Research Part I: Oceanographic Research Papers**, v. 119, n. November 2016, p. 1–15, jan. 2017.

SCAMBOS, T. A.; HULBE, C.; FAHNESTOCK, M.; BOHLANDER, J. The link between climate warming and break-up of ice shelves in the Antarctic Peninsula. **Journal of Glaciology**, v. 46, n. 154, p. 516–530, 2000.

SHEPHERD, A. *et al.* Mass balance of the Antarctic Ice Sheet from 1992 to 2017. **Nature**, v. 558, n. 7709, p. 219–222, 13 jun. 2018.

SHEPHERD, A.; WINGHAM, D.; RIGNOT, E. Warm ocean is eroding West Antarctic Ice Sheet. **Geophysical Research Letters**, v. 31, n. 23, p. 1–4, 2004.

SIEGERT, M. *et al.* The Antarctic Peninsula under a 1.5°C global warming scenario. **Frontiers in Environmental Science**, v. 7, n. JUN, p. 1–7, 2019.

SIGNORI, C. N.; THOMAS, F.; ENRICH-PRAST, A.; POLLERY, R. C. G.; SIEVERT, S. M. Microbial diversity and community structure across environmental gradients in Bransfield Strait, Western Antarctic Peninsula. **Frontiers in Microbiology**, v. 5, n. DEC, p. 1–12, 2014.

STIPS, A.; BOLDING, K.; MACIAS, D.; BRUGGEMAN, J.; COUGHLAN, C. **Scoping report on the potential impact of on-board desulphurisation on the water quality in SOx Emission Control Areas 2016**. [s.l: s.n.].

TAKAHASHI, T.; SUTHERLAND, S. C.; CHIPMAN, D. W.; GODDARD, J. G.; HO, C. Climatological distributions of pH, pCO2, total CO2, alkalinity, and CaCO3 saturation in the global surface ocean, and temporal changes at selected locations. **Marine Chemistry**, v. 164, p. 95–125, 2014.

THOMPSON, D. W. J.; SOLOMON, S. Interpretation of recent Southern Hemisphere climate change. **Science**, v. 296, n. 5569, p. 895–899, 2002.

TORRES-LASSO, J. C. **Acidificação oceânica e variação interanual de CO2**

antropogênico no estreito de Bransfield, Antártica. [s.l.] Universidade Federal do Rio Grande, 2019.

TORRES PARRA, R. R.; CAICEDO LAURIDO, A. L.; IRIARTE SÁNCHEZ, J. D. Hydrographic conditions during two austral summer situations (2015 and 2017) in the Gerlache and Bismarck straits, northern Antarctic Peninsula. **Deep-Sea Research Part I: Oceanographic Research Papers**, v. 161, n. April, 2020.

TOURATIER, F.; AZOUZI, L.; GOYET, C. CFC-11, Δ14C and 3H tracers as a means to assess anthropogenic CO2 concentrations in the ocean. **Tellus, Series B: Chemical and Physical Meteorology**, v. 59, n. 2, p. 318–325, 2007.

TOURATIER, F.; GOYET, C. Definition, properties, and Atlantic Ocean distribution of the new tracer TrOCA. **Journal of Marine Systems**, v. 46, n. 1–4, p. 169–179, 2004a.

___. Applying the new TrOCA approach to assess the distribution of anthropogenic CO2 in the Atlantic Ocean. **Journal of Marine Systems**, v. 46, n. 1–4, p. 181–197, 2004b.

TURLEY, C.; FINDLAY, H. S. **Ocean Acidification**. Second Edi ed. [s.l.] Elsevier B.V., 2016. v. 1

TURNER, S.; TONARINI, S.; BINDEMAN, I.; LEEMAN, W. P.; SCHAEFER, B. F. Boron and oxygen isotope evidence for recycling of subducted components over the past 2.5 Gyr. **Nature**, v. 447, n. 7145, p. 702–705, 2007.

TYNAN, E.; CLARKE, J. S.; HUMPHREYS, M. P.; RIBAS-RIBAS, M.; ESPOSITO, M.; RÉROLLE, V. M. C.; SCHLOSSER, C.; THORPE, S. E.; TYRRELL, T.; ACHTERBERG, E. P. Physical and biogeochemical controls on

the variability in surface pH and calcium carbonate saturation states in the Atlantic sectors of the Arctic and Southern Oceans. **Deep Sea Research Part II: Topical Studies in Oceanography**, v. 127, p. 7–27, maio 2016.

UPPSTRÖM, L. R. The boron/chlorinity ratio of deep-sea water from the Pacific Ocean. **Deep-Sea Research and Oceanographic Abstracts**, v. 21, n. 2, p. 161–162, 1974.

WANG, X.; MOFFAT, C.; DINNIMAN, M. S.; KLINCK, J. M.; SUTHERLAND, D. A.; AGUIAR-GONZÁLEZ, B. Variability and Dynamics of Along-Shore Exchange on the West Antarctic Peninsula (WAP) Continental Shelf. **Journal of Geophysical Research: Oceans**, v. 127, n. 2, 2022.

WANNINKHOF, R.; LEWIS, E.; FEELY, R. A.; MILLERO, F. J. The optimal carbonate dissociation constants for determining surface water pCO2 from alkalinity and total inorganic carbon. **Marine Chemistry**, v. 65, n. 3–4, p. 291–301, 1999.

WATSON, A. J.; SCHUSTER, U.; SHUTLER, J. D.; HOLDING, T.; ASHTON, I. G. C.; LANDSCHÜTZER, P.; WOOLF, D. K.; GODDIJN-MURPHY, L. Revised estimates of ocean-atmosphere CO2 flux are consistent with ocean carbon inventory. **Nature Communications**, v. 11, n. 1, p. 1–6, 2020.

WILLE, J. D. *et al.* Intense atmospheric rivers can weaken ice shelf stability at the Antarctic Peninsula. **Communications Earth & Environment**, v. 3, n. 90, p. 1–14, 2022.

WILSON, C.; KLINKHAMMER, G. P.; CHIN, C. S. Hydrography within the central and east basins of the Bransfield Strait, Antarctica. **Journal of Physical Oceanography**, v. 29, n. 3, p. 465–479, 1999.

WOLF-GLADROW, D. A.; ZEEBE, R. E.; KLAAS, C.; KÖRTZINGER, A.; DICKSON, A. G. Total alkalinity: The explicit conservative expression and its application to biogeochemical processes. **Marine Chemistry**, v. 106, n. 1- 2 SPEC. ISS., p. 287–300, 2007.

YANJUN, W.; LI, X.; SONG, J.; LI, X.; ZHONG, G.; ZHANG, B. Carbon Sinks and Variations of pCO2 in the Southern Ocean from 1998 to 2018 Based on a Deep Learning Approach. **IEEE Journal of Selected Topics in Applied Earth Observations and Remote Sensing**, n. March, p. 1–1, 2021.

ZEEBE, R. E. History of seawater carbonate chemistry, atmospheric CO 2, and ocean acidification. **Annual Review of Earth and Planetary Sciences**, v. 40, p. 141–165, 2012.

ZEEBE, R. E.; WOLF-GLADROW, D. A. **CO2 in Seawater: Equilibrium, Kinetics, Isotopes**. Second pri ed. [s.l.] Elsevier, 2001.

ZHOU, M.; NIILER, P. P.; ZHU, Y.; DORLAND, R. D. The western boundary current in the Bransfield Strait, Antarctica. **Deep-Sea Research Part I: Oceanographic Research Papers**, v. 53, n. 7, p. 1244–1252, 2006.